ECMWF COPERNICUS REPORT

Copernicus Climate Change Service

Ozone
Algorithm Theoretical Basis Document (ATBD)

Version: Multiple Ozone products and related versions

Issued by: BIRA-IASB / Michel Van Roozendael

Date: 01/02/2024

Ref: C3S2_312a_Lot2_D-WP2-FDDP-ATBD_202311_O3_v3.6

Official reference number service contract: 2021/C3S2_312a_Lot2_DLR/SC1

PROGRAMME OF THE EUROPEAN UNION

IMPLEMENTED BY ECMWF

Contributors

ROYAL BELGIAN INSTITUTE FOR SPACE AERONOMY
BRUSSELS, BELGIUM
(BIRA-IASB)
M. Van Roozendael
J. Vlietinck
A. Keppens
T. Verhoelst
D. Hubert
J.-C. Lambert

LABORATOIRE ATMOSPHÈRES, MILIEUX, OBSERVATIONS SPATIALES
UNIVERSITY PIERRE ET MARIE CURIE, PARIS, FRANCE
(LATMOS/UPMC)
A. Boynard
C. Clerbaux

GERMAN AEROSPACE CENTER
WESSLING, GERMANY
(DLR)
D. Loyola
K.-P. Heue
M. Coldewey-Egbers

INSTITUTE OF ENVIRONMENTAL PHYSICS,
UNIVERSITY OF BREMEN, BREMEN, GERMANY
(UiB)
N. Rahpoe
K.-U. Eichmann
M. Weber

ROYAL NETHERLANDS METEOROLOGICAL INSTITUTE
DE BILT, THE NETHERLANDS
(KNMI)
M. van Weele
R. van der A
O. Tuinder

RUTHERFORD APPLETON LABORATORY
DIDCOT, UNITED KINGDOM
(RAL)
B. Latter
R. Siddans
B. Kerridge

FINNISH METEOROLOGICAL INSTITUTE
HELSINKI, FINLAND
(FMI)
V. Sofieva
M. Szelag
J. Tamminen

History of modifications

Version	Date	Description of modification	Chapters / Sections
v1.0	7-8.02.2019	C3S_312a_Lot4 Ozone ATBD updated	Related documents; Acronyms; Scope of the document; Executive summary; 2.1and 4
v1.1	11.02.2019	Information on IASI updated	1.1.6, 2.1,3.2, 4.3 and 5
	12.02.2019	Information on OMPS nadir mapper added (L2 to L3)	3.1.3, 4.1 and 4.2
	15.02.2019	Information on limb and occultation profiles updated	1.2.9, 2.1 and 1.2.10
		Information on SMR updated	1.2.5
		Information on OMPS limb profiler updated	2.1
	18.02.2019	Information on OMPS nadir mapper added (L1 to L2)	1.1.5 and 2.1
		Information on L2 TC updated	3.1.2.1, 3.1.2.4, 3.1.2.9 and 3.1.2.12 and 5
	22.02.2019	Information on FY-3/TOU added	1.1.10 and 2.1
v2.0	25.03.2021	Update	Related documents
v2.1	30.04.2021	Update after revision by ASSIMILA	All
v3.0	20.04.2023	Overall update of document, reflecting status of ozone service at start of C3S2_312a_Lot2	All
V3.1	06/07/2023	Document amended to account for feedback from independent reviewers	All sections
V3.2	03/08/2023	Document amended to restore hyperlinks, adjust equation numbering and harmonise captions throughout the text	All sections
V3.3	09/10/2023	Updates for final Climate Data Records	All sections
V3.4	03/01/2024	Updates and format issues corrections from ECMWF feedback.	All sections
V3.5	01/02/2024	The ATBD now covers the final datasets in c3s2_312a_Lot2 for ozone.	All sections
V3.6	22/04/2024	Taken into account feedback from independent reviewers. Broken links repaired + figures improved in 3.3.2 + acronym table + TOC updated.	All sections
V3.7	08/07/2024	Correction in Table 27 and Table 41.	2.4.5 and 4.1

List of datasets covered by this document

This table summarises the C3S ozone products covered by this document. Note that the CDR products contain a (*) reference in the Deliverable ID column, meaning that those products were produced in a previous C3S contract. The version number mentioned here is the latest version number, for more details, see the Product User Guide and Specification document [D24].

Deliverable ID	Product title	Product type (CDR, ICDR)	Version number	Delivery date
WP2-ICDR-O3-TC-v1	GOME-2B TC GOME-2C TC OMI TC OMPS TC S5P TC	ICDR ICDR ICDR ICDR ICDR	V0200 V0100 V0200 V0100 V0100	28/02/2022
(*)	GOME TC GOME-2A TC SCIA TC	CDR CDR CDR	V0100 V0100 V0100	30/04/2017
(*)	IASI-A TC / trop. Col.	CDR	V0004	30/04/2017
WP2-ICDR-O3-IASI-TCC-v1	IASI-B TC / trop. Col. IASI-C TC / trop. Col.	ICDR ICDR	V0004 V0004	28/02/2022
WP2-ICDR-O3-GTO-TC-v1	GTO merged TC	ICDR	V2000	28/02/2022
WP2-ICDR-O3-MSR-TC-v1	MSR TC	ICDR	V0025	28/02/2022
WP2-ICDR-O3-NP-v1	GOME-2B NP OMI NP	ICDR ICDR	V0008 V0007	28/02/2022
(*)	GOME-2A NP GOME NP SCIA NP	CDR CDR CDR	V0007 V0006 V0006	30/04/2017
WP2-ICDR-O3-LP-v1	OSIRIS LP OMPS-SASK LP OMPS-UB LP ACE LP MLS LP SABER LP SAGE-III LP CDR Merged zonal mean LP Merged gridded LP	ICDR ICDR ICDR ICDR ICDR ICDR CDR ICDR ICDR	V0002 V0002 V0002 V0002 V0003 V0002 V0003 V0008 V0004	28/02/2022
(*)	MIPAS LP GOMOS LP SCIA LP SAGE2 LP HALOE LP SMR LP	CDR CDR CDR CDR CDR CDR	V0002 V0001 V0001 V0001 V0001 V0001	30/04/2017
WP2-FDDP-O3	NP_GOP-ECV	CDR	V0100	30/11/2023

Related documents

Reference ID	Document
D1	OMI Algorithm Theoretical Basis Document, Volume II, OMI Ozone Products, Ed. Pawan K Bhartia, NASA Goddard Space Flight Center, Greenbelt, Maryland, USA, ATBD-OMI-02, Version 2.0, August 2002.
D2	OMI Level 2 Ozone DOAS Data Product Specification, SD-OMIE-KNMI-298, Issue 1.1, January 2004.
D3	Product Specification Document of the GOME Data Processor, ER–PS–DLR–GO–0016, Iss./Rev. 4/B, December 2004.
D4	GOMOS Product Handbook, European Space Agency, issue 3.0, May 2007.
D5	GOME-2 Product Guide, EUM/OPS-EPS/MAN/07/0445, Issue: v2D, March 2009.
D6	GDPS Input / Output Data Specification (IODS) Volume 2: Level 1B output products and metadata, SD-OMIE-7200-DS-467, issue 8, November 2009.
D7	GDP 5.0, Upgrade of the GOME Data Processor for Improved Total Ozone Columns, Algorithm Theoretical Basis Document, ERS D-PAF, GDP5-ATBD-1, December 2009.
D8	ENVISAT-1 Products Specifications, Volume 15: SCIAMACHY Products Specifications, ESA, IDEAS-SER-IPF-SPE-0398, issue 3L, January 2010.
D9	Regner, P., CCI EO Satellite Data Requirements, ESA publication, November 2011.
D10	Joint Polar Satellite System (JPSS) Operational Algorithm Description (OAD) Document for Ozone Mapping and Profiler Suite (OMPS) Total Columns (TC) Sensor Data Record (SDR) Software, September 2014, available at http://npp.gsfc.nasa.gov/sciencedocuments/2014-10/474-00077_OAD-OMPS-TC-SDR_F.pdf
D11	Joint Polar Satellite System (JPSS) Operational Algorithm Description (OAD) Document for Ozone Mapping and Profiler Suite (OMPS) Nadir Profile (NP) Sensor Data Record (SDR) Software, September 2014, available at http://npp.gsfc.nasa.gov/sciencedocuments/2014-10/474-00081_OAD-OMPS-NP-SDR_D.pdf
D12	Algorithm Theoretical Basis Document (ATBD) for the Sensor Data Record (SDR) Algorithm Limb Profiler Ozone Mapping And Profiler Suite (OMPS) National Polar-Orbiting Operational Environmental Satellite System Preparatory Project (NPP), available at https://ozoneaq.gsfc.nasa.gov/media/docs/ATBD_NASA_LP_SDR_v3.pdf
D13	Sofieva, V. *(ed.)* and R. van der A, M. Coldewey-Egbers, C. Lerot, D. Loyola, J. van Peet, R. Siddans, N. Rahpoe, K.-P. Heue and R. Astoreca, Ozone_cci Phase-II Product User Guide (PUG), Issue 1, Revision 2, Ozone_cci_PUG_01_02, December 2015.

D14	van Weele, M. and the Ozone_cci science team, Ozone_cci Phase-II User Requirement Document (URD), Version 3, Ozone_cci_URD_3.0, April 2016.
D15	Van Roozendael, M. *(ed.)* and M. Koukouli, A. Laeng, J.-C. Lambert, D. Loyola, R. Siddans, G. Miles, G. Stieler, J. Tamminen, R. van der A, M. Weber, E. Maillard, P. Coheur, C. Wespes, D. Degenstein, J. Urban, K. Walker and C. Lerot, Ozone_cci Phase-II Data Access Requirement Document (DARD), Issue 2, Revision 1, Ozone_cci_DARD_2.1, May 2016.
D16	Lambert, J.-C. *(ed.)* and D. Balis, A. Delcloo, F. Goutail, J. Granville, D. Hubert, A. Keppens, R. Kivi, M. Koukouli, J.-P. Pommereau, R. Stübi, T. Verhoelst, D. Loyola, R. Siddans, R. van der A, C. Clerbaux, A. Laeng, V. Sofieva and M. Weber, Ozone_cci Phase-II Product Validation and Intercomparison Report (PVIR), Issue 2, Revision 0, Ozone_cci_Phase-II_PVIR_2.0, June 2016.
D17	Laeng, A. *(ed.)* and T. von Clarmann, G. Stiller, V. Sofieva, N. Rahpoe, D. Degenstein, K. Walker, D. Murtagh, J.-C. Lambert, T. Verhoelst, C. Lerot, C. Clerbaux, A. Boynard, K.-P. Heue, J. van Peet, R. Siddans, R. Astoreca and J. Hadji-Lazaro, Ozone_cci Phase-II Comprehensive Error Characterization Report (CECR), Version 2, Issue 1, Revision 2, Ozone_cci_KIT_CECR_02_01_02, December 2016.
D18	Dameris, M. (ed.) and P. Braesicke, M. Coldewey-Egbers and M. van Weele, Ozone_cci Phase-II Climate Assessment Report (CAR), CAR_Ozone_CCI-phase-2, March 2017.
D19	Wolfmüller, M. *(ed.)* and W. Som de Cerff, R. van der A, C. Lerot, D. Loyola, G. Miles, P.-F. Coheur, V. Sofieva, A. Laeng, N. Rahpoe, K. Walker, C. Roth and N. Kalb, Ozone_cci Phase-II System Specification Document (SSD), Issue 1, Revision 2, Ozone_cci_DLR_SS_01_02, May 2017.
D20	Wolfmüller, M. *(ed.)* and C. Lerot, D. Loyola, M. Coldewey-Egbers, K.-P. Heue, G. Miles, R. van der A, N. Rahpoe, V.Sofieva, A. Laeng, C. Roth, J. Urban, P.-F. Coheur, R. Astoreca, R. Hargreaves, V. Sofieva and M. Weber, Ozone_cci Phase-II System Verification Report (SVR), Issue 1, Revision 2, Ozone_cci_DLR_SVR_02, May 2017.
D21	van der A, R.J. *(ed.)* and the Ozone_cci science team, Ozone_cci Phase-II Product Specification Document (PSD), Issue 5, Revision 0, Ozone_cci_PSD_5.0, December 2017.
D22	Rahpoe, N., A. Laeng, G. Stiller, M. Weber *(eds)* and R. van der A, C. Adams, P. Bernath, T. von Clarmann, M. Coldewey-Egbers, D. Degenstein, A. Dudhia, R. Hargreaves, C. Lerot, D. Loyola, J. van Peet, V. Sofieva, J. Tamminen, J. Urban, M. Van Roozendael, T. Danckaert, R. Astoreca, K.-P. Heue, P. Sheese, K. Walker and S. Tukiainen, Ozone_cci Phase-II Algorithm Theoretical Basis Document (ATBD), Version 2, Issue 0, Revision 0, Ozone_cci_ATBD_Phase2_V2, December 2017.

D23	E.U. Copernicus Climate Change Service (2022), C3S2_312a_Lot2 Ozone Target Requirements and Gap Analysis Document (TRGAD), Version 5.1, C3S2_312a_Lot2_D-WP3-TRDGAD-v2-2022(O3)_v5.1
D24	E.U. Copernicus Climate Change Service (2023), C3S2_312a_Lot2 Ozone Product User Guide and Specification (PUGS), Version 3.2, C3S2_312a_Lot2_D-WP2-PUGS_202302_O3_v3.2
D25	E.U. Copernicus Climate Change Service (2021), C3S_312b_Lot2 Ozone Product Quality Assurance Document (PQAD), Version 3.0, C3S_D312b_Lot2.2.1.1_202102_PQAD_O3_v2.0
D26	The 2022 GCOS Implementation Plan, GCOS-244, WMO, Geneva, 2022, https://library.wmo.int/doc_num.php?explnum_id=11317
D27	The 2022 GCOS ECVs Requirements, GCOS-245, WMO, Geneva, 2022, https://library.wmo.int/doc_num.php?explnum_id=11318

General definitions

Essential climate variable (ECV)

An ECV is a physical, chemical, or biological variable or a group of linked variables that critically contributes to the characterization of Earth's climate (Bojinski et al., 2014).

Climate data record (CDR)

The US National Research Council (NRC) defines a CDR as a time series of measurements of sufficient length, consistency, and continuity to determine climate variability and change *(National Research Council, 2004)*.

Fundamental climate data record (FCDR)

A fundamental climate data record (FCDR) is a CDR of calibrated and quality-controlled data designed to allow the generation of homogeneous products that are accurate and stable enough for climate monitoring.

Thematic climate data record (TCDR)

A thematic climate data record (TCDR) is a long time series of an essential climate variable (ECV) (Werscheck, 2015).

Intermediate climate data record (ICDR)

An intermediate climate data record (ICDR) is a TCDR which undergoes regular and consistent updates (Werscheck, 2015), for example because it is being generated by a satellite sensor in operation.

Satellite data processing levels

The NASA Earth Observing System (EOS) distinguishes six processing levels of satellite data, ranging from Level 0 (L0) to Level 4 (L4) as follows (Parkinson et al., 2006).

L0	Unprocessed instrument data
L1A	Unprocessed instrument data alongside ancillary information
L1B	Data processed to sensor units (geo-located calibrated spectral radiance and solar irradiance)
L2	Derived geophysical variables (e.g. ozone column) over one orbit
L3	Geophysical variables averaged in time and mapped on a global longitude/latitude horizontal grid
L4	Model output derived by assimilation of observations, or variables derived from multiple measurements (or both)

The C3S ozone data products include the following types of data.

- Level 3 data:
  - Gridded monthly averages covering the globe.
  - Monthly zonal averages over 10° latitude bands (ozone profiles from individual limb instruments and LMZ_MERGED merged dataset).
- Level 4 data:
  - Gridded monthly averaged assimilated ozone total column (TC_MSR).

Acronyms

Acronym	Definition
ACE-FTS	Atmospheric Chemistry Experiment – Fourier Transform Spectrometer
ASDC	Atmospheric Science Data Center
ATBD	Algorithm Theoretical Basis Document
ATSR	Along Track Scanning Radiometer
BIRA-IASB	Belgian royal Institute for Space Aeronomy
C3S	Copernicus Climate Change Service (EU)
CCI	Climate Change Initiative
CDR	Climate Data Record
CF	Climate Forecast (Conventions and Metadata)
CMA	China Meteorological Administration
CNES	Centre National d'Études Spatiales (France)
CNR	Consiglio Nazionale delle Ricerche (Italy)
CNSA	China National Space Administration
CRG	Climate Research Group
CSA	Canadian Space Agency
D-PAF	German processing and archiving facility
DAAC	EOSDIS Distributed Active Archive Centres
DARD	Data Access Requirements Document
DEM	Digital Elevation Model
DHF	Data Host Facility
DIAL	Differential Absorption Lidar
DLR	German Aerospace Centre
DOAS	Differential optical absorption spectroscopy
DoD	Department of Defense (USA)
DU	Dobson unit
ECMWF	European Centre for Medium-Range Weather Forecasts
ECV	Essential Climate Variable
Envisat	Environmental Satellite (ESA)
EO	Earth Observation
EOF	Empirical orthogonal function
EOS	Earth Observing System
EOSDIS	NASA's Earth Observing System Data and Information System
EP	Earth Probe
ERBS	Earth Radiation Budget Satellite
ERS	European Remote-Sensing Satellite
ESA	European Space Agency
ESD	Estimated Standard Deviation
EU	European Union

Acronym	Definition
EUMETSAT	European Organisation for the Exploitation of Meteorological Satellites
FMI	Finnish Meteorological Institute
FOR	Field Of Regard
FORLI	Fast Optimal/Operational Retrieval on Layers for IASI
GAW	Global Atmosphere Watch
GCOS	Global Climate Observation System
GDP	GOME Data Processor
GODFIT	GOME-type direct-fitting retrieval algorithm
GOME	Global Ozone Monitoring Experiment (aboard ERS-2)
GOME-2	Global Ozone Monitoring Experiment – 2 (aboard Metop-A)
GOMOS	Global Ozone Monitoring by Occultation of Stars
GOP	GOME-type Ozone Profile
GTO	GOME-type Total Ozone
HALOE	Halogen Occultation Experiment
HARMOZ	Harmonised Level-2 ozone profiles from limb and occultation sensors
IAA	Instituto de Astrofisica de Andalucia
IAMAP	International Association of Meteorology and Atmospheric Physics
IASI	Infrared Atmospheric Sounding Interferometer
IFAC	Istituto di Fisica Applicata “Nello Carrara”
IO3C	International Ozone Commission
IMK	Institute for Meteorology and Climate Research
IPA	Independent pixel approximation
IR	Infra-Red
IRI	Infra-Red Imager
IUP	Institute of Environmental Physics, University of Bremen
ICDR	Intermediate Climate Data Record
KIT	Karlsruhe Institute of Technology
KMI-IRM	Royal Meteorological Institute of Belgium
KNMI	Royal Netherlands Meteorological Institute
LATMOS	Laboratoire Atmosphères et Observations Spatiales
LS	Low Stratosphere
LTE	Local thermodynamic equilibrium
LUT	Look-up table
Metop	Meteorological Operational Platform (EUMETSAT)
MIPAS	Michelson Interferometer for Passive Atmospheric Sounding
MLER	Minimum Lambertian Equivalent Reflectivity
MLS	Microwave Limb Sounder
MS	Multiple scattering
MSR	Multi-Sensor Reanalysis
MZM	Monthly Zonal Mean
NASA	US National Aeronautics and Space Administration

Acronym	Definition
NDACC	Network for the Detection of Atmospheric Composition Change
NetCDF	Network Common Data Form (data file format)
NKUA	National and Kapodistrian University of Athens
NOAA	US National Oceanic and Atmospheric Administration
NPP	Suomi National Polar-orbiting Partnership (NOAA / NASA / DoD)
NSMC	National Satellite Meteorological Center (China)
O_3	Ozone
OMI	Ozone Monitoring Instrument (aboard EOS-Aura)
OMPS	Ozone Mapping and Profiler Suite
OMPS-LP	OMPS Limb Profiler
OMPS-NM	OMPS Nadir Mapper
OSIRIS	Optical Spectrograph and InfraRed Imaging System (aboard Odin)
PCA	Principal component analysis
POAM-III	Polar Ozone and Aerosol Measurement - III
PPF	Product Processing Facility
PSD	Product Specification Document
PUG	Product User Guide
RAL	Rutherford Appleton Laboratory
RMIB	Royal Meteorological Institute of Belgium
RMS	Root mean square
RT	Radiative transfer
SAA	Solar azimuth angle
SABER	Sounding of the Atmosphere using Broadband Emission Radiometry
SAGE	Stratospheric Aerosol and Gas Experiment
SBUV	Solar Backscatter Ultraviolet Radiometer
SCIAMACHY	Scanning Imaging Absorption Spectrometer for Atmospheric CHartographY (aboard Envisat)
SHADOZ	Southern Hemisphere Additional Ozonesondes programme
SMR	Sub-Millimetre Radiometer (aboard Odin)
SNSB	Swedish National Space Board
SPARC	Stratosphere-troposphere Processes And their Role in Climate
SPARC-DI	SPARC Data Initiative
SPOT-4	Satellite Pour l'Observation de la Terre - 4
SQWG	SCIAMACHY Quality Working Group
SVD	Singular Value Decomposition
SZA	Solar Zenith Angle
TEC	Technical Expertise Centre of CNES
TIMED	Thermosphere Ionosphere Mesosphere Energetics Dynamics
TOA	Top of the atmosphere
TOMS	Total Ozone Mapping Spectrometer
TPM	ESA Third Party Mission

Acronym	Definition
UARS	Upper Atmosphere Research Satellite
UBr	University of Bremen
UiB	Universität Bremen
UNEP	United Nations Environment Programme
UPMC	Université Pierre et Marie Curie
UT	Upper Troposphere
UV	Ultraviolet
UV-Vis	Ultraviolet and visible light
VMR	Volume Mixing Ratio
VZA	Viewing Zenith Angle
WMO	World Meteorological Organization
WOUDC	World Ozone and Ultraviolet Radiation Data Centre

Table of Contents

Scope of the document

This document is the C3S2_312a_Lot2 Ozone Algorithm Theoretical Basis Document (ATBD). Its purpose is to provide a comprehensive description of all the retrieval algorithms implemented in view of generating the C3S2_312a_Lot2 ozone data package delivery. This includes specifications of data characterization, error budgets, quality flags, and auxiliary information provided with the products (e.g. averaging kernels).

Most of the algorithms described here have been developed as part of the ESA Ozone Climate Change Initiative project ([D13] to [D22]). They represent the current state-of-the-art in Europe for satellite-based ozone climate data record production, in line with the “Systematic observation requirements for satellite-based products for climate” as defined by GCOS (Global Climate Observing System) in [D26] and [D27].

Executive summary

The C3S2_312a_Lot2 Ozone Algorithm Theoretical Basis Document contains a full description of the retrieval algorithms needed to produce level-3 (and accompanying level-2) ozone column and profile data sets from a large number of satellite sensors operated in nadir or limb geometries in spectral ranges extending from the UV to the microwave region.

The document is organized in 4 main sections, describing respectively the satellite instruments, the input and ancillary data sets needed for the processing, the retrieval algorithms and associated forward models and finally the generated output variables. We provide a complete description of the level-1 and level-2 data sets that are used as an input for the level-3 products generated in the project. For level-2 products that are processed as part of the C3S service, we provide a complete description of the algorithms used, as well as the input variables and ancillary data needed for the processing. Finally, the output of the different algorithms is documented.

Algorithms and data products are classified in 4 main categories:

- Ozone total column retrieval from UV-nadir sensors

  This includes total column ozone products derived from the GOME, SCIAMACHY, OMI, GOME-2, OMPS and Sentinel 5P sensors, as well as the merged data sets generated from these sensors (GTO-ECV). Also included in this category are the assimilated Multi-Sensor Reanalysis (MSR) data products generated from a complete suite of nadir ozone sensors dating back to the early days of the satellite ozone monitoring.

- Ozone total and tropospheric column retrieval from IASI

  This includes total column and 0-6km tropospheric column data products derived from IASI level-2 profiles. The Metop-A, B and C platforms are concerned.

- Ozone profile retrieval from UV-nadir sensors

  This covers ozone vertical profiles derived from the GOME, SCIAMACHY, OMI and GOME-2 sensors. The algorithm used for the processing optimises the sensitivity of the retrievals in the troposphere. Also included in this category is a merged data set generated from the individual sensors.

- Ozone profile retrieval from limb and occultation sensors

  This last category of data products includes ozone profiles derived at high vertical resolution (typically 2-3 km) from the lower stratosphere up to the mesosphere. The sensors concerned are GOMOS, SCIAMACHY and MIPAS on ENVISAT complemented by Aura MLS, ODIN OSIRIS, SAGE-II, SAGE-III, SABER, ACE, HALOE and OMPS.

Tables

Figures

1 Instruments

Ozone can be measured by a variety of sensors and measurement techniques. In this project, we focus more particularly on ESA and ESA Third Party Mission (ESA-TPM) sensors from which three distinct lines of ozone data products are derived: total ozone, ozone profiles at low vertical resolution from nadir sensors and ozone profiles at high vertical resolution in the stratosphere and Upper Troposphere/ Lower Stratosphere (UT/LS) from limb-type sensors.

1.1 Nadir-type sensors

1.1.1 ERS-2/GOME

The GOME (Global Ozone Monitoring Experiment) instrument is a 4 channel UV/Vis grating spectrometer which observed the earth's atmosphere in nadir viewing geometry. It has a moderate spectral resolution of 0.2 - 0.4 nm and a ground-pixel size of 320 x 40 km^2 (960 x 40 km^2 for the back scan). A detailed description of the instrument is given in Burrows et al. (1999). GOME was launched on ERS-2 into a sun synchronous polar orbit in April 1995, and delivered data until June 2011 when the ERS-2 platform was shut down. However as a result of aging problems of the ERS-2 platform, pointing accuracy is reduced from February 2001. This affects mainly the solar measurements of GOME, decreasing the frequency of good solar irradiance measurements and thereby increasing noise in some products. Further, since June 2003, a permanent failure of the last tape recorder on ERS-2 limits GOME coverage to areas where direct downlink of data was possible. In Ozone_cci, GOME measurements are used to retrieve total columns and vertical distributions of ozone. Because of its proven stability and of its long lifetime (16 years), GOME is generally considered as the European “Gold Standard” for total ozone measurements.

1.1.2 METOP/GOME-2

The first GOME-2 instrument was launched on-board the EUMETSAT satellite Metop-A in October 2006 (Munro et al., 2016). Built on a design almost identical to GOME, it covers the same spectral range as its predecessor but with an improved spatial resolution. The nominal ground-pixel size is 80 x 40 km^2 with a global coverage in almost one day (swath of 1920 km). GOME-2 continues the measurement series started with GOME, and in this project it is therefore used to retrieve total columns and vertical distributions of ozone. Data are available since January 2007 on an operational basis. A second GOME-2 instrument was launched in 2012 on the Metop-B platform, and a third one was launched in November 2018 on Metop-C.

1.1.3 AURA/OMI

The Ozone Monitoring Instrument (OMI) is a nadir viewing imaging spectrograph that measures the solar radiation backscattered by the Earth's atmosphere and surface over the entire wavelength range from 270 to 500 nm with a spectral resolution of about 0.5 nm. OMI was launched on-board the NASA satellite AURA in July 2004. In comparison to the GOME and SCIAMACHY sensors, OMI is

characterized by a larger swath width of 2600 km, which enables measurements with a daily global coverage at all latitudes. The nominal OMI pixel size of 13 × 24 km^2 at nadir is also significantly smaller. The small pixel size enables OMI to look in between the clouds, which is important for retrieving tropospheric information. The light entering the telescope is also depolarised using a scrambler, which avoids polarization-related artefacts. OMI data are available since 2004 and the instrument is still operational, however in 2007 OMI started to experience the so-called row anomaly which reduces the amount of useful measurements, despite correction algorithms being implemented in the level-1 processing chain.

1.1.4 ENVISAT/SCIAMACHY

SCIAMACHY (Scanning Imaging Absorption Spectrometer for Atmospheric CHartographY) is a multi-channel UV-Vis-NIR spectrometer launched on the ENVISAT platform in 2002. Its primary mission objective was the global monitoring of trace gases in the troposphere and in the stratosphere (Bovensmann et al., 1999). The solar radiation transmitted, backscattered and reflected from the atmosphere is recorded at medium resolution (0.2 nm to 1.5 nm) over the range 240 nm to 1700 nm, and in selected regions between 2.0 µm and 2.4 µm. SCIAMACHY is particular since it has three different viewing geometries: nadir, limb, and sun/moon occultation, which yield total column values as well as distribution profiles in the stratosphere and upper troposphere. In this project both nadir and limb measurements are used in Channels 1, 2 and 3. In nadir view, used for ozone total column and vertical profile retrievals, the ground pixel size for channels 2-3 is 30x60 km^2, i.e. a resolution intermediate between GOME and OMI. The swath width of SCIAMACHY at nadir is similar to GOME (960 km), however due to the alternate nadir and limb mode operation, global coverage is only obtained in approximately 6 days. In limb view, ozone number density profiles are derived in the stratosphere by exploiting the Hartley and Chappuis spectral absorption bands in channels 1 and 3. SCIAMACHY data are available from July 2002 till April 2012 when communication with ENVISAT was lost.

1.1.5 Suomi NPP/OMPS-NM

The Ozone Mapping and Profiler Suite, aboard the Suomi-NPP platform launched in 2011, has three different instruments: two nadir modules and the limb module. The Nadir mapper (NM) aims at measuring total ozone columns and relies on 2-D CCD like OMI. With a swath width of 2800 km separated into 36 cross-track footprints, it provides daily global coverage with a spatial resolution of 50 x 50 km^2 in the nominal operations. It records backscattered radiances in the range 300-380 nm with a coarse spectral resolution of about 1.0 nm. More details on the instrument can be found in Seftor et al. (2014).

1.1.6 METOP/IASI

The Infrared Atmospheric Sounding Interferometer (IASI) is a nadir looking Fourier Transform Spectrometer associated with an imaging instrument launched on the Metop series of European meteorological EUMETSAT's polar-orbit satellites. The mission is dedicated to high-resolution atmospheric sounding of trace gases like ozone, methane or carbon monoxide on a global scale and to operational meteorological soundings with a high accuracy requirement (1 K for tropospheric temperature and 10% for humidity with a vertical resolution of 1 km). Three IASI instruments have been successively launched in October 2006, in September 2012 and in November 2018 on Metop-A,

-B and –C respectively. The Metop satellites are sun-synchronous with a 98.7° inclination to the equator, and a global coverage twice daily at about 09:30 and 21:30 local time. Each of the three launched Metop platforms makes a little more than 14 orbits a day. IASI is a cross-track scanner covering the infrared spectral domain from 645 to 2,760 cm^{-1} (3.62–15.5 µm) with a total of 30 ground fields of regard (FOR) per scan. The spectrum is measured in three wavelength bands (8.26–15.5, 5.0–8.26, and 3.62–5.0 µm), with a separate detector allowing the continuous spectral coverage with no gaps, and each FOR measures a 2×2 array of footprints characterized by a 12-km diameter at nadir. The apodized spectral resolution is 0.5 cm^{-1} and each spectrum is sampled every 0.25 cm^{-1} providing a total of 8461 radiance channels.

1.1.7 BUV

The Backscatter UltraViolet experiment (BUV) on-board the Nimbus 4 satellite was the first satellite measuring ozone. It operated from April 1970 till May 1977 but with several big gaps in time without observations. The instrument measured the earth spectrum in several small bands between 252 and 340 nm. From this the total ozone and an ozone profile is derived.

1.1.8 SBUV

The Solar Backscatter Ultraviolet Radiometer, or SBUV, is a series of operational instruments on NOAA weather satellites in Sun-synchronous orbits. This instrument has flown on the Nimbus-7, NOAA-9, NOAA-11, NOAA-14, NOAA-16, NOAA-17, NOAA-18, and NOAA-19 in the period from November 1978 to Dec 2011. The instrument is very similar to its predecessor BUV.

1.1.9 TOMS

The Total Ozone Mapping Spectrometer (TOMS) is a NASA satellite instrument for measuring ozone values. Of the four TOMS instruments which were successfully launched only two are used because of the length of time period of observations: TOMS on Nimbus-7 and on EarthProbe. This covers the time periods from November 1978 to May 1993 and July 1996 to December 2002. Besides ozone a few other gases can be derived from TOMS observations.

1.1.10 Sentinel-5 Precursor/TROPOMI

The TROPOMI instrument is a space-borne, nadir-viewing, imaging spectrometer covering wavelength bands between the ultraviolet and the shortwave infrared. It is the single payload of Sentinel-5 Precursor, the first Copernicus mission dedicated to the monitoring of atmospheric composition. Launched on 13 October 2017 for a mission of minimum seven years, it operates in a push-broom configuration (non-scanning), with a swath width of ~2600 km on the Earth's surface. The TROPOMI instrument is similar in concept to OMI, but it offers a much-improved spatial resolution of about 5.5x3.5 km^2 at nadir, with similar or better radiometric performance than OMI. Covering the ultraviolet (UV), visible (VIS), near (NIR) and short-wavelength infrared (SWIR), it provides daily global measurements of a number of gases in the atmosphere, including ozone, methane (CH_4), HCHO, NO_2, SO_2, aerosol and carbon monoxide (CO).

1.2 Limb and occultation type sensors

1.2.1 ENVISAT/MIPAS

MIPAS (Michelson Interferometer for Passive Atmospheric Sounding) is an infrared limb emission sounder on ENVISAT, designed and operated for measurements of constituents between the upper troposphere and the mesosphere. MIPAS is a rear looking instrument with the lines of sight approximately in the orbit plane. In the original measurement mode, which was operational from July 2002 to March 2004, 17 tangent altitudes between 6 and 68 km were measured per limb scan at a spectral resolution of 0.035 cm^{-1} (unapodized). However from January 2005, due to a mirror failure, MIPAS operated in reduced spectral resolution mode (0.0625 cm^{-1}). MIPAS measured ozone vertical profiles day and night on the altitude range from 6 to 70 km, pole-to-pole. Data are available for July 2002-March 2004 and January 2005 until April 2012 when communication with ENVISAT was lost. Global coverage was obtained in approximately 3 days.

1.2.2 ENVISAT/GOMOS

GOMOS (Global Ozone Monitoring by Occultation of Stars) is a medium resolution spectrometer covering the wavelength range from 250 nm to 950 nm. It measures attenuation of stellar light in occultation geometry. From dark-limb occultations in the UV-Visible and IR spectral ranges, the vertical profiles of ozone are retrieved in the altitude region from 15 to 100 km. In comparison to other limb-type sensors on ENVISAT, GOMOS features a high vertical resolution of the retrieved ozone profiles: 2 km below 30 km, 3 km above 40 km, with a linear growth from 2 km to 3 km in the altitude range 30-40 km. However the quality of the retrieved profiles can depend on the type of star used as a source. Careful selection and error characterization are necessary to make best use of the data products. GOMOS data are available from 2002 till 2012. Summer poles are not covered, due to the absence of night-time conditions. Data from May-June 2003, January-July 2005 and February-November 2009 are not available due to the instrument technical anomalies.

1.2.3 ENVISAT/SCIAMACHY

See Section 1.1.4.

1.2.4 ODIN/OSIRIS

OSIRIS (Optical Spectrograph and InfraRed Imaging System) is a Canadian instrument on board the Swedish satellite Odin that was launched in February of 2001. It is a limb-viewing device that makes repeated measurements of the limb scattered radiance with a sampling of approximately 2 km between 10 km and 100 km of altitude. OSIRIS uses limb radiance spectra to generate ozone profiles in a range from 80° S to 80° N. Concentrations are retrieved on a 1 km grid from 10.5 km to 59.5 km and have the vertical resolution ~2 km. The ozone retrieval by University of Saskatchewan using a multiplicative algebraic reconstruction technique is described in (Degenstein et al., 2009). The OSIRIS instrument is still operational.

1.2.5 ODIN/SMR

The Sub-Millimetre Radiometer (SMR) on-board the Odin satellite, was launched in February 2001. Measurements of thermal emission lines are performed during day and night and global coverage is achieved during one observation day. Vertical profiles of ozone and many other species are retrieved

using retrieval algorithms based on the Optimal Estimation Method. The official operational level-2 data are produced by the Chalmers University of Technology in Göteborg, Sweden. In this project, we use the currently recommended version 2.1 ozone data product that provides stratospheric ozone data in the ~12-50km range with 2.5-3.5km vertical resolution and single-profile precision of about 20%. The Odin data set is available from November 2001 until present. The validation activity performed in the framework of the Ozone_cci project identified corrupted data after 2010. The reprocessing of the whole SMR mission is ongoing.

1.2.6 SCISAT/ACE-FTS

ACE-FTS is on-board the Canadian satellite SCISAT launched in August 2003, and data is available from Feb. 2004 to present. It provides latitudinal coverage from about 85°N to 85°S with complete coverage every 3 months. The ACE-FTS is a high-resolution (0.02 cm^{-1}) Fourier transform spectrometer measuring from 2.2 to 13 µm (750 – 4400 cm^{-1}). Operating in solar occultation mode, the ACE-FTS provides detailed profiles of the Earth's atmosphere for more than 30 chemical species. The altitude range of the retrieved ozone profiles is from cloud tops (~5 km) to 95 km and the vertical resolution is ~3-4 km (based on the field-of-view of the ACE-FTS instrument).

1.2.7 ERBS/SAGE2

The SAGE II (Stratospheric Aerosol and Gas Experiment) operated in 1984-2005 on board the Earth Radiation Budget Satellite (ERBS) into a 57° inclination. It exploits the atmospheric species by using the solar occultation technique at sunrise and sunset geometries by measuring the attenuated sun light. The wavelengths used are ranging from 385 to 1200 nm in 7 channels. The 'onion-peeling' method (Chu et al., 1989) is used in order to invert the measured spectrum into aerosol extinction, ozone, nitrogen dioxide, and water vapour with a vertical resolution of 1 km. In this work, the version V7 of SAGE II is used (Damadeo et al., 2013). Ozone is inferred from spectral measurements near 600 nm, at the peak of the Chappuis band. SAGE II provides high-quality ozone profiles with a random uncertainty < 1% in the stratosphere.

1.2.8 ISS/SAGE-III

SAGE III on ISS is the fourth generation of a series of NASA Earth-observing instruments, known as the Stratospheric Aerosol and Gas Experiment (SAGE). The first SAGE III instrument was launched on a Russian Meteor-3M satellite. The recently revised SAGE III was mounted to the International Space Station where it uses the unique vantage point of ISS to make long-term measurements of ozone, aerosols, water vapour, and other gases in Earth's atmosphere.

1.2.9 UARS/HALOE

Halogen Occultation Experiment (HALOE) on board the Upper Atmosphere Research Satellite (UARS) operated in 1991-2005 and provided profiles of middle atmosphere composition, temperature and aerosol extinction. HALOE is a solar occultation instrument which used thermal infrared bands (Russel III et al., 1993). About 30 measurements daily split between sunrise and sunset were performed daily, and near global coverage achieved within about one and a half month. The ozone concentrations retrieved have vertical resolution of 1.6 km in the altitude range 15 -90 km.

1.2.10 TIMED/SABER

The Sounding of the Atmosphere using Broadband Emission Radiometry (SABER) instrument is one of four instruments on NASA's TIMED (Thermosphere Ionosphere Mesosphere Energetics Dynamics) satellite. The primary goal of the SABER experiment is to provide the data needed to advance our understanding of the fundamental processes governing the energetics, chemistry, dynamics, and transport in the mesosphere and lower thermosphere. SABER accomplishes this with global measurements of the atmosphere using a 10-channel broadband limb-scanning infrared radiometer covering the spectral range from 1.27 µm to 17 µm. These measurements are used to provide vertical profiles of kinetic temperature, pressure, geopotential height, volume mixing ratios for the trace species O_3, CO_2, H_2O, [O], and [H], volume emission rates for 5.3 µm NO, 2.1 µm OH, 1.6 µm OH, and 1.27 µm O2 (1Δ), cooling and heating rates for many CO_2, O_3, and O_2 bands, and chemical heating rates for 7 important reactions. This study uses the SABER V2.0 ozone profiles.

1.2.11 AURA/MLS

MLS (Microwave Limb Sounder) is one of the instruments on board the Aura satellite. It was launched in 2004. It collects data with 13 orbits per day and is flying at 705 km altitude on a near polar orbit. It measures the thermal microwave emission from Earth's atmosphere and retrieves different species along with pressure, cloud ice density, and temperature (Waters et al. 2006; Livesey, Snyder and Wagner 2006). MLS measures continuously the thermal emission from broad band spectra at 118, 190, 240, 640, and 2500 GHz using limb viewing geometry. The vertical resolution is 2.5 km in the stratosphere and degrades to 4 - 6 km in the mesosphere and to 3 km at 316 hPa. Supplementary information regarding screening flags, the quality of fitted spectra, and retrieval status are included along with the Level 2 data sets (Froidevaux et al., 2008). The retrieved MLS ozone profiles V 4.2 are used in this study.

1.2.12 SUOMI NPP/OMPS-LP

The Ozone Mapping and Profiler Suite Limb Profiler (OMPS-LP) on board the Suomi-NPP satellite has been taking measurements of limb-scattered sunlight from early 2012 to present (Flynn et al., 2006). OMPS-LP images the atmosphere using three vertical slits, one aligned with the orbital plane and the others separated by 250 km at the tangent point on either side of the orbital track. Imaging allows OMPS-LP to obtain along track and vertical sampling of approximately 125 km and 1 km respectively. Spectral information in the range 270—1000 nm is obtained employing a prism spectrometer.

For our analyses, two OMPS-LP ozone data products are used, one processed in the University of Saskatchewan (USask 2D v1.1.0, Zawada et al., 2017) and the second in the University of Bremen (UBr v3.3, Arosio et al., 2018).

1.2.12.1 USask 2D product

The USask 2D retrieval accounts for atmospheric variations along the orbital track by using the SASKTRAN-HR forward model (Zawada et al., 2015) and simultaneously retrieving the ozone field for an entire orbit, rather than processing each vertical image separately. Only data from the centre slit of OMPS is used as the other two slits are not aligned with the orbital track. Profiles are retrieved with a vertical resolution of 1–2 km and an along track resolution of 300–400 km. Individual profiles

have a mean uncertainty of 4–6% for most of the upper and middle stratosphere, with values increasing to approximately 30% just below the tropopause.

1.2.12.2 UBr product

The UBr retrieval uses the radiative transfer model SCIATRAN along with a Tikhonov regularization approach to constrain the profile. Four spectral segments are selected: three in the UV region and one in the Chappuis band. The altitude range over which the retrieval is performed spans between 8 and 60 km above the sea level. Limb radiance in each spectral interval is first normalized with respect to a limb measurement at an upper TH. Simultaneously with the ozone retrieval, surface reflectance estimation is performed exploiting the sun normalized radiance. Beforehand, a cloud filter is applied and the retrieval of aerosol extinction profiles is performed. In addition, a retrieval of polar mesospheric cloud (PMC) properties is implemented and this information is used in the ozone retrieval in the presence of a PMC. This improves the coverage of the data set in Polar Regions during local summer. For a detailed description of the retrieval scheme, see Arosio et al., 2018. The typical vertical resolution of the retrieved profiles is about 2–3 km, with worse values in the 30–35 km range, below 20 km in the tropics and above 50 km at all latitudes. A thorough uncertainty analysis was performed and presented in Arosio et al. (2022). The typical retrieval noise spans 2–3 % between 15 and 50 km. The total random uncertainty is estimated in the range 3–5 % in the middle stratosphere increasing in the UTLS. The total systematic uncertainty is mainly related to cloud contamination and model errors in the lower stratosphere and to the retrieval bias at high altitudes, with total absolute values of about 5 % above 50 km and below 20 km.

1.2.13 SPOT-4/POAM-III

POAM-III was a solar occultation instrument on the SPOT satellite, which operated from 1998 to 2005. It flew in a sun-synchronous polar orbit, performing solar occultation observations in nine band channels, covering the spectral range from 354 to 1018 nm. Successive measurements cover a fairly constant latitude band (55–71° N for sunrise and 63–88° S for sunset).

The altitude range for the retrieved profiles spans the 5–60 km range, with a vertical resolution of 1 km in the stratosphere and 2–5 km in the upper troposphere. Typical retrieval errors are reported to be within 5% in the stratosphere and increasing up to 15–30 % in the troposphere. Aerosol extinction and sunspots are known to affect the retrievals from POAM observations, mainly in the 20–40 km altitude range. However, according to (Lumpe et al., 2002), less than 10% of the ozone profiles are reported to suffer from sunspot-related artefacts, which results in random errors of more than about 10% in the stratosphere.

The POAM-III ozone product was validated against SAGE II, HALOE, and balloon-borne observations as described in (Lumpe et al., 2002) and (Randall et al., 2003). Results showed agreement within 5% in the 13–50 km range, whereas a 15–20% high bias was found at lower altitudes.

2 Input and auxiliary data

This section lists the satellite data sets used as an input for the retrieval algorithms described in this ATBD.

2.1 Overview

Table 1 gives an overview of the satellite data needed for the generation of the C3S Ozone ECV Data products.

Table 1. Overview of satellite data required to generate the C3S ozone ECV products.

Agency	Satellite	Sensor	Period	Product	Version	Subset or complete needed	Volume	Available from	Comments
CSA	Scisat	ACE-FTS	2004-2016	Level 2	v4.1/4.2	Complete	1 GB	ESA	On ftp server and available on Ozone_cci server
ESA	ERS-2	GOME	1995-2011	Level 1b	V4	Complete	1 TB	ESA	On D-PAF ftp server
ESA	Envisat	SCIAMACHY	2002-2012	Level 1b	V8.01	Complete	16 TB	ESA	Current version v8 available now from ftp server
ESA	Envisat	SCIAMACHY	2002-2012	Level 2	V3.5	Complete	6.6 Gb	UBr	
ESA	Envisat	SCIAMACHY	2002-2012	Level 2	V5.04			ESA	
ESA	Envisat	GOMOS	2002-2012	Level 2	ALGOM2s	Complete	400 MB	ESA & FMI	On ESA/ALGOM and Ozone_cci ftp server
ESA	Envisat	MIPAS	2002-2012	Level 2	V8	Complete	6 GB	KIT/IMK	On ftp server
ESA	Sentinel-5P	TROPOMI	2018-2022	Level 2	V2	Complete	6.4 TB	Copernicus	
EUMETSAT	Metop-A	GOME-2	2007-2021	Level 1b	V4	Complete	70 TB	EUMETSAT	On media and on ftp server
EUMETSAT	Metop-B	GOME-2	2013-2022	Level 1b	V4	Complete	50 TB	EUMETSAT	On media and on ftp server
EUMETSAT	Metop-C	GOME-2	2018-2022	Level 1b	V4	Complete	20 TB	EUMETSAT	On media and on ftp server
EUMETSAT	Metop-A	IASI	2007-2021	Level 2	V1	Complete	12 TB	AERIS	On AERIS and Ozone_cci server
EUMETSAT	Metop-B	IASI	2013-2022	Level 2	V1	Complete	8 TB	AERIS	On AERIS and Ozone_cci server
EUMETSAT	Metop-C	IASI	2018-2022	Level 2	V1	Complete	3 TB	AERIS	On AERIS and Ozone_cci server

Agency	Satellite	Sensor	Period	Product	Version	Subset or complete needed	Volume	Available from	Comments
NASA	Nimbus4	BUV	1970-1977	Level 2	V8.6	Complete	3 GB	NOAA/NASA	On ftp server
NASA	Nimbus7 / Earthprobe	TOMS	1978-2002	Level 2	V8	Complete	300 GB	NASA	On ftp server
NASA	Nimbus-7/ NOAA-9-19	SBUV	1978-2011	Level 2	V8.6	Complete	100 GB	NOAA/NASA	On ftp server
NASA	ERBS	SAGE-2	1984-2005	Level 2	V7	Complete	330 Mb	NASA	
NASA	ISS	SAGE-III	2018-2022	Level-2	V5.2	Complete		NASA	
CNES	SPOT-4	POAM-III	1998-2005	Level-2	V4	Complete		NASA	
NASA	UARS	HALOE	1991-2005	Level 2	V19	Complete	210 Mb	NASA	
NASA	TIMED	SABER	2002-	Level 2	V2.0	Complete	18 Gb	NASA	
NASA	AURA	OMI	2004-2022	Level 1b	V3	Complete	30 TB	NASA	On ftp server
NASA	AURA	OMI	2004-2022	OMITO3 Level 2	V3	Complete	2.7 TB	NASA	On ftp server
NASA	AURA	OMI	2004-2022	OMIDOAO3 Level 2	V3	Complete	2.7 TB	NASA	On ftp server
NASA	AURA	MLS	2004-2022	Level 2	V5	Complete	46 Gb	NASA	
NASA	Suomi-NPP	OMPS-NM	2012-2022	Level1b	V2.0	Complete	7.5 TB	NASA	On ftp server
NASA	Suomi-NPP	OMPS-LP	2012-2021	Level 2	V1.1.0	Complete	22 GB	USask & UBr	On ftp server (Univ. Saskatchewan) and Ozone_cci server
SNSB CSA -TPM	ODIN	SMR	2001-2016	Level 2	V2.1	Complete	15 GB	ESA / Chalmers	On ftp server (Univ. Chalmers) and Ozone_cci server
SNSB CSA -TPM	ODIN	OSIRIS	2001-2022	Level 2	V7.2	Complete	21 TB	ESA	On ftp server (Univ. Saskatchewan) and Ozone_cci server

2.2 Level-1 data

Level-1 data are required from the following sensors to generate total column and vertical ozone profiles. They serve as input for the level-2 retrieval algorithms that are applied in the project for the generation of the nadir ozone ECV data products. Input data and wavelength channels are described in the following tables:

- ERS-2/GOME (Table 2). The wavelength range and spectral resolution of the four GOME channels are provided in Table 3
- Envisat / SCIAMACHY (Table 4). The wavelength range and spectral resolution of the eight SCIAMACHY channels are provided in Table 5
- Metop-A, Metop-B and Metop-C/ GOME-2 (Table 6)
- EOS-AURA/OMI (Table 7)
- Suomi-NPP /OMPS-NM (Table 8)

Table 2. ERS-2/GOME L-1b data required as input to the C3S Ozone data processing.

Originating system	GOME flew on-board the ESA satellite ERS-2, which was launched in April 1995 and operated until September 2011. The GOME level-1b data products were generated from the ESA level 0 product at DLR.
Data class	Earth Observation Data
Sensor type and key technical characteristics	The GOME (Global Ozone Monitoring Experiment) instrument is a 4 channel UV/Vis grating spectrometer observing the earth's atmosphere in nadir viewing geometry. It has a moderate spectral resolution of 0.2 - 0.4 nm and a ground-pixel size of 320 x 40 km^2 (960 x 40 km^2 for the back scan). GOME was launched on ERS-2 into a sun synchronous polar orbit in April 1995, and delivered data until September 2011. In this project GOME measurements in Channels 1 and 2 will be used to retrieve total and vertical distribution of ozone.
Data availability & coverage	GOME data are available from April 1995 until September 2011 when the instrument was switched off. However, because of aging problems of the ERS-2 platform, pointing accuracy has been reduced since February 2001. This affects mainly the solar measurements of GOME, decreasing the frequency of good solar irradiance measurements and thereby increasing noise in some products. Further, since June 2003, a permanent failure of the last tape recorder on ERS-2 has limited GOME coverage to areas where direct downlink of data was possible. With the nominal swath of 960 km, global coverage was achieved every three days at the equator and earlier at higher latitudes.
Source data product name and reference to product technical specification documents	ERS-2 GOME level 1b data [D3].
Data quantity	Approximately 70 Gb/year (until 2003). Total volume is about 1 TB.

Data quality and reliability	The data quality is monitored as part of the operational off-line ground segment of GOME at DLR[1]. For details about the quality of the GOME level-1 products we refer to the GOME Product Information.
Ordering and delivery mechanism	These ESA standard GOME products are generated at DLR on behalf of ESA and are freely available. After registering at ESA EO help and Order Desk, level 1 data can be copied free-of-charge from a FTP Server.
Access conditions & pricing	The team has default access to the GOME Level-1 data. The GOME level-1 products are free of charge.
Issues	GOME level 1 version 5 using the latest calibration corrections valid for the complete GOME mission are needed. Note that the current GOME level 1 version 4 products only contain a subset of the data acquired after the ERS-2 recorder problem in 2003. A revised version is under development and will be available for processing of CCI Phase-2 products.

Table 3. Wavelength range and spectral resolution of the four GOME channels.

Channel	Wavelength range (nm)	Spectral resolution (nm)
1A	237-283	0.20
1B	283-316	0.20
2	311-405	0.17
3	405-611	0.29
4	595-793	0.33

Table 4. Envisat/SCIAMACHY L-1b data required as input to the C3S Ozone data processing.

Originating system	SCIAMACHY operated on-board the ESA satellite ENVISAT from March 2002 until April 2012. The SCIAMACHY level-1b data product is generated from the level 0 product by ESA and DLR.
Data class	Earth Observation Data
Sensor type and key technical characteristics	SCIAMACHY (Scanning Imaging Absorption Spectrometer for Atmospheric CHartographY) is an imaging spectrometer whose primary mission objective was the global monitoring of trace gases in the troposphere and in the stratosphere. The solar radiation transmitted, backscattered and reflected from the atmosphere is recorded at medium resolution (0.2 nm to 1.5 nm) over the range 240 nm to 1700 nm, and in selected regions between 2.0 µm and 2.4 µm. SCIAMACHY has three different viewing geometries: nadir, limb, and sun/moon occultation, which yield total column values as well as distribution profiles in the stratosphere and upper troposphere. In this project both nadir and limb measurements will be used in Channels 1 to 3. The ground pixel size for channels 2-3 is 30x60 km^2 (nadir view).

[1] All weblinks last accessed on 22/04/2024.

Data availability & coverage	SCIAMACHY data are available since 2002 and the instrument operation ended by April 2012, when the communication with ENVISAT was lost. Global coverage is obtained in approximately 6 days.
Source data product name and reference to product technical specification documents	SCIAMACHY level 1b data [D8].
Data quantity	1.95 TB / year. Total volume is about 20 TB.
Data quality and reliability	The data quality was monitored by ESA and results were reported in SCIAMACHY bimonthly report documents that described the status and changes to the SCIAMACHY instrument, its data processing chain and its data products. It was the result of input received from the different groups working on SCIAMACHY operation, calibration, product validation, and data quality. The groups contributing to the report were SOST-DLR and SOST-IFE, ESA-ESRIN PCF, ESA-ESTEC PLSO and DLR-IMF. The geophysical quality monitoring was under responsibility of the SQWG and the SCIAVALIG groups. Other monitoring services are summarized here.
Ordering and delivery mechanism	SCIAMACHY level-1 data are available from ESA and are free of charge for the team.
Access conditions & pricing	The team has default access to the SCIAMACHY Level-1 data. The SCIAMACHY level-1 products are free of charge.
Issues	The SCIAMACHY level-1 version 8 (or higher) data set including the most advanced degradation corrections is required.

Table 5. Wavelength range and spectral resolution of the eight SCIAMACHY channels.

Channel	Wavelength range (nm)	Resolution (nm)
1	240(214) – 314	0.24
2	309 – 405	0.26
3	394 – 620	0.44
4	604 – 805	0.48
5	785 – 1050	0.54
6	1000 – 1750	1.48
7	1940 – 2040	0.22
8	2265 – 2380	0.26

Table 6. Metop/GOME-2 L-1b data required as input to the C3S Ozone data processing.

Originating system	GOME-2 is on-board the EUMETSAT satellite Metop-A which was launched in October 2006. A second GOME-2 instrument was launched in September 2012 on the Metop-B platform and a third one on Metop-C in November 2018. The GOME-2 level-1b data product is generated from the level 0 product by EUMETSAT. Metop-C data are not included in the C3S ozone products.
Data class	Earth Observation Data

Sensor type and key technical characteristics	The GOME-2 instrument covers the same spectral range as GOME with an improved spatial resolution. When operated in full swath, the nominal ground-pixel size is 80 x 40 km^2 with a global coverage in almost one day (swath of 1920 km). After the launch of Metop-B, it has been decided to operate the two instruments in tandem, GOME-2B in full-swath mode and GOME-2A in reduced swath (960 km) mode. In this configuration, the nominal ground-pixel size of GOME-2A is 40 x 40 km^2. When combining the two instruments, full earth coverage is obtained in one day. In this project GOME-2 measurements in Channels 1 and 2 are used to retrieve total and vertical distribution of ozone.
Data availability & coverage	GOME-2A data are available since January 2007 on an operational basis. Likewise GOME-2B data are operationally available since July 2013. Global coverage is obtained in around 1.5 days (in 1 day when GOME-2A and GOME2-B are combined) at the equator and daily on higher latitudes.
Source data product name and reference to product technical specification documents	GOME-2 level 1b data [D5].
Data quantity	4 TB/ year/ instrument.
Data quality and reliability	The data quality is monitored by EUMETSAT and results are reported in Newsletters. All GOME-2 instruments suffer from time-dependent degradation especially in the UV region.
Ordering and delivery mechanism	GOME-2 level-1 data are available from EUMETSAT and are free of charge for the team.
Access conditions & pricing	The team has default access to the GOME-2 A/B/C Level-1 data. The GOME-2 level-1 products are free of charge.
Issues	The GOME-2 level-1b version 5 data set is required.

Table 7. Aura/OMI L-1b data required as input to the C3S Ozone data processing.

Originating system	OMI is on-board the NASA satellite AURA which was launched in July 2004. The OMI level-1b data product is generated from the KNMI/NASA level 0 product at NASA.
Data class	Earth Observation Data
Sensor type and key technical characteristics	The OMI instrument is a nadir viewing imaging spectrograph that measures the solar radiation backscattered by the Earth's atmosphere and surface over the entire wavelength range from 270 to 500 nm with a spectral resolution of about 0.5 nm. The 114° viewing angle of the telescope corresponds to a 2600 km wide swath on the surface, which enables measurements with a daily global coverage. The light entering the telescope is depolarised using a scrambler and then split into two channels: the UV channel (wavelength range 270 - 380 nm) and the VIS channel (wavelength range 350 - 500 nm). In the normal global operation mode, the OMI pixel size is 13 km× 24 km at nadir (along x across track). In the zoom mode the spatial resolution can be reduced to 13 km × 12 km. The small pixel size enables OMI to look in between the clouds, which is very important for retrieving tropospheric information.

Data availability & coverage	OMI data are available since 2004 and the instrument is still operational. OMI has a daily global coverage except when operated in zoom-in mode. In 2007 OMI started to experience the so-called row anomaly. Two rows seemed to be (partially) blocked. This row anomaly was followed by other row anomalies in 2008, 2009 and 2011. Like the first row anomaly a few rows seemed to be (partially) blocked. But these rows also suffered from reflected sunlight during part of the orbit and earthshine from another scene. These new row anomalies are changing through time. Currently, progress has been made with a correction algorithm for these rows.
Source data product name and reference to product technical specification documents	Version 003 OMI Level 1B Products [D6]. Orbital Swath Pixels (UV1, 13x48 km^2; UV2 & VIS, 13x24 km^2; Zoom, 13x12 km^2).
Data quantity	Approximately 1 TB/year.
Data quality and reliability	The quality flags "PixelQualityFlags", "GroundPixelQualityFlags", "XTrackQualityFlags", and"MeasurementQualityFlags" are available in the data for all possible errors/warning [D6].
Ordering and delivery mechanism	The data is available via the browsable web-interface Mirador of NASA.
Access conditions & pricing	The OMI level-1 products are free of charge.
Issues	None.

Table 8. Suomi-NPP/OMPS-NM L-1b data required as input to the C3S Ozone data processing.

Originating system	OMPS-NM is on-board the NASA satellite Suomi-NPP which was launched in end of 2011. The level-1b data product v2.0 is generated from the NASA level 0 product at NASA.
Data class	Earth Observation Data
Sensor type and key technical characteristics	The Ozone Mapping and Profiler Suite, aboard the Suomi-NPP platform launched in 2011, has three different instruments: two nadir modules and the limb module. The Nadir mapper (NM) aims at measuring total ozone columns and relies on 2-D CCD like OMI. With a swath width of 2800 km separated into 36 cross-track footprints, it provides daily global coverage with a spatial resolution of 50 x 50 km^2 in the nominal operations. It records backscattered radiances in the range 300-380 nm with a coarse spectral resolution of about 1.0 nm. More details on the instrument can be found in Seftor et al. (2014).
Data availability & coverage	OMPS data are available since 2012 and the instrument is still operational. OMPS has a daily global coverage except when operated in zoom-in mode.
Source data product name and reference to product technical specification documents	Version 2.0 OMPS Level 1B Products.
Data quantity	Approximately 0.5 TB/year.
Data quality and reliability	Data quality monitoring is under the responsibility of NASA.
Ordering and delivery mechanism	The data is available via the browsable web-interface NASA

Access conditions & pricing	The OMPS level-1 products are free of charge and accessible from here.
Issues	None.

2.3 Level-2 data

This section is dedicated to Level-2 data that serve as input to C3S ozone data processing chains and that are not produced within the C3S Ozone project.

2.3.1 Ozone total column data required by the multi-sensor reanalysis (MSR)

The latest total ozone retrievals of 21 satellite instruments are used: BUV-Nimbus4, TOMS-Nimbus7, TOMS-EP, SBUV-7, -9, -11, -14, -16, -17, -18, -19, GOME, SCIAMACHY, OMI, GOME-2A, -2B, -2C, TROPOMI, FY-3A, FY-3B and OMPS (detailed in Table 9). However, the quality of the FY-3A and FY-3B was found insufficient to be included in the MSR processing.

Table 9. The satellite datasets used in the MSR. The columns show (1) the name of the dataset, (2) the satellite instrument, (3) the satellite, (4 and 5) the time period.

Data set	Instrument	Satellite	From	To
BUV	BUV	Nimbus-4	1 April 1970	6 May 1977
TOMS-N7	TOMS	Nimbus-7	31 Oct. 1978	6 May 1993
TOMS-EP	TOMS	Earth probe	25 July 1996	31 Dec. 2002
SBUVN07	SBUV	Nimbus-7	31 Oct. 1978	21 June 1990
SBUVN09	SBUV/2	NOAA-9	2 Feb. 1985	19 Feb. 1998
SBUVN11	SBUV/2	NOAA-11	1 Dec. 1988	27 Mar. 2001
SBUVN14	SBUV/2	NOAA-14	5 Feb. 1995	28 Sep.2006
SBUVN16	SBUV/2	NOAA-16	3 Oct. 2000	31 Dec. 2003
SBUVN17	SBUV/2	NOAA-17	11 July 2002	31 Dec. 2011
SBUVN18	SBUV/2	NOAA-18	5 June 2005	31 Dec. 2011
SBUVN19	SBUV/2	NOAA-19	23 Feb. 2009	31 Dec. 2011
GDP5	GOME-1	ERS-2	27 June 1995	3 July 2011
TOGOMI2	GOME-1	ERS-2	27 June 1995	3 July 2011
SGP5	SCIAMACHY	Envisat	2 Aug. 2002	8 Apr. 2012
TOSOMI2	SCIAMACHY	Envisat	2 Aug. 2002	8 Apr. 2012
OMDOAO3	OMI	Aura	1 Oct. 2004	Now
OMTO3	OMI	Aura	1 Oct. 2004	Now
GOME2A	GOME-2	Metop-A	4 Jan. 2007	1 Nov. 2021
GOME2B	GOME-2	Metop-B	1 Nov. 2012	Now
GOME2C	GOME-2	Metop-C	1 Jul. 2019	Now
OMPS	OMPS	Suomi-NPP	7 Nov. 2011	Now
TROPOMI	TROPOMI	Sentinel-5P	30 Apr. 2018	Now

2.3.2 Ozone column data from TROPOMI Sentinel-5 Precursor

TROPOMI ozone column data (OFFL product) are operationally processed using the GODFIT-v4 algorithm, also used for the processing of other nadir ozone ECV data products (see section 3.1).

Table 10. Sentinel-5P/TROPOMI L-2 data required as input to the generation of L3 total ozone products

Originating system	TROPOMI is the single sensor on board of the Copernicus Sentinel-5 Precursor mission which was launched in October 2017. The TROPOMI total ozone level-2 data are generated using a DOAS approach for the NRT product, while the OFFL product is based on the GODFIT-v4 direct-fitting algorithm developed within the ESA CCI programme. For the nadir ozone ECV TROPOMI product, we used the OFFL product V02.
Data class	Earth Observation Data
Sensor type and key technical characteristics	see Section 1.1.10
Data availability & coverage	S5P/TROPOMI data are available from April 30 2018 until present.
Data quantity	Approximately 1.6 TB/ year.
Data quality and reliability	Independent validation by Mission Performance Centre (MPC) Cal/Val experts and the Sentinel-5 Precursor Validation Team (S5PVT) conclude that the OFFL ozone data is in good overall agreement reference measurements collected from global ground-based reference networks. The global bias with respect to the ground-based measurements is found to be below 1%, which is well within the mission requirements of maximum 5%. The biases at individual stations also satisfy this requirement. The scatter of the differences around this bias also complies with mission requirements of ±2.5%.
Ordering and delivery mechanism	The data are available on the Copernicus S5p Open Access Hub.

2.3.3 Ozone column data from IASI

The IASI/Metop-A and IASI/Metop-B Level 2 data required for creation of the gridded nadir ozone column data set are described in Table 11.

Table 11. Metop/IASI L-2 data required as input to the generation of C3S ozone products.

Originating system	IASI is on-board the EUMETSAT satellite Metop-A which was launched in October 2006. A second IASI instrument was launched in September 2012 on the Metop-B platform. The IASI level-2 data products are generated by applying the FORLI v20151001 radiative transfer model and retrieval algorithm to level 1C radiances to retrieve the ozone nadir vertical profile.
Data class	Earth Observation Data
Sensor type and key technical characteristics	see Section 1.1.6
Data availability & coverage	IASI/Metop-A data are available from October 2007 until November 2021. IASI/Metop-B data are available from March 2013 until present. IASI/Metop-C data are available from October 2019 until present.
Data quantity	Approximately 1 Gb / year.
Data quality and reliability	Total ozone: positive bias of 1-2% compared to UV observations Tropospheric ozone: negative bias of ~10% compared to ozone sondes Boynard et al. (2016, 2018)

Ordering and delivery mechanism	The data are available from the AERIS website.

2.3.4 Limb and occultation ozone profile data

The following Level 2 data are required for creation of Level 3 data and the merged limb ozone profile data set.

- Envisat / GOMOS (Table 12)
- Envisat / MIPAS (Table 13)
- Envisat / SCIAMACHY (Table 14)
- Odin / OSIRIS (Table 15)
- Odin / SMR
- SciSat / ACE-FTS (Table 16)
- UARS / HALOE (Table 17)
- ERBS / SAGE-2 (Table 18)
- TIMED / SABER (Table 19)
- Aura /MLS (Table 20)
- Suomi NPP/OMPS-LP (Table 21)

Table 12. Envisat/GOMOS L-2 data required as input to the generation of C3S ozone profiles.

Originating system	GOMOS was on-board the ESA satellite ENVISAT from March 2002 until May 2012. The GOMOS Level 2 data product (ALGOM2s v 1.0) is generated from the Level 1B product by FMI in the framework of the ESA ALGOM project.
Data class	Earth Observation Data
Sensor type and key technical characteristics	GOMOS (Global Ozone Monitoring by Occultation of Stars) is a medium resolution spectrometer covering the wavelength range from 250 nm to 950 nm. It measures attenuation of stellar light in occultation geometry. Although GOMOS measures during day and night, only dark-limb occultations are used in this project. Ozone profiles are retrieved from UV-Visible atmospheric transmission spectra. Ozone data adequate for atmospheric studies are obtained in the 15–100 km range. The vertical resolution of the retrieved ozone profiles is 2 km below 30 km, 3 km above 40 km, with a linear growth from 2 km to 3 km in the altitude range 30-40 km. It does not depend either on stellar properties or occultation geometry.
Data availability & coverage	GOMOS data are available from May 2002 until December 2011. Until early January 2005, the daily number of measurements was about 400. After July 2005, the number of occultations has been reduced down to ~280 daily. Summer poles are not covered (absence of night-time conditions). Data from May-June 2003, January-July 2005 and February-November 2009 are non-available due to the instrument technical anomalies.
Source data product name and reference to product technical specification documents	GOMOS Level 2 data [D4]. The ozone ALGOM2s dataset algorithm and data description can be found in (Sofieva et al., 2017a). The ALGOM2s retrievals use IPF V6 data in the middle atmosphere.
Data quantity	The user-friendly gridded ozone dataset is 357 Mb.

Data quality and reliability	The assessment of the GOMOS data quality and reliability is performed part of the GOMOS Quality Working Group activities. The validation and intercomparisons of IPF V6 and ALGOM 2S data can be found in (Kyrölä et al., 2013; Adams et al., 2014; Hubert et al., 2016; Sofieva et al., 2017a*)*.
Ordering and delivery mechanism	Available from the ESA ALGOM website. HARMOZ data are available from the Ozone_cci website.
Access conditions & pricing	The team has default access to the GOMOS Level 2 data. The GOMOS Level 2 products are free of charge.
Issues	None.

Table 13. Envisat/MIPAS L-2 data required as input to the generation of C3S ozone profiles.

Originating system	The MIPAS Level-1b data serve as input for several level-2 retrieval processors. Within the project, the KIT/IAA algorithm is used after the round robin exercise performed within the O3CCI project Phase I and is used for the ozone limb vertical profile ECV product.
Data class	Earth Observation Data
Sensor type and key technical characteristics	MIPAS is an infrared limb emission sounder on ENVISAT, designed and operated for measurements of constituents between the upper troposphere and the mesosphere. MIPAS has several observation modes: NOM (6-70 km; 500 km along track-sampling), UTLS (6-50km), MA (18-100km), UA (40-170km), and various others. MIPAS is a rear looking instrument with the lines of sight approximately in the orbit plane. In the original measurement mode, which was operational from July 2002 to March 2004, 17 tangent altitudes between 6 and 68 km were measured per limb scan. Spectral resolution: 0.035 cm-1 unapodized. The altitude of the ENVISAT orbit was about 800 km and the ground track speed is about 510 km per 76.5 s which are needed to record one full limb scan. The field of view covers about 3 km in altitude at the tangent point. The horizontal extension of the field of view is about 30 km at the tangent point. Since January 2005, due to a mirror failure, MIPAS was operating on reduced spectral resolution mode (0.0625 cm-1 unapodized).
Data availability & coverage	MIPAS measures day and night on the altitude range from 6 to 70 km (170 km), pole-to-pole, which gives rise to more than 1000 vertical profiles/day. So far, the VMR of 30 trace species, as well as temperature and cloud composition are generated. Global coverage is obtained in approximately 3 days. In current project the complete MIPAS Level 2 V8-240 data are available for Aug-2002 – April 2012 with two modes V8H (High Resolution) and V8R (Reduced Resolution)
Source data product name and reference to product technical specification documents	MIPAS level 1b data (ENVISAT-1 Products Specifications, Vol. 12: MIPAS). MIPAS V8RH_O3-40 +V8H_O3-240
Data quantity	2x5 GB for the O3CCI HARMOZ_ALT and HARMOZ_PRS product
Data quality and reliability	Validation of MIPAS V8 IMK/IAA is ongoing. Intercomparisons with satellite data are shown in (Sofieva et al., 2023)
Ordering and delivery mechanism	MIPAS level-2 data are available from the KIT/IMK/IAA. HARMOZ data are available from the Ozone_cci website.
Access conditions & pricing	The team has default access to the MIPAS Level 2 O3CCI data. The MIPAS Level 2 products are free of charge.

Issues	None.

The SCIAMACHY level-2 version 2.9 data (current version, see Table 14) is produced by applying the SCIATRAN radiative transfer model and retrieval package to level 1-b data (see Ozone_cci ATBD [D23]) to retrieve the ozone limb vertical profile.

Table 14. Envisat/SCIAMACHY L-2 data required as input to the generation of C3S ozone profiles.

Originating system	SCIAMACHY has been operated on-board the ESA satellite Envisat from March 2002 until May 2012 in a sun-synchronous orbit. SCIAMACHY performs observations in 3 different geometries, i.e., limb, nadir and occultation. The SCIAMACHY level-2 data products are generated from level 1-b data (see Ozone_cci ATBD [D22]).
Data class	Earth Observation Data
Sensor type and key technical characteristics	The main difference of the current version (V3.5) with respect to V2.9 (O3CCI_ATBD_Phase1), is the use of different spectral windows and a DOAS (Differential Optical Absorption Spectroscopy) type polynomial fitting in the near UV and visible (Huggins and Chappuis ozone bands). The SCIAMACHY IUP limb retrieval algorithm (V3.5) exploits the scattered radiances in the UV and visible ranges separated in several spectral windows to retrieve ozone number density profiles (window A: 264-274.9 nm, window B: 276.5-287 nm, window C: 289-334 nm, window D 325.5 - 331 nm and window E: 495 - 576 nm) substituting the prior retrieval at discrete wavelengths in the UV and the use of the triplet method in the visible. The ozone number density is retrieved in the altitude range from 8 to 65 km at the measurement grid. The random error for V 3.5 is on the order of 3-5%. The vertical resolution of the SCIAMACHY profile is 3.2 km or lower.
Auxiliary data	The temperature and pressure are derived by using the ECMWF operational stratospheric analysis data (ECMWF). The ground albedo distribution is extracted from the albedo data base from Matthews (1983), a Goddard Institute for Space Studies (GISS) dataset. High precision integrated albedo data at 1°x1° resolution are available for different seasons. The aerosol extinction profiles are taken from the ECSTRA (Extinction Coefficient for STRatospheric Aerosol) model which depends on altitude, latitude and wavelength and is used as input in the retrieval (Fussen & Bingen, 1999). This data base was derived from SAGE II solar occultation measurements. Covariance matrices, diagonal elements of the a priori covariance matrix, and averaging kernels are available in addition to the limb ozone profiles.
Data quantity	Approximately 200 MB/day. Total volume of level-2 version 2.9 data is about 700 GB. (Ozone profiles: 34 GB, a priori diagonal elements: ~ 10 GB, covariance matrices: 330 GB, averaging kernels: 330 GB).
Data quality and reliability	Intercomparison of SCIAMACHY IUP limb ozone V3.0 with ozone sonde stations has shown improvements with average differences being below 10% from about 15% in V2.9 *(*Jia et al. 2015*)*.
Ordering and delivery mechanism	SCIAMACHY level-2 data are available from the Institute für Umweltphysik (IUP) University of Bremen. HARMOZ data are available at the Ozone_cci website.

Table 15. Odin/OSIRIS L-2 data required as input to the generation of C3S ozone profiles.

Originating system	OSIRIS (Optical Spectrograph and InfraRed Imaging System) is a Canadian device on board the Swedish satellite Odin that was launched in February of 2001.
Data class	Earth Observation Data
Sensor type and key technical characteristics	Odin has a circular, sun-synchronous orbit, inclined 98° from the equator, at an altitude near 600 km, with a 96 minute period so OSIRIS is very near local dusk on the ascending track and near local dawn on the descending track, going through local midnight near the southern pole and local noon near the northern pole. OSIRIS is a limb-viewing device and the Optical Spectrograph (OS) has a field of view that spans approximately 40km horizontally and 1km vertically. It makes repeated measurements approximately every 2km while scanning up and down between tangent altitudes of about 10 km to 100 km. The scan period is around 1.5 minutes which allows nearly 60 scans every orbit. The OS only sees the summer hemisphere illuminated by the sun, except during the equinoxes when the entire orbit is illuminated. The OS measures 280nm to 810nm with a 1353 pixel-wide CCD, with a spectral resolution of approximately 1 nm. Data from the wavelength range of 475 to 535nm is discarded due to contamination from the spectrograph's order sorter. The InfraRed Imager (IRI) consists of three channels that record the limb radiance at 1260, 1270, and 1530 nm. Each consists of an array of 100 photodetectors with a tangent altitude resolution of about 1 km. The IRI simultaneously measures 100 vertical kilometres in tangent altitude.
Data availability and coverage	OSIRIS Level 2 data covers from 80° S to 80° N for all longitudes. Ozone concentrations are retrieved on a 1km grid from 10.5 km to 59.5 km. The most recent version of OSIRIS Level 2 data product is available from 2002 to 2010. From 2002-2007 Odin's time was shared with other instruments, so OSIRIS was operational for only half time. From 2008-present the other instruments were decommissioned and OSIRIS became operation full time.
Source data product name and reference to product technical specification documents	OSIRIS Level 2 Ozone, documents not available.
Data quantity	The OSIRIS Level 2 data (including aerosol) is currently 5.05 Gb.
Data quality and reliability	The OSIRIS Level 2 ozone data are extensively validated in the Ozone_cci project. Additional data assessment can be found in (Bourassa et al., 2018) and (Bognar et al, 2022).
Ordering and delivery mechanism	Requests for Odin/OSIRIS data access must go through the ESA data user online registration. HARMOZ data are available at the Ozone_cci website.
Access conditions and pricing	Access is free of charge.

The Sub-Millimetre Radiometer (SMR) on-board the Odin satellite, launched in February 2001, makes time-shared limb measurements of strato-mesospheric ozone using several independent bands within the 486-581GHz frequency range. Odin is on a sun-synchronous orbit at about 600km altitude with ~6am/6pm equator crossing time. Measurements of thermal emission lines are performed

during day and night and global coverage is achieved during one observation day based on about 15 orbits per day and 45-65 vertical scans between nominally 8 and 70km or 110km per orbit (depending on observation mode). Vertical profiles of ozone and many other species are retrieved using retrieval algorithms based on the Optimal Estimation Method.

The official operational level-2 ozone data are produced by the Chalmers University of Technology in Göteborg, Sweden. The currently recommended version 2.1 ozone data product is measured in a stratospheric mode band centred at 501.8GHz and can be obtained after registration from http://odin.rss.chalmers.se. Ozone data retrieved from other lines are also available. The 501.8GHz v2.1 level-2 product provides stratospheric ozone data in the ~12-50km range with 2.5-3.5km vertical resolution and single-profile precision of about 20%. The systematic error is estimated to be smaller than 0.75ppmv. The Odin data set is available from November 2001 until present. The stratospheric mode measurements relevant here have been performed on every third day until April 2007 and on every other day since then.

Table 16. SciSat/ACE-FTS L-2 data required as input to the generation of C3S ozone profiles.

Originating system	ACE-FTS is on-board the CSA satellite SCISAT which was launched in August 2003, data is available from Feb. 2004 to present. The ACE-FTS level-2 data products (VMR profiles) are generated from the ACE-FTS level 1-b product (infrared limb spectra) at the University of Waterloo.
Data class	Earth Observation Data
Sensor type and key technical characteristics	The ACE-FTS is a high-resolution (0.02 cm-1) Fourier transform spectrometer measuring from 2.2 to 13 µm (750 – 4400 cm-1). It has a circular field of view and uses 2 photovoltaic detectors (InSb and HgCdTe) with a dichroic element to obtain the same field of view. Operating in solar occultation mode, the ACE-FTS provides detailed profiles of the Earth's atmosphere for more than 30 chemical species. More information is available from the ACE website at University of Waterloo.
Data availability and coverage	ACE-FTS data are available since Feb. 2004 and is still operational. It provides latitudinal coverage from about 85°N to 85°S with complete coverage every 3 months.
Source data product name and reference to product technical specification documents	Current validated version of processing is v4.1/4.2.
Data quantity	Approximately 1 Gb/year (level 2). Total volume is about 8 Gb.
Data quality and reliability	Only reliable data (that satisfy QA/QC criteria) are included in HARMOZ ACE-FTS dataset. Extensive validation is performed in Ozone_cci and by ACE-FTS team (Sheese et al., 2022)
Ordering and delivery mechanism	ACE is an ESA third party mission and with data available from the ACE site at University of Waterloo. HARMOZ data are available at the Ozone_cci website.
Access conditions and pricing	The ACE-FTS level-2 products are free of charge.

Table 17. UARS/HALOE L-2 data required as input to the generation of C3S ozone profiles.

Originating system	Halogen Occultation Experiment (HALOE) operated in 1991-2005 on board the Upper Atmosphere Research Satellite (UARS).
Data class	Earth Observation Data

Sensor type and key technical characteristics	Solar occultation. Level -2 data with VMR on pressure grid.
Data availability and coverage	October 1991 – November 2005.
Source data product name and reference to product technical specification documents	HALOE GATTS V19 on **HALOE website.**
Data quantity	Harmonized HALOE data: • V19 • File version HARMOZ_PRS fv0003 • File version HARMOZ_ALT fv0001 • 2x177 monthly files with total of 400 MB • Harmonized at UiB-IUP
Data quality and reliability	No filtering applied. Quality has to be determined. Full citation about two problems in profiles: Link to two problems.
Ordering and delivery mechanism	Original data can be downloaded from HALOE GATTS.
Access conditions and pricing	The UARS HALOE level-2 products are free of charge.

Table 18. ERBS/SAGE-2 L-2 data required as input to the generation of C3S ozone profiles.

Originating system	SAGE II (Stratospheric Aerosol and Gas Experiment II) was launched aboard the Earth Budget Satellite (ERBS) in October 1984. The ozone profiles are retrieved in number density (ND) on a geometrical altitude.
Data class	Earth Observation Data
Sensor type and key technical characteristics	Solar occultation.
Data availability and coverage	October 1984 – August 2005.
Source data product name and reference to product technical specification documents	SAGE II V7 on SAGE-II website of NASA Atmospheric Science Data Center (ASDC).
Data quantity	Harmonized SAGE II data: • V7 • File version HARMOZ_PRS fv0006 • File version HARMOZ_ALT fv0006 • 2x248 monthly files with total of 600 MB • Harmonized at UiB-IUP
Data quality and reliability	SAGE -II data are considered as a “gold standard” of ozone profile measurements.ZM Ozone values during Pinatubo period should be excluded. Full filtering and screening have been applied as recommended by the data provider. Only reliable data (that satisfy QA/QC criteria) are included in the HARMOZ dataset. See Section 1.2.7.
Ordering and delivery mechanism	Available from SAGE-II website of the NASA ASDC (click on DATA)

Access conditions and pricing	The ERBS SAGE-2 level-2 products are free of charge.

Table 19. TIMED/SABER L-2 data required as input to the generation of C3S ozone profiles.

Originating system	The Sounding of the Atmosphere using Broadband Emission Radiometry (SABER) instrument is one of four instruments on NASA's TIMED (Thermosphere Ionosphere Mesosphere Energetics Dynamics) satellite. It has been launched in Dec. 2001 and is operating.
Data class	Earth Observation Data
Sensor type and key technical characteristics	Infrared Sounder.
Data availability and coverage	January 2002 – December 2018.
Source data product name and reference to product technical specification documents	SABER V 2.0. Website Documentation.
Data quantity	Harmonized SABER data: • V2.0 Channel 96 • File version HARMOZ_PRS fv0003 • File version HARMOZ_ALT fv0001 • 2x157 monthly files with total of 30 GB • Harmonized at UiB-IUP
Data quality and reliability	5 of the files have corrupt time values.
Ordering and delivery mechanism	Download Page.
Access conditions and pricing	The TIMED SABER level-2 products are free of charge.

Table 20. Aura/MLS L-2 data required as input to the generation of C3S ozone profiles.

Originating system	Microwave Limb Sounder (MLS) on-board the Aura satellite and part of the A-Train constellation, was launched in 2004. The ozone values are VMR on pressure grid.
Data class	Earth Observation Data
Sensor type and key technical characteristics	Microwave Limb.
Data availability and coverage	August 2004 – December 2018.
Source data product name and reference to product technical specification documents	Product overview MLS.

Data quantity	• V4.2 • File version HARMOZ_PRS fv0005 • File version HARMOZ_ALT fv0004 • 2x137 monthly files with total of 50 GB • Harmonized at UiB-IUP
Data quality and reliability	The filtering applied in the current version following the recommendation of MLS/Aura team.
Ordering and delivery mechanism	Data available from the MLS website.
Access conditions and pricing	The MLS AURA level-2 products are free of charge.

Table 21. SUOMI NPP/OMPS L-2 data required as input to the generation of C3S ozone profiles.

Originating system	OMPS-LP is on-board the NASA satellite SUOMI NPP, launched in 2012 and is operational. The OMPS-LP level-2 data products (ozone number density profiles) are generated at the University of Saskatchewan.
Data class	Earth Observation Data
Sensor type and key technical characteristics	The OMPS Limb Profiler measures limb-scattered sunlight in the wavelength range 270—1000 nm employing a prism spectrometer. OMPS-LP images the atmosphere using three vertical slits, one aligned with the orbital plane and the others separated by 250 km at the tangent point on either side of the orbital track. Imaging allows OMPS-LP to obtain along track and vertical sampling of approximately 125 km and 1 km respectively. More information is available at the NASA OMPS EarthData website.
Data availability and coverage	OMPS data are available since Feb. 2012 and is still operational. It provides ~1600 profiles per day with global coverage.
Source data product name and reference to product technical specification documents	The current version of processing is USask 2D v1.1.0.
Data quantity	Approximately 1 Gb/year (level 2). Total volume is about 8 Gb.
Data quality and reliability	The harmonized dataset (HARMOZ), which contains only valid data, is provided by the University of Saskatchewan. The data from first months of OMPS operation (Feb and March 2012) have lower coverage and possibly some pointing issues.
Ordering and delivery mechanism	liOMPS HARMOZ data are available at the Ozone_cci website.
Access conditions and pricing	The OMPS-LP level-2 products are free of charge.

2.4 Ancillary data

2.4.1 Surface albedo

Spectral surface albedo data (Table 22) are required as input for the total column and nadir ozone profile retrieval algorithms. These data sets must be available at the UV wavelengths used for the inversion, and at suitable spatial and temporal resolutions.

Table 22. Surface albedo data required for C3S ozone data processing.

Originating system	TOMS, GOME, OMI sensors.
Data class	Climatological data base.
Sensor type and key technical characteristics	Minimum Lambertian Equivalent Reflectivity (MLER) data bases derived from the TOMS, GOME and OMI sensors are available and suitable for nadir UV ozone retrievals.
Data availability & coverage	MLER climatologies are available from TOMS, GOME and OMI. These data sets are specified as global monthly averaged maps, representative for one yearly cycle (i.e. they are distributed in the form of 12 maps for each wavelength interval).
Source data product name and reference to product technical specification documents	The TOMS, GOME and OMI LER climatologies are documented in the following scientific publications: Herman and Celarier, 1997; Koelemeijer et al., 2003 and Kleipool et al., 2008.
Data quantity	The full data base of GOME LER amounts to approximately 100 MB.
Data quality and reliability	The quality of the TOMS, GOME and OMI LER climatologies is documented in the respective scientific publications (see above).
Ordering and delivery mechanism	LER climatologies from relevant sensors are available from the TEMIS web-site and from the NASA OMI web-site.
Access conditions & pricing	Albedo climatologies from TOMS, GOME and OMI are available free of charge.
Issues	None.

2.4.2 Ozone climatology

Ozone vertical profile climatology's are required as input for the total column retrieval algorithms. These data sets must be global in coverage, classified according to the total column and be representative for the main sources of ozone variability in both the troposphere and the stratosphere.

Within C3S_Ozone we use as baseline the total column-classified ozone profile climatology constructed using MLS and sondes measurements *(*Labow et al., 2015) (Table 23) combined with the tropospheric ozone column climatology built using OMI and MLS observations (Ziemke et al., 2011) (

Table 24).

Table 23. Ozone profile climatology *(*Labow et al., 2015*).*

Originating system	Combination of data from MLS and ozone sondes.
Data class	Climatological data base.
Sensor type and key technical characteristics	The Labow et al. climatology was formed by combining data from the Microwave Limb Sounder (MLS) with data from balloon sondes. It consists of average ozone profiles for 30° latitude zones covering altitudes from 0 to 60 km (in Z* pressure altitude coordinates).
Data availability & coverage	The climatology is global in scope and available from the web.
Source data product name and reference to product technical specification documents	The ozone profile climatology is fully described in Labow et al. (2015).
Data quantity	Approximately 200 kB.
Data quality and reliability	See Labow et al. (2015).

Ordering and delivery mechanism	The data base is available from the authors.
Access conditions & pricing	The data base is freely available.
Issues	None.

Table 24. Tropospheric ozone column climatology (Ziemke et al., 2011).

Originating system	Combination of data from OMI and MLS observations.
Data class	Climatological data base.
Sensor type and key technical characteristics	The Ziemke et al. climatology was formed by combining data from the Ozone Monitoring Instrument and the Microwave Limb Sounder. It consists of monthly mean tropospheric ozone columns provided on a grid with a spatial resolution of 1.25° x 1° (Lon x lat) for all latitudes comprised between -60° and + 60°. Corresponding tropopause altitudes are also provided.
Data availability & coverage	The climatology is available at this website.
Source data product name and reference to product technical specification documents	This tropospheric climatology is fully described in Ziemke et al. (2011).
Data quantity	< 10 Mb.
Data quality and reliability	See Ziemke et al. (2011)
Ordering and delivery mechanism	The data base is available here.
Access conditions & pricing	The data base is freely available.
Issues	None.

2.4.3 Digital Elevation Model (DEM)

A global digital elevation model (DEM) is required as input for the total column and nadir profile retrieval algorithms. Within Ozone_cci we use as baseline GTOPO30 DEM (https://www.usgs.gov/science-explorer-results?es=GTOPO30) with a horizontal grid spacing of 30 arc seconds (approximately 1 kilometre) (Table 25).

Table 25. Digital elevation model (DEM).

Originating system	GTOPO30 was derived from several raster and vector sources of topographic information.
Data class	Elevation data base.
Sensor type and key technical characteristics	GTOPO30, completed in late 1996, was developed over a three year period through a collaborative effort led by staff at the U.S. Geological Survey's Center for Earth Resources Observation and Science.
Data availability & coverage	The DEM data is global in scope and available from this website.
This Source data product name and reference to product technical specification documents	The GTOPO30 is fully described in the web link.
Data quantity	Approximately 2 Gb.
Data quality and reliability	See Web link.
Ordering and delivery mechanism	The data base is available from the web.

Access conditions & pricing	The data base is freely available.
Issues	None.

2.4.4 Ozone UV absorption cross-sections

Spectroscopic databases of absorption cross-sections are required as input for the total column and nadir profile ozone retrieval algorithms. Within C3S_Ozone we use as baseline temperature-dependent ozone absorption cross-sections covering the Hartley-Huggins bands from 270 to 340 nm (Table 26).

Table 26. Ozone UV absorption cross-sections.

Originating system	Laboratory data by Daumont et al. (1992), Malicet et al. (1995), and Brion et al. (1998). Laboratory data by Gorshelev et al. (2014) and Serdyuchenko et al. (2014).
Data class	Spectroscopic data base.
Sensor type and key technical characteristics	**BDM data set** Absorption cross-sections are measured in the laboratory using a grating spectrometer and an absorption cell. A capacitive manometer measures the pressure of gaseous mixture in the absorption cell all through the experiment. To allow measurement at low temperatures down to 215 K, a two-stage cryostat is used. For details see Malicet, Brion and Daumont (1989) and Daumont et al. (1992). ***Serdyuchenko et al.* data set** These new ozone absorption cross-section measurements are performed in the solar spectral region using a combination of Fourier transform and echelle spectrometers. The cross-sections cover the spectral range 213–1100nm at a spectral resolution of 0.02– 0.06nm in the UV–visible and 0.12–0.24nm in the IR at eleven temperatures from 193 to 293K in steps of 10 K. The absolute accuracy is better than three percent for most parts of the spectral region and wavelength calibration accuracy is better than 0.005 nm. For details see Gorshelev et al. (2014) and Serdyuchenko et al. (2014).
Data availability & coverage	The data are available from the authors and from public data bases.
Source data product name and reference to product technical specification documents	Laboratory data by Daumont et al. (1992), Malicet et al. (1995), and Brion et al. (1998). Laboratory data by Gorshelev et al. (2014) and Serdyuchenko et al. (2014).
Data quantity	BDM: Approximately 10 MB. Serdyuchenko et al.: Approximately 36 MB.
Data quality and reliability	See author's references, Orphal (2003) and the ESA Ozone cross-sections review study by J. Orphal.
Ordering and delivery mechanism	The data base is available from the web.
Access conditions & pricing	The data base is freely available.

Issues	The Brion, Daumont and Malicet (BDM) ozone absorption cross-section data set has been recommended for use in remote-sensing applications, notably as part of the activities of the ACSO IGACO-O3 committee. However the recent availability of the high quality data set of Serdychenko et al. (2014) which covers an extended range of temperatures has motivated new investigations. In comparison to past historical references such as Bass and Paur (1985), these data sets are characterised by (1) improved wavelength registration, (2) more accurate characterization of the temperature dependence of the cross-section, (3) high spectral resolution, and (4) high signal to noise ratio. Although the current baseline for CCI total ozone and ozone profile retrievals in the Hartley and Huggins bands is BDM, the eventual possibility of switching to the new Serdyuchenko et al. data set will be investigated.

2.4.5 ECMWF meteorological data

ECMWF meteorological data (Table 27) are needed for the retrieval of ozone data products and for assimilation tools that will be used as one of the approaches to data merging.

Table 27. ECMWF meteorological data.

Originating system	ECMWF is providing forecasts, up to 10 days ahead, of meteorological parameters to the European Meteorological institutes. Re-analysis of these parameters are also available from the ERA5 collection.
Data class	Meteorological parameters (e.g. temperature, humidity, wind fields, surface pressure, etc.).
Sensor type and key technical characteristics	The ECMWF model spectral resolution, T1279L91, consists of a dynamical component, a physical component and a coupled ocean wave component. The model formulation can be summarised by six basic physical equations, the way the numerical computations are carried out and the resolution in time and space.
Data availability & coverage	The global data is operationally delivered on a 12 hour basis and can be downloaded by the meteorological institutes via dedicated internet-access. The global ERA5 data is available for 1940 till almost today. The most recent ERA5 data is available after a few months.
Source data product name and reference to product technical specification documents	A full set of parameters is available to ECMWF Member States through the ECMWF operational dissemination system. As a matter of fact, more parameters are produced and disseminated, than are archived. They are available in Gaussian regular and reduced grid, regular and rotated lat-lon grid forms. Upper air parameters (except humidity) are also available in spectral form.
Data quantity	Approximately 1 Gb per day. Total amount of data at ECMWF is 150 TB.
Data quality and reliability	See the ECMWF website.

Ordering and delivery mechanism	Data is accessible for meteorological institutes of the Member States.
Access conditions & pricing	The data base is only freely available for meteorological institutes of the Member States.
Issues	https://confluence.ecmwf.int/display/FCST/Known+IFS+forecasting+issues

The current status of the usage of ECMWF data sets for generating of the ozone ECV products is summarized in Table 28. As can be seen, most retrieval algorithms make use of meteorological input data, either as a-priori information (when for example temperature is retrieved as part of the state vector) or to constrain model parameters used in the inversion process. In addition, ECMWF data are also used at KNMI for the assimilation of total ozone columns.

Table 28. Source of meteorological data sets (pressure/temperature) used for generating the C3S_Ozone data products.

Source of PT data	**retrieved**	**climatology**	**ECMWF data**		
Product			**Operational**	**ERA5**	**ERA-Interim**
Total ozone	X [2]	X			
Nadir ozone profile					X
SCIAMACHY limb ozone profile			X		X [3]
MIPAS ozone profile	X		X [4]		
GOMOS ozone profile			X		
Assimilated ozone products				X	

2.4.6 Atmospheric state input to FORLI RTM

2.4.6.1 L1C radiances

FORLI-O_3 v20151001 (see 3.2.2) uses the Level1C radiances disseminated by EumetCast. A subset of the spectral range, covering 1025–1075 cm^{-1}, is used for the O_3 retrieval.

[2] The total ozone algorithm retrieves an effective ozone-weighted mean temperature. A priori T° profiles are taken from the TOMS v8 climatology.

[3] Some of the reprocessed level-2 and level-3 data used ERA-Interim, however there is a limitation in the range of altitude covered by ERA-Interim which prevents its use on a systematic basis.

[4] ECMWF data are used as a-priori in the inversion process.

2.4.6.2 *Ozone climatology*

The *a priori* profile x_a covariance matrix S_a are constructed from the McPeters/Labow/Logan climatology of ozone profiles (McPeters, Labow and Logan, 2007), which combines long term satellite limb measurements (from the Stratospheric Aerosol and Gas Experiment II and the Microwave Limb Sounder) and measurements from ozone sondes. The *a priori* profile x_a is the mean of the ensemble. Figure 1 illustrates this *a priori* information: the *a priori* profile x_a has values slowly increasing from around 25 ppbv at the surface to 100 ppbv at 10km, reaching a maximum of 7.3 ppmv in the middle stratosphere. The variability (taken hereafter as the square root of the variance, i.e. of the diagonal elements ofS_a) is below 30% in the boundary layer and the free troposphere; it is maximum in the upper troposphere–lower stratosphere, between 10 and 20 km, where it is of the order of 60%. There are significant correlations between the concentrations in the layers 0–10, 10–25 and 25–40 km, but weak correlation between these three (Figure 1).

Figure 1 - Left: x_a (ppmv, blueline) and associated variance (shaded blue) for the FORLI-O3. The dashed red line indicates the top altitude of the last retrieved layer. Right: correlations and S_a variance–covariance matrices in unitless multiplicative factor (from Hurtmans et al. 2012).

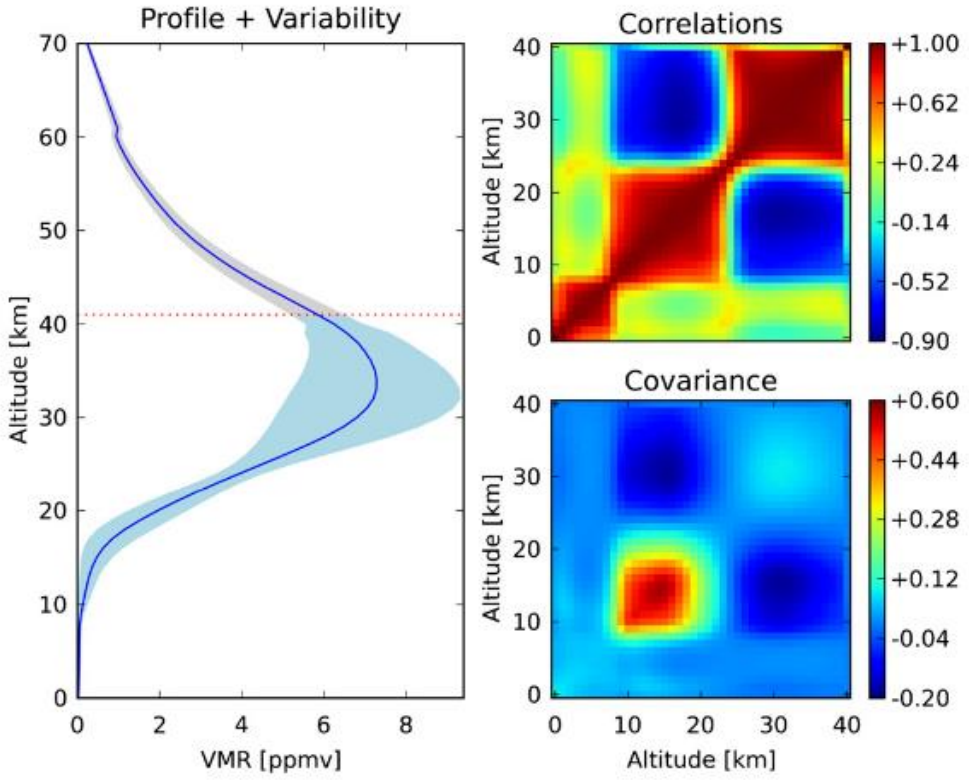

2.4.6.3 *Temperature and humidity profiles*

Profiles of temperature and humidity are from the IASI L2 PPF (*August et al., 2012*). The atmospheric temperatures are kept fixed whereas the water profile is used as a priori and further adjusted.

2.4.6.4 Surface temperature

Surface temperatures (land and sea) are from the IASI L2 PPF. Surface temperature is part of the parameters to be retrieved.

2.4.6.5 Cloud fraction

FORLI v20151001 uses the cloud fraction from the IASI L2 PPF. All pixels with a cloud fraction equal to or lower than 13 % are processed.

2.4.6.6 CO_2 profile

A constant vertical profile at 380 ppm is assumed for CO_2.

2.4.6.7 Orography

Orography is from the GTOPO30 global digital elevation model and is integrated in the entire IASI FOV.

2.4.6.8 Emissivity

A wavenumber-dependent surface emissivity above continental surfaces is used while for ocean a single standard emissivity is considered. For continental surfaces it relies on the climatology of Zhou et al. (2011). In cases of missing values in the Zhou et al. climatology, the MODIS climatology of Wan (2008) is used. It is available on a finer 0.05° x 0.05° grid but is restricted to only 12 channels in the IASI spectral range. In order to deal with this, the spectrally resolved mean emissivity of the Zhou climatology is scaled to match as closely as possible the values in these 12 channels and it is this resulting emissivity that is considered. Finally when there is no correspondence between the IASI FOV and either climatology's, then the mean emissivity of the Zhou et al. (2011) climatology is used.

2.4.6.9 Look-up tables

Tabulated absorption cross-sections at various pressures and temperatures are used to speed up the radiative transfer calculation. The spectral range for the LUTs used in v20151001 is 960-1105 cm^{-1} and the spectral oversampling is 100. The absorption cross-sections are computed on a logarithmic grid for pressure from 4.5×10^{-5} to 1 atm with a grid step of 0.2 for the logarithm of pressure, and on a linear grid for temperature (162.8–322.6 K with a grid step of 5K). Relative humidity is also introduced in the LUT, varying linearly between 0 and 100%, by steps of 10%.

2.4.6.10 Spectroscopy

Line integrated absorption cross section, air broadening, self-broadening, line shifting and absorption cross section data are taken from the widely used HITRAN spectroscopic database version 2012 (Rothman et al., 2013). Continuum formulations are taken from MT-CKD (Clough et al., 2005).

3 Retrieval algorithms and forward models

3.1 Ozone total column retrieval from UV-nadir sensors

Total ozone columns are generally measured from space using earthshine backscattered radiance observations from nadir-viewing instruments. Within C3S, a total ozone climate data record is produced operationally based on the experience built as part of the ESA CCI programme. This data record combines individual regularly extended and updated L2 total ozone data sets from different ESA, ESA Third Party Mission (ESA-TPM) and NOAA/NASA sensors, i.e. GOME/ERS-2, SCIAMACHY/Envisat, GOME-2/Metop, OMI/Aura and OMPS-NM/SNPP. These sensors are described in Sections 1.1.1, 1.1.2, 1.1.3, 1.1.4 and 1.1.5.

3.1.1 Heritage

In the USA, total ozone has been measured since 1978 by NASA and NOAA using a series of TOMS and SBUV instruments (Bhartia, 2003; Miller et al., 2002). In Europe, total ozone measurements from space have been initiated with the GOME instrument, and continued with the successor instruments SCIAMACHY, GOME-2 and OMI. Two different approaches have been used to retrieve total ozone columns from those sensors: DOAS and direct-fitting.

The DOAS technique for total ozone retrieval was used from the start of the GOME/ERS-2 mission in 1995 (GDP Versions 1-4, see for example Van Roozendael et al., 2006), DOAS retrieval is currently implemented in the SCIAMACHY and GOME-2 operational processors, respectively SGP 6.0 (Lerot et al., 2008), GDP 4.7 (Hao et al., 2014). The DOAS technique is fast and provides ozone columns at the 1% level of accuracy in most situations (Van Roozendael et al., 2006).

The Direct-fitting approach provides more accurate total ozone columns, at the cost of slower computational performance. The heritage of this approach can be traced back to the analysis of ozone column measurements obtained from the continuous scan Nimbus-7 data (Joiner and Bhartia, 1997). The upgraded GOME operational processor GDP 5 is based on Direct-fitting; the complete 16-year GOME data record has been recently reprocessed (Van Roozendael et al., 2012). The Direct-fitting algorithm GODFIT developed at BIRA-IASB has been further developed as part of the ESA Ozone_CCI activities and has been used to generate L2 total ozone data sets from GOME, SCIAMACHY, GOME-2A/B and OMI with a high level of inter-sensor consistency (Lerot et al., 2014). Chiou et al. (2014) have shown that the CCI phase-I GOME, SCIAMACHY and GOME-2 data sets agree at the −0.32 to 0.76% level with the recently published monthly zonal mean total ozone SBUV data. Koukouli et al. (2015) have shown that these satellite records agree with ground-based observations to within a percent of relative difference.

The total ozone production system implemented within C3S is directly inherited from the distributed production system developed as part of the CCI programme: individual L2 data sets have been extended and updated at BIRA-IASB using the GODFIT algorithm, and then merged into one single L3 record using the merging algorithm developed at DLR (Coldewey-Egbers et al., 2015).

3.1.2 Level 1 to Level 2

Within C3S, the baseline algorithm for L2 total ozone retrieval from backscatter UV sensors is an updated version of the GOME-type direct-fitting (GODFIT) algorithm jointly developed at BIRA-IASB,

DLR-IMF and RT-Solutions for implementation in version 5 of the GOME Data Processor (GDP) operational system. In contrast to previous versions of the GDP, which were based on the DOAS method, GODFIT uses a least-squares fitting inverse algorithm including direct multi-spectral radiative transfer simulation of earthshine radiances and Jacobians with respect to total ozone, albedo closure and other ancillary fitting parameters. The basis of the algorithm has been described in detail in the GDP5 Algorithm Theoretical Basis Document (Spurr et al. 2011). More details about description below can also be found in (Lerot et al. 2014), (Van Roozendael, et al. 2012) and in the Ozone_cci ATBD [D22]. This section presents the general features of the algorithm.

3.1.2.1 Overview

The direct fitting algorithm employs a classical inverse method of iterative least squares minimization which is based on a linearized forward model, that is, a multiple-scatter radiative transfer (RT) simulation of earthshine radiances and associated weighting functions (Jacobians) with respect to state vector elements. The latter are the total ozone column and several ancillary parameters including albedo closure coefficients, a temperature shift, amplitudes for Ring and under sampling corrections, and a wavelength registration shift. On-the-fly RT calculations are done using the LIDORT discrete ordinate model (Spurr, 2008). The performance of the radiative transfer computations has been significantly enhanced with the development of a new scheme based on the application of Principal Components Analysis (PCA) to the optical property data sets (Spurr et al. 2013). Alternatively, the simulated radiances and Jacobians can be extracted from pre-computed tables in order to further accelerate the retrievals. This facilitates greatly the treatment of large amount of data provided by sensors with a very high spatial resolution such as OMI aboard the AURA platform and the future Sentinel-4 and -5(p) instruments.

One specificity of the C3S total ozone L2 processing is that it includes a soft-calibration procedure of the L1 reflectance's for some of the sensors considered for the production of the climate L3 merged total ozone data record (see Section 3.1.2.9). This allows to further enhance the inter-sensor consistency between the individual level-2 data sets by empirically correcting for some remaining discrepancies caused by limitations in the calibration and/or instrumental degradation.

Before processing the individual satellite pixels, a recalibration of the L1 irradiance wavelength grid is carried out for each satellite orbit data to have the required high accuracy for the alignment between the earthshine and reference irradiance spectra on one hand and the cross-sections on the other. This recalibration consists in aligning the solar Fraunhofer lines in the L1 sun spectrum to the position provided by a reference solar atlas (Chance and Kurucz, 2010) degraded to the resolution of the instrument. During this procedure, the instrumental slit function can also be characterized in a dynamic way by convolving the reference solar atlas with a predetermined line shape of which key parameters (e.g. the Full Width at Half-Maximum (FWHM)) are adjusted simultaneously to the wavelength grid shift parameters. The various cross sections are then convolved dynamically using the slit function fitted during the wavelength calibration. This capability may be particularly useful if the real slit function turns out to differ significantly from the key data slit function or if the instrumental degradation leads to some slit function change over time. Once this is done, total ozone can be inverted for each measured radiance.

The flowchart in Figure 2 gives an overview of the inversion procedure. It is straightforward stepwise process, with one major decision point. Following the initial reading of satellite radiance and

irradiance data (possibly soft-calibrated), and the input of auxiliary data (topography fields, optional temperature profiles, fractional cloud cover and cloud-top-height), the iteration counter is set (n=0), and an initial guess is made for the state vector (total ozone amount, temperature shift, closure coefficients, etc.). A unique ozone profile $P(n)$ is then constructed from the total column estimate $C(n)$, using a 1-1 column-profile map based on column-classified ozone profile climatology. For this, we use the climatological database recently released by Labow et al. (2015) and constructed using MLS and sondes observations, combined with the tropospheric climatology based on OMI and MLS measurements published by Ziemke et al. (2011). Next, pressure, temperature and height profiles are constructed; this is where the current value of the temperature shift $S(n)$ is applied.

Figure 2 - Flow Diagram of the GOME-type direct fitting retrieval algorithm (GODFIT).

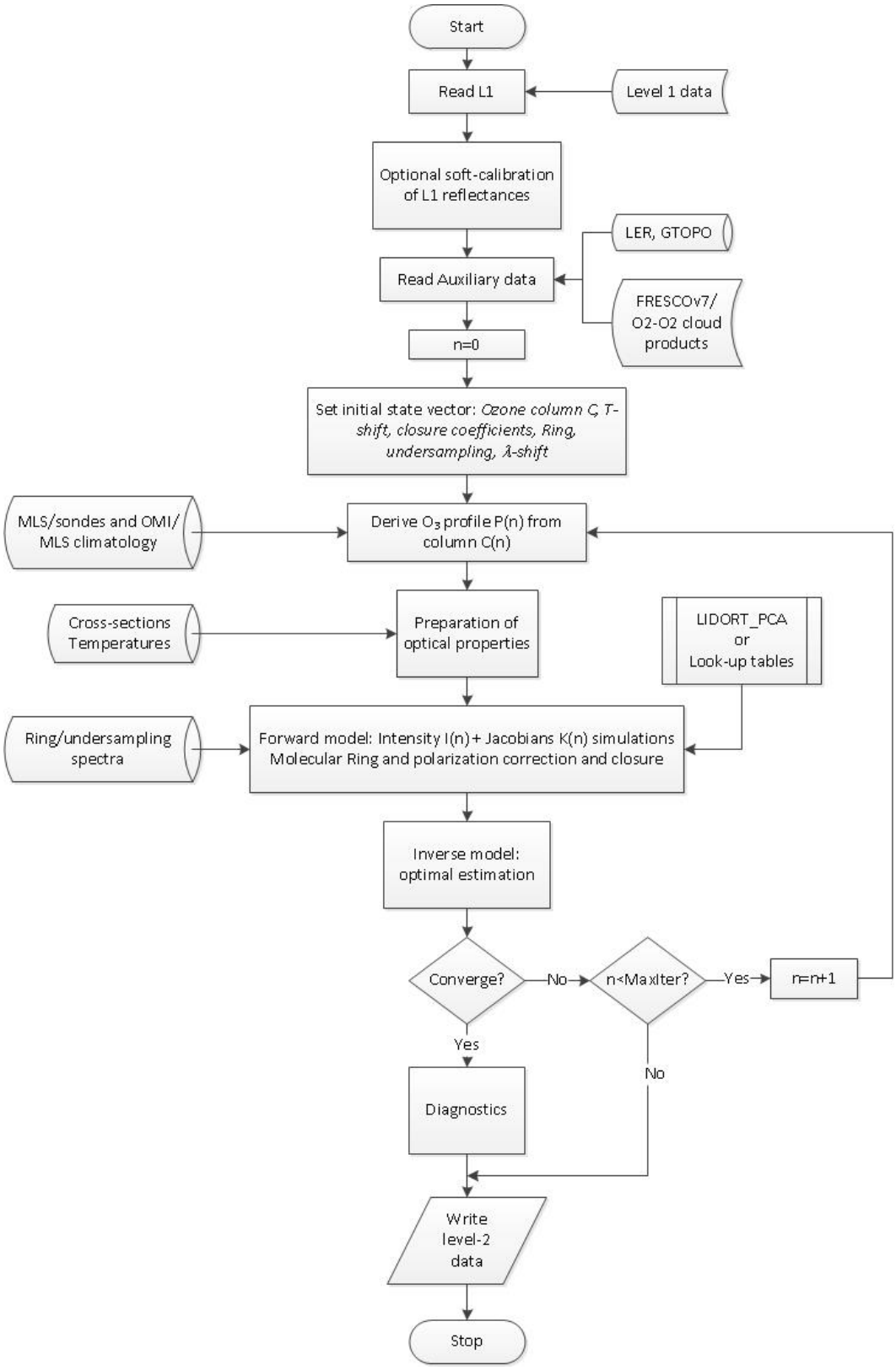

The algorithm then enters the forward model step, in which optical properties are created and the LIDORT model called to deliver top-of-atmosphere (TOA) radiances *I(n)*, and the associated ozone column, albedo, T-shift and other weighting functions *K(n)* at each iteration step *n*. These simulated quantities are then corrected for the molecular Ring effect. Next, the inversion module yields a new guess for the ozone column and ancillary state vector parameters. The iteration stops when suitable convergence criteria have been satisfied, or when the maximum number of iterations has been reached (in which case, there is no established convergence and final product). The ozone total column and other parameter errors are computed directly from the inverse variance-covariance matrix.

When the simulated spectra are extracted from a lookup table (LUT) instead of being computed online, the inversion procedure is further simplified. The optical properties do not have to be computed and the calls to the RT model LIDORT are replaced by interpolation procedures through the LUT using directly the state vector variables as input in addition to the geolocation parameters. The radiance LUT was computed using the same forward model as the online scheme in order to have full consistency between the two approaches (see below).

Table 29 lists static and dynamic auxiliary data needed by the retrieval algorithm GODFIT to generate the total ozone ECV. More details are given in Section 2.4 for each of those input data sets.

Table 29. List of auxiliary input needs for generating the total ozone product.

Parameter	Physical unit	Source	Comments
High-resolution solar spectrum	[mol s−1 m−2 nm−1]	Chance and Kurucz [2010]	Static
Absorption O_3 cross sections at various temperatures	[$cm^2 molec.^{-1}$]	Serdyuchenko et al., [2014]	Static
Ring cross-sections	---	Generated internally	Static
Surface Albedo	---	OMI-based monthly LER database (Kleipool et al., 2008)	Static Values at 335 nm are used
Surface height	m	GTOPO30	Static Degraded at instrumental resolution
A-priori O_3 vertical profile shapes	DU	Total O_3-classified climatology (Labow et al., 2015) combined with the OMI/MLS tropospheric O_3 climatology (Ziemke et al., 2011)	Static
Cloud fraction	---	Cloud product FRESCOv7/O2-02 OMI product or extracted from NASA TO3 OMPS product	Dynamic

Parameter	Physical unit	Source	Comments
Cloud top height/pressure	Pa	Cloud product FRESCOv7/O2-02 OMI product or extracted from NASA TO3 OMPS product	Dynamic
Temperature profiles	°K	ECMWF - ERA Interim	Dynamic Only to compute soft-calibration factors.

3.1.2.2 Forward model

Simulation of earthshine radiances and retrieval-parameter Jacobians is done using the multi-layer multiple scattering radiative transfer code LIDORT (Spurr, 2008). LIDORT generates analytic Jacobians (or radiancepartial derivatives) for atmospheric and/or surface properties. In particular Jacobians are calculated for total ozone, surface albedo and temperature shift. LIDORT solves the radiative transfer equation in each layer using the discrete-ordinate method (Stamnes, et al. 1988). Boundary conditions (surface reflectance, level continuity, direct incoming sunlight at top-of-atmosphere) are applied to generate the whole-atmosphere field at discrete ordinates. Source function integration is then used to generate solutions at any desired viewing geometry and output level. The entire discrete ordinate RT solution is analytically differentiable with respect to any atmospheric and/or surface parameter used to construct optical properties (Spurr, 2002), and this allows weighting functions to be determined accurately with very little additional numerical computation.

In addition to the usual pseudo-spherical (P-S) approximation (solar beam attenuation treated for a curved atmosphere) LIDORT also has an outgoing sphericity correction, in which both solar and viewing angles are allowed to vary along the line-of-sight (LOS) path treated for a spherical-shell atmosphere. This approach gives sufficient accuracy[5] for off-nadir viewing geometries (maximum 60°) encountered with polar orbiting sun-synchronous sensors.

A new accelerated-performance scheme for the radiative transfer computation has been implemented within GODFIT. This scheme is based on the application of Principal Component Analysis (PCA) to optical property data sets used for RT simulation – most of the variance in the mean-removed optical data is contained in the first and most important principal components. Thus, full multiple-scattering (MS) computations with LIDORT are done only for the mean profile and the first few EOF optical profiles. These LIDORT MS results are then compared with MS radiances from a 2-stream (2S) RT code (Spurr and Natraj, 2011), and a second-order central difference scheme based on these LIDORT/2S difference and on the data Principal Components is then used to provide correction factors to the MS field at every wavelength. Thus it is only necessary to compute the MS radiances at every wavelength using the much faster 2S code.

LIDORT is a scalar code and therefore polarization is neglected in the RT modelling. Ideally, a vector code such as VLIDORT should be used in the forward model. However, to minimize the computational burden, polarization correction factors are applied to simulated scalar radiances. These factors are extracted from a lookup table of VLIDORT-LIDORT intensity relative differences. This LUT provides correction factors classified according to ranges of the solar zenith, viewing zenith, and relative azimuth angles (from 20 to 85 degrees, 0 to 70 degrees and 0 to 180 degrees respectively), surface

[5] In this context," accuracy" is the total error of the retrieval.

altitude (from 0 to 15 km), ground albedo (from 0 to 1) and the total ozone column (from 125 to 575 DU).

3.1.2.3 Atmospheric profiles and the T-shift procedure

In a multilayer atmosphere, the forward model requires the specification of a complete ozone profile. In GODFIT, the ozone profile is parameterized by total column, and latitude. The use of total column as a proxy for the ozone profile was recognized a number of years ago and column-classified ozone profile climatologies were created for the TOMS Version 7 (Wellemeyer, et al. 1997), and Version 8 (V8) retrieval algorithms (Bhartia 2003). The same mapping is used for GODFIT with the recent climatology based on MLS and sonde data (Labow et al., 2015). This climatology neglects the seasonal and longitudinal variations of tropospheric ozone. To improve the representativeness of the *a priori* profiles, it is combined with the OMI/MLS tropospheric ozone column climatology (Ziemke, et al. 2011).

Since ozone absorption in the Huggins bands is highly sensitive to temperature, temperature profiles are not only required for hydrostatic balance but also for the determination of ozone cross sections. In GODFIT, a-priori temperature profiles are taken from the monthly zonal temperature climatology supplied with the TOMS Version 8 ozone profiles (Bhartia 2003). In addition, a temperature shift adjustment is being used to improve total ozone accuracy[6] and better reflect the dependence of the ozone absorption signature on temperature at the scale of satellite pixels (Van Roozendael, et al. 2012).

3.1.2.4 Surface and cloud treatment

Lower boundary reflection properties must be specified as an input for the forward model. By default one assumes a Lambertian surface characterized by a total albedo *L.* Most ozone being above the tropopause, clouds can be treated as a first-order correction to the basic ozone retrieval using the independent pixel approximation (IPA). TOA radiance in a partially cloudy scenario is simulated as a linear combination of radiances from clear and fully cloudy scenes, weighted by the effective cloud fractional cover f_c assuming clouds as Lambertian reflecting boundary surfaces. Alternatively, the observed scene can be treated as a single effective surface, located at an altitude resulting from the cloud fraction weighted mean of the ground and cloud altitudes (Coldewey-Egbers, et al. 2005). The effective surface albedo is retrieved simultaneously to the total ozone column using the internal closure mode of GODFIT. We found that this approach minimizes the impact of cloud contamination on the retrieved ozone columns, especially for high clouds and it has been consequently adopted in the current version of the algorithm. By default, cloud optical properties (cloud fraction, cloud top albedo and height) come from the FRESCOv7 algorithm (Wang et al., 2008) for GOME, SCIAMACHY and GOME-2 and from the O2-O2 cloud product (Acarreta et al., 2004) for OMI or, for OMPS, from the cloud parameters provided in the operational TO3 NASA product (McPeters et al., 2019).

3.1.2.5 Albedo and other forward model closure terms

For internal closure, tropospheric aerosol scattering and absorption and surface reflectivity are brought together in an albedo closure term that is fitted internally, in the sense that coupling between surface and atmosphere is treated properly in a full multiple scattering context. The code thus

[6] I.e. to diminish the total error of the retrieval.

determines an effective wavelength-dependent albedo in a molecular atmosphere. Assuming that surface albedo *R* is a quadratic or cubic polynomial function, we write:

$$R(\lambda) = \gamma_0 + \sum_{m=1}^{M} \gamma_m (1 - \lambda/\lambda_0)^m \qquad \text{Eq. (1)}$$

We assume first guess values $\gamma_m = 0$ for polynomial orders $m > 0$ and an initial value for γ_0 (surface albedo at wavelength λ_0) is taken from a suitable database.

In order to complete the forward model process, additional effects must be taken into account before simulated intensities can be compared with Level 1b measurements in the inverse model. In particular the Ring effect which shows up as small-amplitude distortions in earthshine and sky spectra due to the effect of inelastic rotational Raman scattering by air molecules (Grainger and Ring 1962) must be corrected for. To this aim, we use a revisited semi-empirical formulation including tabulated effective air mass factors and reproducing closely filling-in factors calculated with the LIDORT-RRS radiative transfer code (Lerot et al., 2014).

We then simulate sun-normalized radiances at wavelengths specified by the solar irradiance spectrum supplied with every orbit. There is a wavelength registration mismatch between irradiance and radiance spectra, arising mainly from the solar spectrum Doppler shift; this mismatch varies across an orbit due to changes in the instrument temperature. To correct for this, an earthshine spectrum shift is fitted as part of the retrieval procedure, and this shift value is then an element in the state vector of retrieval parameters. In general, the retrieved spectrum shift value is around 0.008 nm, in line with a Doppler shift. Re-sampling is always done by cubic-spline interpolation.

3.1.2.6 Lookup tables of LIDORT sun-normalized radiances

The goal of the lookup table approach is to replace the online radiative transfer calculation by an interpolation of precalculated radiances. Therefore, we construct a multi-dimensional lookup table of radiances as a function of all varying parameters that enter the LIDORT simulation: the fitted parameters (total ozone column and the ancillary fitting parameters scene albedo and temperature shift), angles describing the observation geometry, surface pressure, as well as latitude, by which we select the appropriate temperature and ozone profile shapes from the TOMSv8 and MLS/sonde climatology's. The tabulated radiances are then calculated for a fixed wavelength grid spanning the 325-335 nm range at 3 times the instrument sampling rate, using cross sections convolved with the instrument's slit function.

The forward model calculation for a set of parameter values now becomes an interpolation of the radiances at surrounding grid points. For the total ozone column and solar zenith angle, we use quadratic interpolation through 3 surrounding grid points. For the other dimensions of the table, linear interpolation is sufficient. This results in an interpolated radiance as a function of the lookup table's wavelength grid, which is then resampled onto the wavelength grid of the observed spectrum using cubic spline interpolation. The derivative of this interpolation procedure produces the needed Jacobians.

In order to keep the interpolation procedure simple and efficient, the LUT uses a wavelength-independent scene albedo. Within the inversion procedure, only a wavelength-independent albedo

is fitted, and the possible wavelength dependence of the spectrally-smooth variation of the measured radiance is taken into account via the fit of a polynomial of which the constant term is neglected.

In order for the lookup table approach to be faster than the online algorithm, frequent hard disk access must be avoided. Because all forward model parameters, except for the time of year, vary rapidly within a single orbit file, this restriction translates into the requirement that the radiances for the full range of those parameters fit in memory. This puts a limit on the density of the table's parameter grid, and some experimentation is necessary to obtain a grid which fits in memory and produces accurate interpolation results over the whole parameter space. To save space, the parameter grid does not include a longitudinal dimension. The precalculated radiances are therefore based solely on the MLS/sonde profile database, which has no longitudinal dependence, and do not take into account the tropospheric climatology OMI/MLS, which would be used in the online approach (section above). After the retrieval, we use the averaging kernels and the difference between the profile used in the lookup table and a more accurate profile which matches the tropospheric column prescribed by the OMI/MLS climatology, to apply a correction to the retrieved total column. Using these techniques, we have managed to construct a lookup table which reproduces the retrieved columns of the online algorithm with an accuracy better than 1%, and a tenfold performance improvement.

3.1.2.7 Inversion scheme

GODFIT is a direct fitting algorithm, using iterative non-linear least squares minimization. In the scientific prototype version mostly used for Ozone_cci work, the optimal estimation inverse method is being used with loose a priori regularization on the state vector elements. The optimal estimation method is well known *(C. D. Rodgers 2000)*; we minimize the quadratic functional cost function:

$$\chi^2 = (y_{meas} - f(x))^T S_y^{-1}(y_{meas} - f(x)) + (x - x_a)^T S_a^{-1}(x - x_a) \qquad \text{Eq. (2)}$$

Here, we have the measurement vector of TOA radiances y_{meas}, the state vector x, the forward model simulations $f(x)$, and the error covariance matrix S_y. x_a Is the a priori state vector, with S_a the corresponding covariance matrix. The inversion proceeds iteratively via a series of linearizations about the atmospheric state at each iteration step:

$$x_{i+1} = x_a + D_y[y_{meas} - f(x_i) - K_i(x - x_a)] \qquad \text{Eq. (3)}$$

Where:

$$D_y = S_{i+1}K_i^T S_y^{-1} \quad \text{and} \quad S_{i+1} = \left(K_i^T S_y^{-1} K_i + S_a^{-1}\right)^{-1} \qquad \text{Eq. (4)}$$

$K_i = df(x_i)/dx_i$ is the matrix of Jacobians, D_y is the matrix of contribution functions, and S_{i+1} is the solution covariance matrix. The latter is the main diagnostic output. The iteration stops when one or more convergence criteria are met. The computation proceeds efficiently with an SVD (singular value decomposition) on the scaled matrix Jacobians. Since the total ozone inverse problem is not ill-posed, the regularization is only present to ensure numerical stability. The a priori constraints are

deliberately made very loose, so that the precision is not compromised in any serious way by a priori smoothing. The a priori vector is taken to be the initial state vector.

3.1.2.8 State vector and inverse model settings

There are typically 7 to 8 elements in the retrieval state vector, listed in Table 30, along with their initial value settings. Aside from total ozone, the algorithm fits the temperature-profile shift parameter, 3 polynomial coefficients for internal albedo closure, 2 amplitudes for the semi-empirical molecular Ring correction and the (optional) under sampling correction and an earthshine spectrum wavelength shift.

Table 30. Summary of fitting parameters for direct fitting total ozone algorithm.

State Vector Element Type	# of parameters	Initial Value
Total ozone (unit: [DU])	1	Previous-pixel
Polynomial Coefficient (Internal Closure)	3	R_{335}, 0.0, 0.0
T-shift (unit: [K])	1	0.0
Ring Fraunhofer	1	1.0
Earthshine Shift (unit: [nm])	1	0.008
Undersampling	1	0.0

The total ozone first guess is taken from the previous pixel value. If this value is not available for some reason, the initial total ozone column is taken from a zonal averaged climatology based on TOMS data (Stolarski and Frith 2006). For closure, the initial value R_{335} is extracted from the surface albedo database at 335 nm as described in Section 2.4.1; other albedo parameters are initialized to zero. Initial values of the under-sampling and T-shift parameters are all zero, while the earthshine shift is initialized to 0.008 corresponding to the average Doppler shift due to the platform speed of around 7000 m/s.

3.1.2.9 Soft-calibration of level-1 reflectance's and post-correction of L2 data

Although a common group of retrieval settings are applied consistently to all level-1 data sets from GOME, SCIAMACHY and GOME-2A/B and OMI, systematic differences between the individual total ozone data sets remain. These originate from systematic radiometric errors and degradation effects affecting the measured level-1 reflectance's. To deal with these patterns and enhance the inter-sensor consistency, a soft-calibration scheme has been developed. This procedure relies on comparisons of measured level-1 reflectance's to simulated values in the spectral interval 325-335 nm, the simulations being performed with the same forward model as that used for the retrievals.

Experience and validation have shown that level-2 total ozone data sets produced from the GOME and OMI sensors have an excellent temporal stability, are very consistent with each other and also with ground-based instruments without any need for external soft-calibration. Note however that wavelength-independent correction factors need to be applied to the GOME reflectances in the O_3 fitting window if the absolute radiometric calibration is exploited to derive information on the

effective reflectivity of the scene. Those corrections factors are derived relatively with respect to measurements carried out at the beginning of the mission over a few reference scenes.

To ensure consistency of the other total O_3 data sets with those two instruments, the GOME and OMI ozone columns in a reference sector in the Pacific Ocean have been used as an external reference to realize the simulations within the soft-calibration scheme. The systematic comparison of the level-1 and simulated reflectance's for all satellite observations co-located with the reference O_3 columns allows to identify and characterize possible (broad-band or high-frequency) artefacts in the measured spectra. Based on this analysis, lookup tables (LUTs) of spectral correction factors have been constructed for SCIAMACHY and GOME-2A/B using all computed satellite/simulation reflectance ratios. These LUTs have 3 dimensions: one for the time and two for the viewing and solar zenith angles. Before the total ozone retrieval, the level-1 reflectance is multiplied by the appropriate correction factor spectrum. More details on this soft-calibration scheme are given in Lerot et al. (2014*)*. In the past, a first version of the initial soft-calibration scheme relied on Brewer measurements. We use now the GOME and OMI data sets as the reference, which allows to restore the independency of the satellite data sets with respect to ground-based observations. The reference needs to be available when reprocessing or updating the L2 data sets requiring a soft-calibration. The production of GOME and OMI total ozone data sets is therefore the first step in the C3S L2 total ozone processing chain as illustrated in Figure 3. Then soft-calibration factors are computed for all other sensors and corresponding L2 data sets are finally produced.

The produced L2 data set from OMPS –NM L1 data shows obvious "stripes", i.e. a significant variability of the total ozone column retrieved as a function of the row. Those stripes appear to present a relatively systematic pattern as a function of the row. This is attributed to the coarse spectral resolution of OMPS, leading to an inaccurate spectral wavelength calibration. To circumvent this, a post correction is applied to the retrieved columns by adding systematic offset values, which have been beforehand determined.

Figure 3 - C3S processing chain for generating the L2 total ozone products when soft-calibration of L1 data is required.

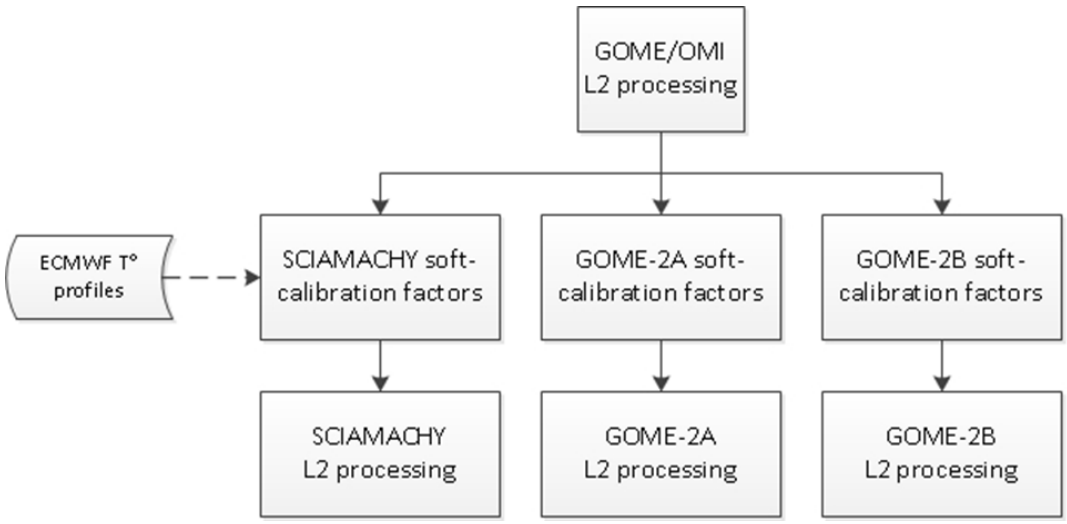

3.1.2.10 Averaging kernels

In optimal estimation, the averaging kernel A is defined as the product of the contribution function matrix D_y and the Jacobian matrix K. Generally speaking, it is a measure of the departure of the estimator from the truth and the dependence on a priori settings. For the total column retrieval, the problem is well-posed. Accordingly, the averaging kernel matrix reduces to a vector that indicates the sensitivity of the retrieved total column to changes in ozone concentration in different layers. We calculate the averaging kernel as follows. At each wavelength, LIDORT is called to derive the ozone profile layer Jacobians K* using the ozone a priori profile corresponding to the final retrieved total column. The contribution function D_y is obtained making use of the column weighting function K_i calculated as part of the retrieval process. The averaging kernel is then given by $A = D_y K^*$.

When using the LUT approach, calculating the averaging kernels would require that all Jacobians at all wavelengths are stored in a table, too, which would multiply the size of the table, again making it impossible to keep all the required data in memory. Therefore, we chose to store precomputed averaging kernels for each grid point, fixing the fitted forward model parameters which are not part of the lookup table grid (closure, Ring amplitude and wavelength shift) at their initial values. We found that this approximation does not have any significant impact.

3.1.2.11 Error budget

Table 31 summarizes our current assessment of the main contributions to the global error budget on total ozone retrieval by direct-fitting. The error budget is given separately in two different regimes, corresponding respectively to low (<80°) and large (>80°) values of the SZA.

Table 31. Estimation of the error sources of the direct-fitting total ozone retrievals (single pixel retrieval).

Error source	Per cent error	
	SZA < 80°	**SZA > 80°**
Instrument signal-to-noise [a]	< 0.5	< 2
Soft calibration: Absolute recalibration + structures removal [b]	< 1.5	< 1.5
O_3 absorption cross-sections and its atmospheric temperature [b]	< 2.5	< 2.5
Interferences with other species (except in case of volcanic eruption)[b]	< 1.5	< 1
Aerosols (except in case of volcanic eruption)[b]	< 1	< 1.5
Instrument spectral stability (wavelength registration)[b]	< 0.5	< 0.5
Solar-I_0 effect [b]	< 0.2	< 0.2
Ring effect (rotational Raman scattering)[b]	< 0.1	< 0.5
O_3 profile shape [b]	< 1	< 4
Cloud fraction [c]	< 0.5	< 0.5
Cloud top height [c]	< 1.5	< 1.5
Total random error (including cloud fields)	**< 1.7**	**< 2.6**
Total systematic error	**< 3.6**	**< 5.3**

[a] random error (precision) associated with instrument's noise. This error can be derived by the propagation of radiance and irradiance statistical errors provided in the level-1 products

[b] systematic errors

[c] random or systematic errors depending on the time scale

It includes the random error (or precision) associated with instrument signal-to-noise and which can be derived easily by the propagation of radiance and irradiance statistical errors provided in the level-1 products through the inversion algorithm. It is generally less than 0.5% at moderate SZAs and may reach 2% at SZAs larger than 80°.

The smoothing error associated to the a priori ozone profile shape used in the forward model is assessed using the formalism of Rodgers (Rodgers, 2000). Once we have the averaging kernel *A*, the error S_p due to the profile shape may be estimated as $S_p = A^T S_a A$ where S_a is the covariance matrix associated with the *a priori* profile climatology used in the inversion. What is really required here is the covariance associated with the particular retrieved total column for a specific latitude band and season. Covariance matrices associated to the MLS/Sonde climatology have been constructed allowing an estimate of S_p on a pixel-per-pixel basis. As illustrated in Figure 4, the mean total ozone

error due to the profile shape is generally less than 1% at low SZAs and is as large as 5% at extreme SZAs.

Figure 4 - Mean total ozone error due to a priori O_3 profile shape, as a function of the SZA.

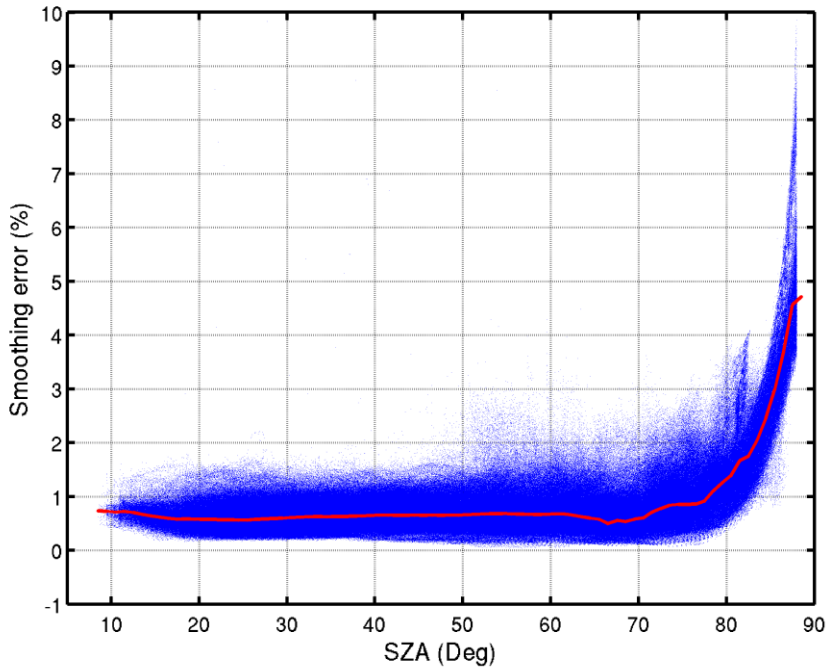

In GODFIT, both absorption by trace gases other than ozone and the impact of aerosols are neglected in the forward model. Here, we estimate the resulting total ozone errors using closed-loop tests. Synthetic radiances are generated using the GODFIT forward model based on optical inputs that include these sources of error (e.g. NO_2 or aerosols). Then, total ozone retrieval is performed using these synthetic spectra and the retrieval settings baseline (i.e. neglecting other trace gases or aerosols in the forward model). The difference with respect to the "true" state gives the error estimate.

To simulate the impact of stratospheric NO_2, a typical stratospheric profile as depicted in Figure 5 has been used to generate synthetic radiances. Total ozone columns retrieved from the resulting synthetic spectra show errors of less than 0.5% for all SZAs and all surface albedos. When considering a profile with a large amount of NO_2 in the lowermost layer (e.g. representative of a heavily polluted scenario), total ozone errors increase slightly but are still less than 0.5% for low surface albedo (0.05). The errors are slightly larger than 1% when the surface albedo is high (0.8), but the likelihood of such a high NO_2 concentration above a bright surface is very small. Similar sensitivity tests have been carried out for BrO and SO_2. The errors due to their neglect are generally negligible, except for a major volcanic eruption scenario with SO_2 column amounts exceeding 50-100 DU. In this case, total ozone errors may reach a few percent.

Figure 5 - (a) NO_2 vertical profiles used for generating synthetic radiances. (b) Total ozone error (%) due to neglect of NO_2 in the retrieval scheme, as a function of SZA. For the two profiles shown in (a), ozone errors are plotted for low and high surface albedos (0.05 and 0.8) and for a total ozone column of 400 DU.

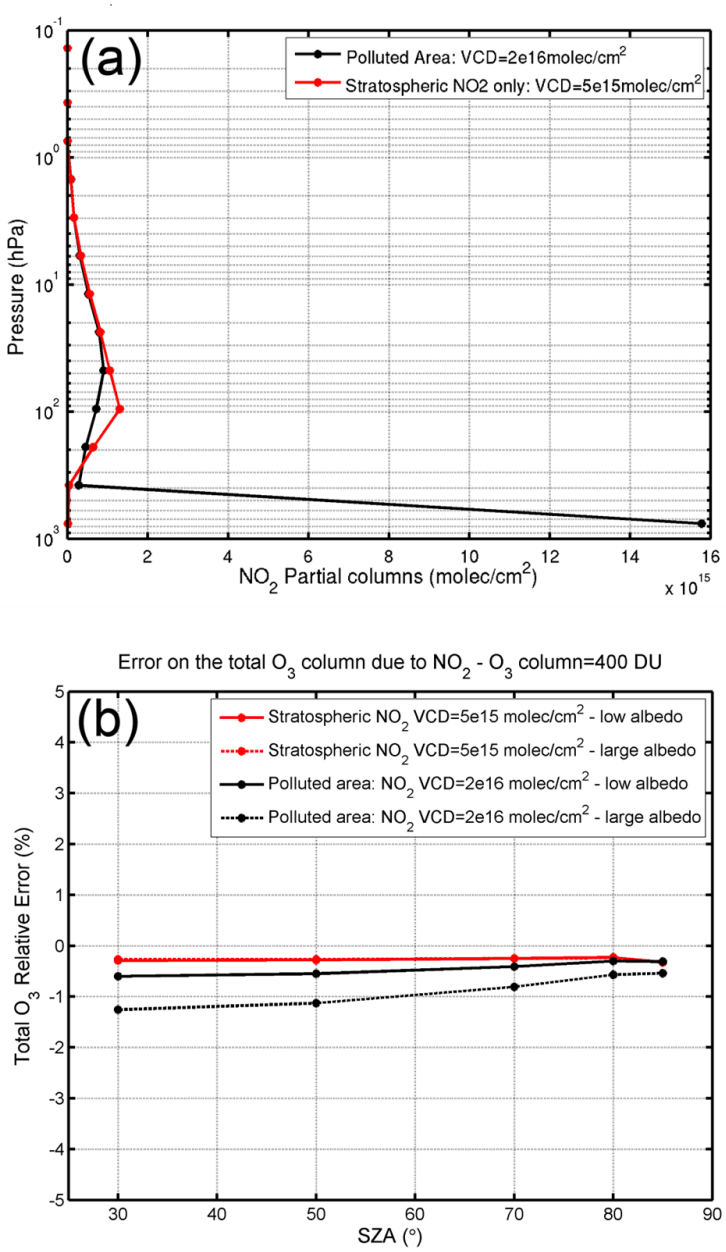

The same closed-loop approach has been adopted to estimate the ozone error due to neglect of aerosols in the forward model. A number of scenarios were considered, including a background aerosol case, a heavily polluted scenario with a large amount of absorbing aerosol in the lowermost layer, a dust storm scenario with a large amount of scattering aerosol in the lowermost layer and finally, two scenarios representing major volcanic eruptions with stratospheric injections of absorbing

or scattering aerosols. Optical property profiles for these scenarios are plotted in Figure 6 (a-b). The associated total ozone errors, plotted as a function of SZA in Figure 6 (c), are generally within 1%. This small impact is mainly due to the simultaneous fit of the effective surface albedo. As seen in Figure 6 (c) for the pollution scenario, total ozone errors are much larger (up to 4%) if the surface albedo is fixed to a climatological value. This nicely illustrates the added value of the internal closure mode of GODFIT, which implicitly accounts for tropospheric absorbing and scattering aerosols and avoids relying on the ingestion of highly uncertain external aerosol optical property information. For a scenario with a strong injection of stratospheric aerosols due to a major volcanic eruption such as Pinatubo, the total errors may reach 10% Figure 6 (d).

Other uncertainty estimates have been derived from similar sensitivity test studies carried out within previous projects (GODFIT A/B, GDP4 and GDP5) or extensively described in Lerot et al. (2014). Total errors are computed assuming all contributions are mutually uncorrelated. The total random errors are estimated to be 1.7 and 2.6 % for the low/moderate and high SZA regimes respectively. The corresponding total systematic errors are less than 3% and 5.7%. Note that this error budget is quite conservative and validation studies show that differences between satellite and ground-based total ozone columns are generally less than 1%.

Figure 6 - (a) Aerosol optical depth and (b) aerosol single scattering profiles used for generating synthetic radiances for a variety of scenarios (see inset and text for more details). (c) Total ozone error (%) due to neglect of aerosols in the retrieval scheme, plotted as a function of SZA for the background, polluted and dust storm scenarios. The red dashed line shows the much larger errors obtained when a fixed (non-fitted) albedo is used. (d) Same as (c) but for strong volcanic eruption scenarios.

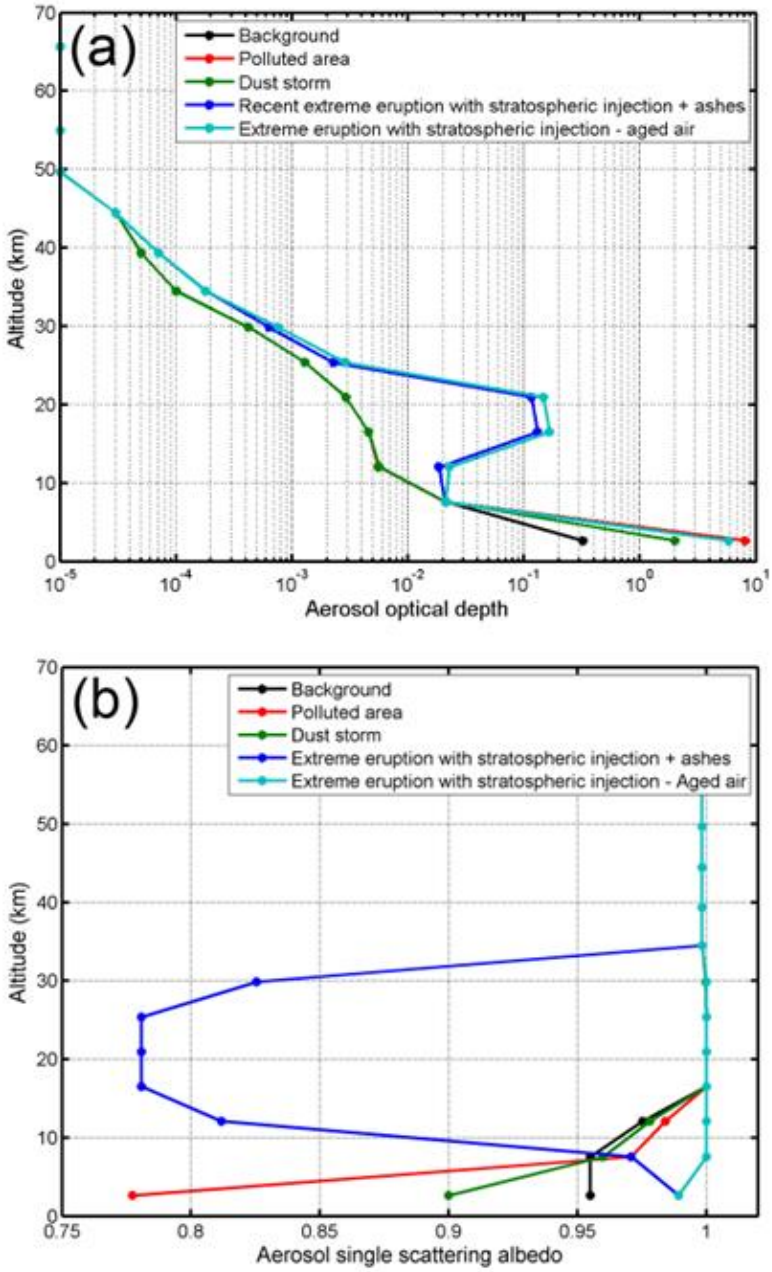

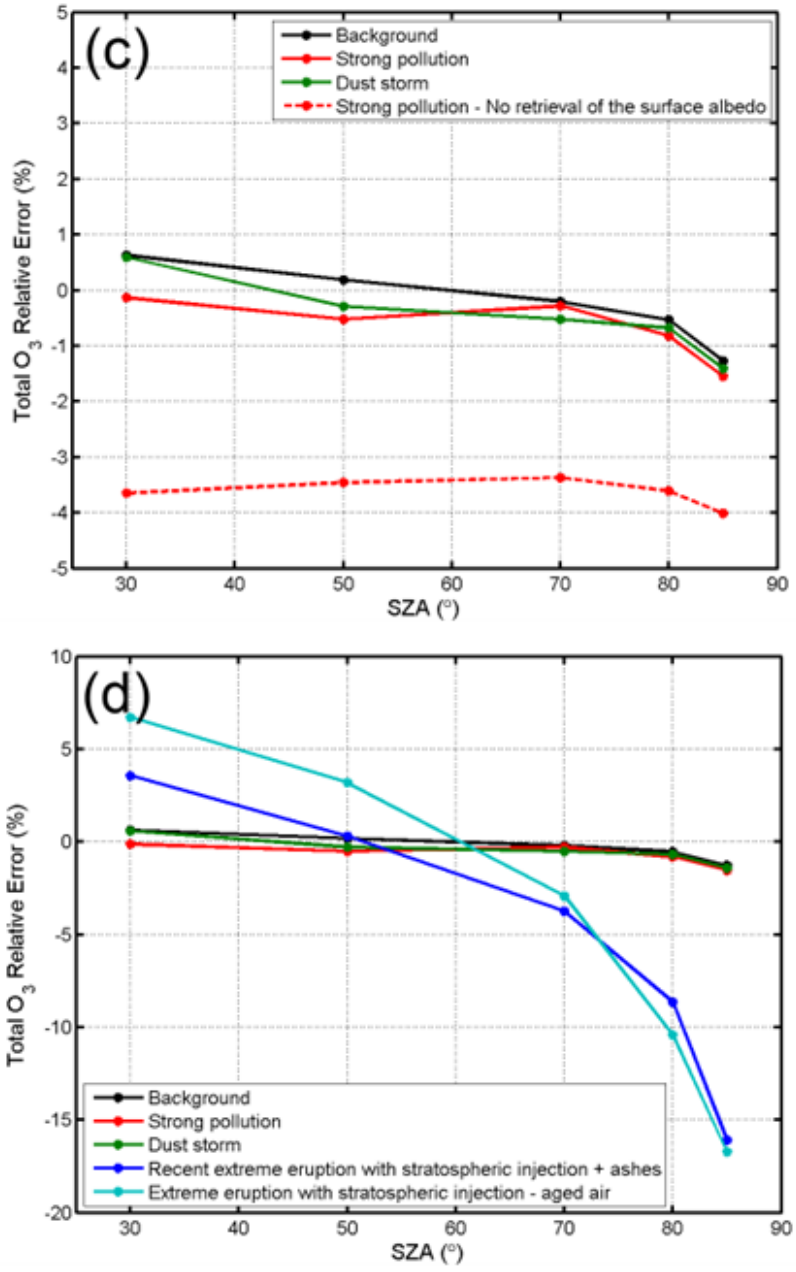

3.1.2.12 Output parameters

Level-2 total ozone column data sets derived from the sensors GOME/ERS-2, SCIAMACHY/ENVISAT, GOME-2/Metop-A, GOME-2/Metop-B and OMI/AURA have been processed with the retrieval algorithm GODFIT. The data sets are provided for the complete instrumental time series, under the condition of availability of the input parameters, and are based on the latest level-1 data (see Table 32).

Table 32. Time coverage of the Ozone_cci total ozone level-2 data sets and level-1 versions used in the processing chains.

Platform/Sensor	Time coverage	Level-1 data
ERS-2/GOME	Jul. 1995 – Jun. 2011	ESA L1 v4.00/4.01/4.03
Envisat/SCIAMACHY	Aug. 2002 – Apr. 2012	ESA L1 v8.0x
Metop-A/GOME-2	Jan. 2007 – Nov. 2021	Eumetsat L1 v5.12/6.12
Metop-B/GOME-2	Jan. 2013 – Dec. 2022	Eumetsat L1 v5.12/6.12
Metop-C/GOME-2	Jan. 2019 – Dec. 2022	Eumetsat L1 v5.12/6.12
Aura/OMI	Oct. 2004 – Dec. 2022	NASA Collection 3
Suomi-NPP/OMPS-NM	Jan 2012 – Dec. 2022	NASA V2.0
Sentinel-5P/TROPOMI	Apr 2018 – Dec. 2022	ESA V02.01

There is one ozone column measurement per ground pixel observed by the sensor and the level-2 data sets are distributed via NetCDF files (one file per orbit). For each measurement, geolocation information, auxiliary and additional fitted parameters, quality indicators, a-priori O_3 profile shape and averaging kernels are also provided in the output files. Table 33 describes the main output variables generated by the level-2 processor.

Table 33. Dimension and description of all variables contained in the UV nadir L2 total ozone NetCDF files. N_p represents the total number of measurements for scanning instruments (GOME, SCIAMACHY, GOME-2) and the number of viewing lines for imaging instruments (OMI). N_r is the number of rows for imaging instruments (60 for OMI; 36 for OMPS) and is 1 for scanning instruments.

Variable Name	Unit	Dimension	Description
total_ozone_column	mol.m-2	N_p x N_r	Retrieved total ozone column
Total_ozone_column_ random_error	mol.m-2	N_p x N_r	Random error associated to the retrieved total column
Total_ozone_column_ smoothing_error	mol.m-2	N_p x N_r	Error due to the a priori profile associated to the retrieved total column
ozone_ghost_column	mol.m-2	N_p x N_r	Partial ozone column comprised between the ground and the effective surface
fitted_ring_coefficient	-	N_p x N_r	Retrieved Ring scaling parameter
effective_temperature	°K	N_p x N_r	Retrieved effective temperature
fitted_state_vector	Various	8 x N_p x N_r	Full fitted state vector (Total O3, T°-shift, 4 polynomial coefficients, Ring scale factor, Radiance wavelength shift)
effective_scene_pressure	hPa	N_p x N_r	Pressure at the effective scene used for the retrieval
effective_scene_albedo	-	N_p x N_r	Retrieved effective albedo of the scene

Variable Name	Unit	Dimension	Description
rms	-	N_p x N_r	Root mean square of fit residuals
reduced_chi_squared	-	N_p x N_r	Reduced chi-square of the fit
nb_of_iterations	-	N_p x N_r	Number of iterations before convergence
convergence_flag	-	N_p x N_r	Convergence flag: 0 for failure, 1 for success
processing_flags	-	N_p x N_r	0: Nominal mode; 1: irregular L1 data - No retrieval; 2: Solar zenith angle larger than 89° - No retrieval; 3: No cloud data - No retrieval; 8: Forward model failure - No retrieval; 9: inversion failure - No retrieval; 21: Pixel affected by row anomaly - No retrieval; 22-24: Pixel might be affected by row anomaly - uncertain output
atmosphere_ pressure_grid	hPa	15 x N_p x N_r	Pressure at levels defining the layers used in the forward model
averaging_kernels	-	14 x N_p x N_r	Averaging kernels in the layers of the forward model
apriori_ozone_profile	mol.m-2	14 x N_p x N_r	A-priori partial ozone columns in the layers of the forward model

Figure 7 shows an example of total ozone columns retrieved from one day of GOME-2/Metop-A observations.

Figure 7 - Total ozone columns retrieved from GOME-2/Metop-A observations on 1st November 2007.

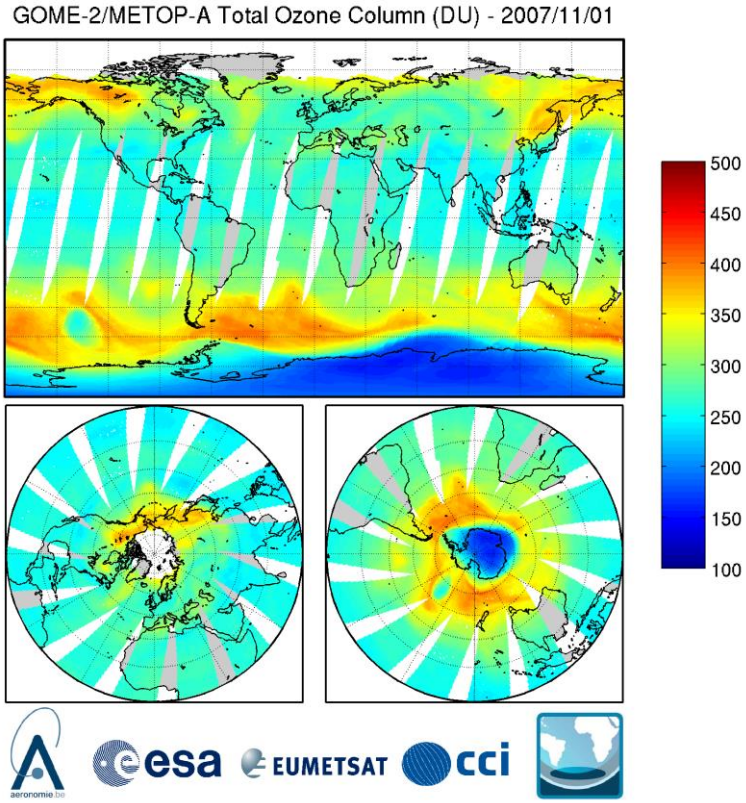

The delivered Net-CDF files contain only measurements for which the convergence has been reached with a number of iterations less than 6 (the typical number of iterations is 3-4). No retrieval is performed for pixels with solar zenith angle larger than 89°. The quality of the total ozone measurements following some specific instrumental operations (e.g. decontamination episodes) may be degraded. These measurements are in general easily detectable and have already been filtered out from the delivered level-2 data sets.

An estimation of the random error is associated to each total ozone column given in the product. This value has been derived via propagation of the level-1 radiance and irradiance statistical errors throughout the inversion algorithm. The reduced chi-squared value is a good indicator of the consistency between the fit residuals and the level-1 errors. Assuming perfectly estimated level-1 errors, the reduced chi-squared will be very close to 1 for a fit without any systematic structures in its residuals. In practice, they are generally ranging between 0.3 and 3. The root mean-squared (RMS) of the fit residuals is another indicator of the fit quality, but does not provide any hint on the nature of the residuals (random or systematic).

As mentioned above, the averaging kernels are also provided for all measurements. They represent the sensitivity of the total column retrieval to a real change in the ozone concentration at a given layer, considering both the observation geometry and the algorithmic features. At low and mid-latitudes, these averaging kernels are generally close to 1 in the stratosphere and upper troposphere

and decrease for the lowermost layers, depending on the surface albedo and cloud contamination. At higher solar zenith angles, they change more rapidly with the altitude, making the retrieval quality much more dependent on the a priori profile shape information. Typical averaging kernels are illustrated in Figure 8 for one GOME orbit. The black dots represent the pressure of the effective scene considered for the total ozone retrieval. A smoothing error estimate is also provided in the level-2 files, which represents the impact of the a priori profile shape on the retrieved column. This is computed using both the averaging kernel and the covariance matrices associated to the a priori profile climatology.

Figure 8 - Typical averaging kernels of total ozone retrievals for one GOME orbit. The black dots represent the pressure of the effective scenes considered.

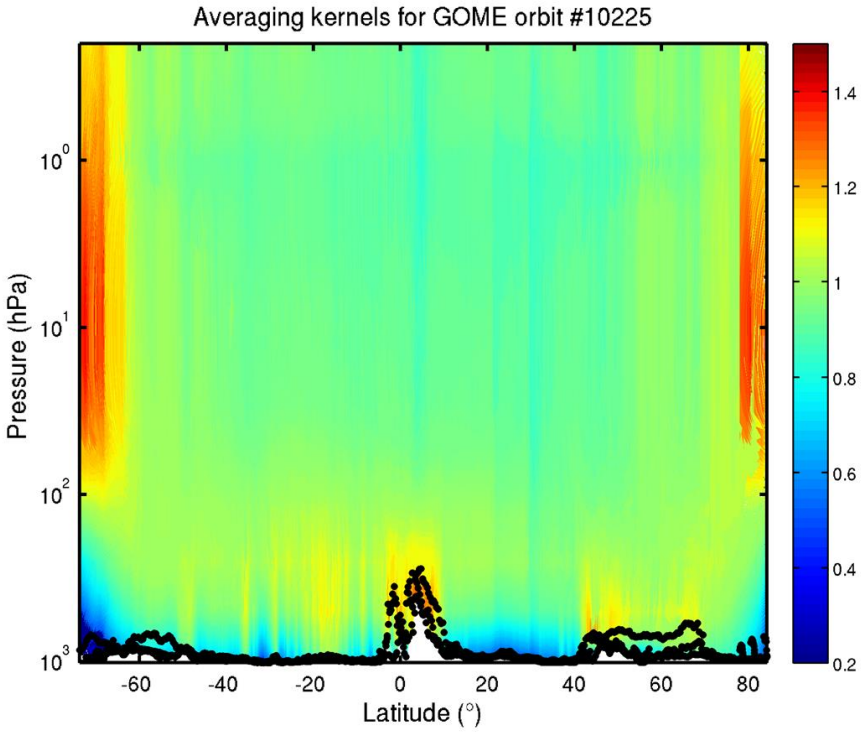

3.1.3 Level 2 to Level 3

3.1.3.1 Total ozone level 3 data from individual sensors

Level 2 ozone column measurements per ground pixel (see Section 3.1.2) serve as input to the level 3 algorithm which is designed to map the level 2 measurements onto a fixed global grid of 1° x 1° in latitude and longitude. This spatial resolution has been selected according to specific requirements of GCOS, IGACO, and WMO for total ozone. Each daily level 3 grid cell contains an average of all level 2 data from the same GMT day that overlap with this cell. Cell values are computed as weighted averages in which the fractional area of overlap of the satellite ground pixel with the given grid cell is used as weight. Level 2 data can be mapped onto more than one grid cell. The daily level 3 gridding algorithm is applied separately to GOME/ERS-2, SCIAMACHY/ENVISAT, GOME-2/Metop-A, GOME-

2/Metop-B, OMPS/SNPP and OMI/AURA measurements. The final step is the calculation of monthly means. In order to provide representative values that contain a sufficient number of measurements equally distributed over all days in a month, cut-off values for latitude as a function of month have been defined (see Table 34). In addition to total ozone column information the delivered NetCDF files contain the sample standard deviation, an estimate of the standard error, and the number of measurements used to calculate the monthly mean ozone column. The estimate of the standard error is derived using the standard deviation, the number of measurements, and a multiplicative factor which accounts for the spatial and temporal sampling patterns of the individual sensors. We provide one NetCDF file per month. An overview of the variables (description and dimension) contained in the NetCDF files is given in Table 35 and an overview of the time coverage and update frequency of the individual data sets is presented in

Table 36.

Table 34. Cut-off values for latitude as a function of month for the individual and merged UV nadir level 3 monthly mean total ozone products.

Month	Latitudes	Month	Latitudes
January	60.0° N – 90.0° S	July	90.0° N – 57.5° S
February	70.0° N – 90.0° S	August	90.0° N – 62.5° S
March	80.0° N – 80.0° S	September	82.5° N – 72.5° S
April	90.0° N – 65.0° S	October	72.5° N – 85.0° S
May	90.0° N – 60.0° S	November	65.0° N – 90.0° S
June	90.0° N – 57.5° S	December	60.0° N – 90.0° S

Table 35. Dimension and description of the variables contained in the individual and merged UV nadir level 3 total ozone NetCDF files. N_{lat} (=180) is the number of latitudes and N_{lon} (=360) is the number of longitudes.

Variable Name	Unit	Dimension	Description
latitude	degree	N_{lat}	Latitude of grid center
longitude	degree	N_{lon}	Longitude of grid center
total_ozone_column	mol.m-2	N_{lat} x N_{lon}	Monthly mean total ozone column
total_ozone_column_ standard_deviation	mol.m-2	N_{lat} x N_{lon}	Sample standard deviation of mean total ozone column
total_ozone_column_ standard_error	mol.m-2	N_{lat} x N_{lon}	Estimated standard error of mean total ozone column
number_of_measurements	-	N_{lat} x N_{lon}	Number of measurements used to derive the monthly mean total ozone column

Table 36. Time coverage and update frequency of the UV nadir total ozone level 3 data sets.

Sensor/Platform	Time coverage	Update frequency
GOME/ERS-2	Jul. 1995 – Jun. 2011	N/A
SCIAMACHY/ENVISAT	Aug. 2002 – Apr. 2012	N/A
OMI/AURA	Oct. 2004 – now	Quarterly
GOME-2/MetOp-A	Jan. 2007 – Nov. 2021	Quarterly
GOME-2/MetOp-B	Jan. 2013 – now	Quarterly
GOME-2/MetOp-C	Jul. 2019 – now	Quarterly
OMPS/SNPP	Jan. 2012 – now	Quarterly
TROPOMI/S5P	Apr. 2018 - now	Quarterly
GTO-ECV Merged	Jul. 1995 – now	semi-annually

3.1.3.2 Merged GOME-type total ozone (GTO-ECV)

Within the second phase of ESA's Ozone_cci project an algorithm has been developed by DLR-IMF for the creation of a level 3 monthly mean merged homogeneous total ozone product combining measurements from the five sensors GOME/ERS-2, SCIAMACHY/Envisat, GOME-2/Metop-A, GOME-2/Metop-B, and OMI/Aura. This subsection is dedicated to the illustration of the selected merging approach. A detailed description of the algorithm can also be found in the Ozone_cci ATBD [D22], in Coldewey-Egbers et al. (2015), and in Garane et al. (2018). Note that OMPS/SNPP data are not included in GTO-ECV.

Level 3 daily data on a 1°x1° grid from the individual sensors – as described in Section 3.1.3.1 – serve as input to the merging algorithm. In order to minimize the differences between the individual products a so-called inter-satellite calibration approach is applied before assembling the data records. OMI/AURA in combination with GOME/ERS-2 is used as a long-term reference in which GOME has first been adjusted to OMI based on comparisons during the overlap period from 2004 to 2011. Next, SCIAMACHY and both GOME-2 data records are adjusted to this reference. For GOME and SCIAMACHY the correction factors with respect to the reference data set depend on latitude and month of the year, i.e., they are constant for all years. For the GOME-2 sensors an additional time-dependence in the correction factors has been imposed since the differences between GOME-2 and the reference indicate a small drift. For all sensors the calculation of the correction factors with respect to the reference is based on comparing 1° monthly zonal means. These pair-wise monthly zonal means are based on collocated daily 1°x1° data in order to minimize differences due to differences in spatial and temporal sampling. Subsequently the correction factors are applied to daily gridded data in which the correction factors are linearly interpolated in time. Despite of all sensors having different equator crossing times, diurnal changes of ozone are not considered in the calibration approach.

Finally, the five individual data sets are averaged on a daily basis and combined into one single record. The last step is the calculation of monthly means. In order to provide representative values that contain a sufficient number of measurements equally distributed over all days in a month, the same cut-off values for latitude as for the individual level 3 products are used for the merged product (see Table 34). In addition to total ozone column information, the standard deviation, an estimate of the standard error, and the total number of measurements used to derive the monthly mean are

provided in the NetCDF files. An overview of the variables (description and dimension) contained in the NetCDF files is given in Table 35. We generate and deliver one NetCDF file per month and the time coverage for the merged product is July 1995 to present. This data product will be updated and extended on a semi-annual basis. Figure 9 shows an example for the merged product (total ozone, standard deviation, and number of available measurements per month) with data from October 2014. Figure 10 shows the total ozone column as a function of latitude and time for the entire period from July 1995 to October 2018.

Figure 9 - GTO-ECV level 3 product for October 2014; left: total ozone column, middle: standard deviation, and right: number of measurements in this month.

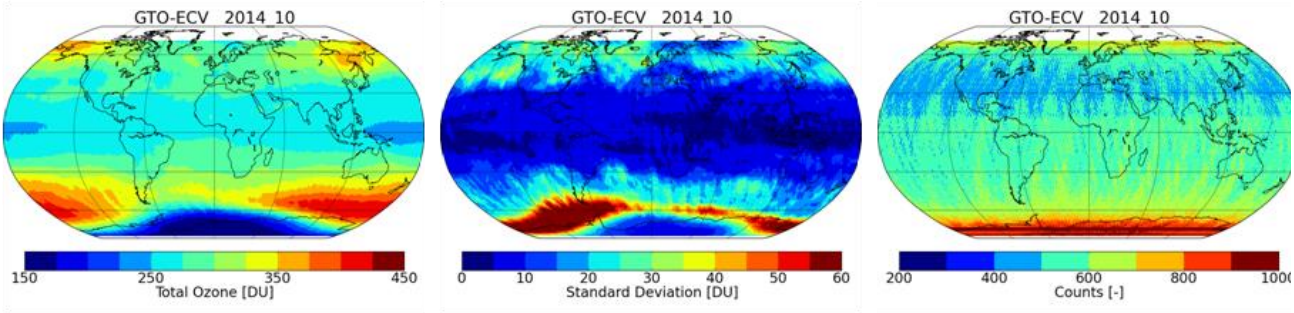

Figure 10 - GTO-ECV level 3 product: total ozone column as a function of latitude and time (07/1995 - 10/2021).

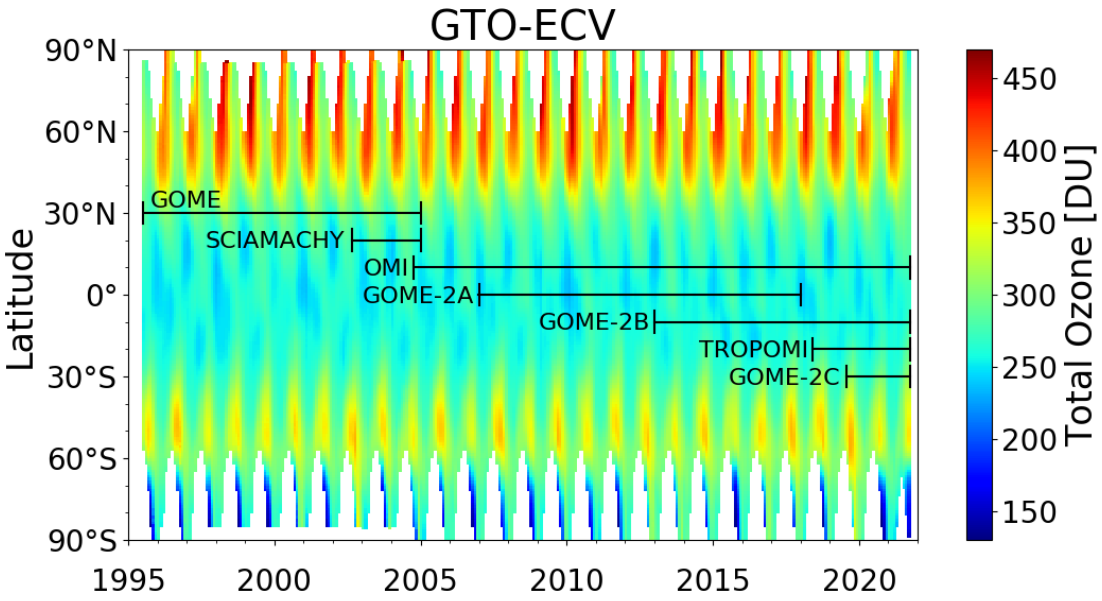

3.1.4 Level 2 to Level 4 – Multi-sensor reanalysis (MSR)

3.1.4.1 Correcting the satellite level 2 dataset

For long-term accuracy and consistency it is crucial to reduce offsets, trends and long-term variations in the satellite data, so that the data can be used as input to the assimilation scheme with minimized biases and with known standard deviations. As in the first version of the ozone multi sensor reanalysis (MSR1), the parameters fitted to correct for the ozone differences (satellite minus ground-based observation) are the Solar Zenith Angle (SZA), the Viewing Zenith Angle (VZA), the effective temperature of stratospheric ozone, time and an offset (with reference year 2000). New compared to the MSR1 correction is the inclusion of a 2nd order SZA correction, since most satellite data sets show a non-linear SZA dependence for low solar elevation angles. A basic assumption is that all corrections are additive to the total ozone amount. By fitting all data together, regional biases that may be caused by offsets of individual ground instruments are avoided. For each satellite product an "overpass" dataset is created for all ground stations and a maximum allowed distance between the centre of the ground pixel and the ground station is defined. This number is typically 50-200 km depending on the ground pixel size. These overpass datasets are fitted to the ground data for the 5 free parameters.

The relevant regression parameters, i.e. those that reduce the RMS (Root Mean Square) between satellite and ground-based observations significantly, are used. The TOMS-EP dataset is corrected for a trend for the last two years only, so this dataset is divided in two. The datasets that show a non-linear dependence on VZA are corrected on a "per pixel" basis. Note that the (S) BUV instruments perform only nadir measurements and the VZA dependence is therefore absent.

Based on the calculated corrections the merged MSR2 level 2 dataset is created. The original satellite datasets were read, filtered for bad data, corrected, and finally merged into a single time ordered dataset. Essential information in the MSR2 level 2 dataset is time, location, satellite id and ozone. In the data assimilation the satellite id is used to assign a corresponding measurement error to this observation. After applying this bias correction procedure, the trend, offset, and seasonal cycle in the satellite observations have been reduced to a negligible level in the MSR2 level 2 data.

3.1.4.2 Ozone model and data assimilation

The chemistry-transport model used is a simplified version of TM5 (Krol et al., 2005; Huijnen et al., 2010), which is driven by ECMWF analyses of wind, pressure and temperature fields. The model is using only one tracer for ozone and a parameterization for the chemical modelling. The assimilation approach is an extension of the work described in Eskes et al., 2005. As input the assimilation uses ozone column values and estimates of the measurement uncertainty. The ozone model setup and data assimilation scheme in TMDAM have been described in van der A et al. (2015), and we refer to this paper for more details.

Several improvements were developed to improve the MSR data for the period before 1979 when few observations were available and the Chlorine content in the atmosphere was less. To have a single algorithm for the whole period, the improvements are also in use for the recent years of the MSR. The improvements consisted of the following 3 adjustments:

Heterogeneous chemistry

The Cariolle parametrisation of chemistry has been adapted so that it is functioning before the era of the ozone hole, when CFC concentrations were less. The EESC (Equivalent Effective Stratospheric Chlorine) dependent heterogeneous chemical destruction of stratospheric ozone factor was incorporated within the exponent of the ozone depletion term following the Braesicke scheme. For the EESC, we collected the daily data of Newman et al. (2007).

Photolysis factor

For better results in the twilight zone, i.e. for Solar zenith angles (SZA) between 84.0-95.0 degrees, we multiply the photolysis with a factor (94.0 – SZA)/ (94.0 – 85.0).

Correlation length of the error in assimilated ozone

For sparse observations (which is the case before 1970) we use a longer and more realistic correlation length in the error covariance in order to increase the physical area which is affected by observations in the data assimilation. This improves the characterisation of the model error (growth) in order to optimal use the information of the observations. One year of assimilation in 2017 using only a sparse Dobson network is compared to the MSR2 (= 'truth') to recalculate the correlation length.

3.2 Ozone total and tropospheric column retrieval from IASI

3.2.1 Heritage

The algorithm used for the retrieval of Level-2 ozone data from Level-1 data collected by IASI nadir sensor is described in the Ozone_CCI ATBD [D22]. In the C3S Ozone project, the Level-2 ozone products serve as input to the generation of Level-3 ozone products (total and tropospheric ozone).

3.2.2 Level 1 to Level 2

The IASI ozone total and tropospheric column products are based on the FORLI (Fast Optimal/Operational Retrieval on Layers for IASI) algorithm v20151001. FORLI is a line-by-line radiative transfer model capable of processing in near-real-time the numerous radiance measurements made by the high-spatial and high-spectral resolution IASI, with the objective to provide global concentration distributions of atmospheric trace gases. Validation of IASI total and tropospheric O_3 retrieved from FORLI-O3 v20151001 was carried out by Boynard et al. (2016, 2018). Both papers report a good agreement between total ozone columns retrieved from IASI and UV independent measurements, with IASI slightly higher than UV observations by 1-2 % on average. The comparison with ozonesondes shows that IASI underestimates O_3 by ~10% in the troposphere.

This part describes the methods used for FORLI. Most is extracted from Hurtmans et al. (2012).

3.2.2.1 Basic retrieval equations

For the inversion step, it relies on a scheme based on the widely used Optimal Estimation theory (Rodgers, 2000).

The forward model equation can be written in a general way as

$$y = F(x; b) + \eta \quad \text{Eq. (5)}$$

where y is the measurement vector containing the measured radiance, x is the state vector containing the molecular concentrations to be retrieved, b represents all the other fixed parameters having an impact on the measurement (temperature, pressure, instrumental parameters...), η is the measurement noise and F is the forward radiative transfer function. The goal of the inverse problem is to find a state vector $\hat{x}$, approximating the true state x, which is most consistent with the measurement and with a certain prior knowledge of the atmospheric state. Specifically, the measured radiances y are combined with an *a priori* state x_a, and both are weighted by covariance matrices representative of their statistical variations, S_η and S_a.

For a linear problem, the retrieved state, solution of the Optimal Estimation, is given by

$$\hat{x} = x_a + \left(K^T S_\eta^{-1} K + S_a^{-1}\right)^{-1} K^T S_\eta^{-1} (y - K x_a) \quad \text{Eq. (6)}$$

Where K is the Jacobian of the forward model F, the rows of which are the derivatives of the spectrum with respect to the retrieved variables.

3.2.2.2 Assumptions, grid and sequence of operations

Spectral ranges

FORLI-O_3 v20151001 uses the Level 1C radiances disseminated by EumetCast. A subset of the spectral range, covering 1025–1075 cm^{-1}, is used for the O_3 retrieval. The spectral range used in the forward model is 960-1105 cm^{-1} and the spectral oversampling is 100.

Vertical grid

FORLI-O3 uses a vertical altitude grid in km.

Ozone state vector

The ozone product from FORLI is a profile retrieved on 40 1km-thick layers between surface and 40 km, with an extra layer from 40 km to TOA.

Other state vector elements

Besides the ozone profile, surface temperature and the water vapour column are retrieved.

Measurement covariance matrix

S_η is taken diagonal. The value of the noise is wavenumber dependent in the spectral range used for the retrieval, varying around 2 x 10^{-8} W/ (cm^2 cm^{-1} sr).

Iterations and convergence

We assume a moderately non-linear problem, where Eq. (6) is iteratively repeated using a Gauss-Newton method until convergence is achieved. For iteration:

$$x_{j+1} = x_a + \left(K_j^T S_\eta^{-1} K_j + S_a^{-1}\right)^{-1} K_j^T S_\eta^{-1}\left[y - F(x_j) + K(x_j - x_a)\right] \quad \text{Eq. (7)}$$

The gain matrix G is the matrix whose rows are the derivatives of the retrieved state with respect to the spectral points. From Eq. (6), it can be shown that

$$G = \left(K^T S_\eta^{-1} K + S_a^{-1}\right)^{-1} K^T S_\eta^{-1} \quad \text{Eq. (8)}$$

Convergence is achieved when

$$d_i^2 = [F(x_{i+1}) - F(x_i)]^T S_{\delta\hat{y}}^{-1} [F(x_{i+1}) - F(x_i)] \ll m \quad \text{Eq. (9)}$$

Where $S_{\delta\hat{y}} = S_\delta\left(\hat{K} S_a \hat{K}^T + S_\delta\right)^{-1} S_\delta$ and m is the degree of freedom.

3.2.2.3 Radiative Transfer Model (RTM)

General formulation

Ray tracing for upward flux

The Ray-tracing defines for off-nadir geometries the path s versus the altitude z. This path depends on the zenith angle of the beam (θ) as seen from the surface, which, under the approximation of a flat atmosphere, is equal to $\sec\theta$. Although the plane-parallel approximation could reasonably be applied for IASI at near-nadir, it is not adapted at larger viewing angles. The spherical shape of the Earth is explicitly accounted for in FORLI by including a local radius of curvature for the Earth $R_\oplus$ and the index of refraction of air. The elementary path is then written as

$$ds = \frac{n(z)(z + R_\oplus)dz}{\sqrt{n^2(z)(z + R_\oplus)^2 - R_\oplus^2 n^2(z_G)\sin\theta}} \quad \text{Eq. (10)}$$

Where $n(z)$ is the index of refraction of air at altitude z. The altitude dependency is expressed through the variation of temperature, pressure and humidity and is modelled using the Birch and Downs formulation (Birch and Downs, 1994). The index of refraction is considered constant in the IASI spectral range. In order to calculate the path along the line of sight, Eq. (10) is integrated using a numerical method, as no analytical closed form exists.

Radiative transfer

Local thermodynamic equilibrium is assumed. The monochromatic upwelling radiance at TOA is then calculated as

$$L^{\uparrow}(\tilde{\nu};\theta,z) = L^{\uparrow}(\tilde{\nu};\theta,0)\tau(\tilde{\nu};\theta,0,z) + \int_0^z J(\tilde{\nu},\Omega,z')\frac{\partial}{\partial z'}\tau(\tilde{\nu};\theta,z',z)dz' \qquad \text{Eq. (11)}$$

Where $L^{\uparrow}(\tilde{\nu};\theta,0)$ is the radiance at the start of the light path (i.e. that of the emitting surface) at wavenumber $\tilde{\nu}$ with a ground zenith angle θ, $\tau(\tilde{\nu};\theta,z',z)$ is the transmittance from altitudes z' to z, and $J(\tilde{\nu},\Omega,z')$ is the atmospheric source term which depends on both thermal emission and scattering.

For FORLI, only clear or almost-clear scenes (cloud fraction in the field--of--view (FOV) lower than typically 20%; see specific documents for CO, O_3 and HNO_3 for threshold values) are analysed and the atmosphere is therefore considered as a non-scattering medium. In that case J becomes independent on geometric angle, thus simplifying to the black-body emission function $B(\tilde{\nu},T)$.

The transmittance $\tau(\tilde{\nu};\theta,z',z)$ in Eq. (11) is related to the absorption coefficient κ by

$$\tau(\tilde{\nu};\theta,z',z) = exp\left[-\int_{z'}^{z}\sum_j \kappa_j(\tilde{\nu};z'')\rho_j(z'')\frac{\partial s(\theta,z'')}{\partial z''}dz''\right] \qquad \text{Eq. (12)}$$

Where j refers to a given gaseous species, $\rho_j(z'')$ is the molecular density of that species at altitude z'', and $s(\theta,z'')$ is the curvilinear path determined by the ray tracing. The absorption coefficient κ contains absorption features described by single spectral lines; regions affected by absorption of heavier species (where cross-sections would need to be used) are avoided. Also absorption continua are explicitly considered in the calculation of κ.

A precise calculation of the Earth's source function $L^{\uparrow}(\tilde{\nu};,\theta,0)$ in Eq. (11) has to be achieved to properly model the spectrum recorded at TOA. That term is basically governed by the black-body emission of the ground surface, modified, however, by the emissivity and reflectivity of that surface. Considering a surface of emissivity $\grave{o}(\tilde{\nu})$:

$$L^{\uparrow}(\tilde{\nu};\theta,0) = \grave{o}(\tilde{\nu})B(T_{skin}) + (1-\grave{o}(\tilde{\nu}))L_0^{\downarrow\dagger}(\tilde{\nu}) + \alpha(\tilde{\nu})L_0^{\downarrow\mathring{a}}(\tilde{\nu}) \qquad \text{Eq. (13)}$$

Where $B(T_{skin})$ is the ground black-body Planck function at the ground temperature T_{skin} ;

$$L_0^{\downarrow\dagger}(\tilde{\nu}) = \frac{1}{\pi}\int_0^{2\pi}d\varphi\int_0^{\pi/2}d\theta L_0^{\downarrow}(\tilde{\nu};\theta)\sin\theta\cos\theta \qquad \text{Eq. (14)}$$

is the mean radiance associated to the total downward flux reaching the surface, integrated upon all the geometries considering a Lambertian surface; $\alpha(\tilde{\nu})L_0^{\downarrow\mathring{a}}(\tilde{\nu})$ is the fraction of sun light that is retro-reflected in the direction of the sounding beam, which depends on the sun azimuthal angle and the surface effective reflectivity $\alpha(\tilde{\nu})$. In FORLI both contribution from Lambertian and specular reflections are explicitly taken into account, following

$$\alpha(\tilde{\nu}) = \left(\left(1 - \dot{\alpha}(\tilde{\nu})\right)\mu_{\delta 0} + \rho\mu_{glint}\right) 6.7995 \times 10^{-5} \quad \text{Eq. (15)}$$

With

$$\mu_{\delta 0} = \frac{\cos\theta^{\text{å}}}{\pi} \quad \text{Eq. (16)}$$

And

$$\mu_{glint} = \frac{\cos\theta + \cos\theta^{\text{å}}}{\sqrt{2[1 + \sin\theta^{\text{å}}\sin\theta\cos(\varphi - \varphi^{\text{å}}) - \cos\theta\cos\theta^{\text{å}}]}} \quad \text{Eq. (17)}$$

Where θ, $\theta^{\text{å}}$, φ and $\varphi^{\text{å}}$ are the sun and satellite zenithal and azimuthal angles respectively, and where ρ in Eq. (15) is the effective reflectivity for specular reflection; the last factor on the right hand side of that equation is the sun solid angle. Note that $L_0^{\downarrow\text{å}}(\tilde{\nu})$ in Eq. (13) is modelled by a Planck blackbody function at 5700 K, without including spectral lines.

Numerical approximations

In order to perform the radiative transfer calculation, a discretized layered atmosphere has to be considered. Typically a 1 km-layered atmosphere is assumed. The convention adopted here is to label the levels from 0 to N, N for altitudes starting from ground to the TOA, with an atmospheric layer bounded by two levels. The layer index is then ranging from 1 to N. For each layer, average parameters (e.g. $\bar{T}_i$, $\bar{P}_i$, …) are computed.

Ray tracing

Eq. (10) is integrated for each layer using a Gauss-Kronrod quadrature scheme. For each layer, the partial column of each molecule j is also computed using

$$PC_{i,j} = \int_{z_i}^{z_{i+1}} \rho_j(z)\frac{ds(z)}{dz}dz \quad \text{Eq. (18)}$$

Where $\rho_j(z)$ is the molecular density (in molecule/cm ^{3}).

Radiative transfer

Assuming clear sky, Eq. (11) is discretized using a recursive representation evaluated successively for each layer $= 1, \ldots, N$:

$$L_i^{\uparrow} = \bar{B}_i + \left(L_{i-1}^{\uparrow} - \bar{B}_i\right)\tilde{\tau}_i \quad \text{Eq. (19)}$$

Where $\bar{B}_i$ is the average constant Planck function for layer i computed at the average temperature $\bar{T}_i$ of that layer and $\tilde{\tau}_i = \tau(\tilde{\nu}, z_i, z_{i-1})$ is the effective transmittance of that layer. $L_0^{\uparrow}$ is evaluated using successively two recursions similar to Eq. (13), the first being to approximate the downward flux $L_0^{\downarrow\dagger}(\tilde{\nu})$. The evaluation of this equivalent downward flux integral in Eq. (19) is simplified by computing an effective downward radiance with a zenith angle of 53.5°, which approximates the integral within a few percent (Elsasser, 1942; Turner et al., 2004). Accordingly, the computational cost gain is made at a minor error cost in most situations.

Effective transmittances are computed for each layer using a formulation close to the analytical form Eq. (15), but using the average parameters:

$$\tilde{\tau}_i = exp\left[-\sum_j PC_{i,j} \sum_l \kappa_{j,l}(\tilde{\nu}; \bar{T}_i, \bar{P}_i)\right] \qquad \text{Eq. (20)}$$

Where i refers to the layer, j to the molecular species; and l, to the spectral line when relevant. For water vapour, the water concentration enters in the line shapes definition, and we should rigorously write $\kappa_{j,l}(\tilde{\nu}; \bar{T}_i, \bar{P}_i, VMR_{j,l})$.

A special feature of FORLI is to work with unit less multiplying factors $M_{i,j}$ instead of the partial columns $PC_{i,j}$ themselves. The multiplying factors are calculated with respect to the *a priori* profiles, except for water vapour for which the level 2 first guess retrieved at EUMETSAT CAF (August et al., 2012) is used instead. Therefore Eq. (20) becomes

$$\tilde{\tau}_i = exp\left[-\sum_{j=fitted} M_{i,j} PC_{i,j} \sum_l \kappa_{j,l}(\tilde{\nu}; \bar{T}_i, \bar{P}_i) - \sum_{j=fixed} PC_{i,j} \sum_l \kappa_{j,l}(\tilde{\nu}; \bar{T}_i, \bar{P}_i)\right] \qquad \text{Eq. (21)}$$

Where the sum runs over the fitted molecules and the j-fixed molecules.

The total state vector ends up to be all the multiplying factors $M_{i,j}$ and all the non-molecular parameters (ground temperature T_{skin}, emissivity or spectral/radiometric calibration parameters) that have to be adjusted. Specifically in FORLI, only $M_{i,j}$ (the trace gas profile and the water vapour column) and T_{skin} are retrieved.

Error description

The fitted variance-covariance matrix $\hat{s}$, representing the total statistical error after the retrieval, is written

$$\hat{s} = \left(K^T S_\eta^{-1} K + S_a^{-1}\right)^{-1} \qquad \text{Eq. (22)}$$

It includes the contribution from the smoothing error and the measurement error, which can be decomposed according to Rodgers (2000).

Averaging kernels are calculated as

$$A = GK \qquad \text{Eq. (23)}$$

where

$$G = \left(K^T S_\eta^{-1} K + S_a^{-1}\right)^{-1} K^T S_\eta^{-1} \qquad \text{Eq. (24)}$$

Typical averaging kernels are represented in Figure 11.

Figure 11 - Example of averaging kernels for FORLI-O3 retrievals. The coloured lines represent the vertical range of sensitivity for retrieved values at altitudes denoted by dots of the same colour. The black and grey curves represent the successive sub-columns providing independent information content on the ozone vertical profile. DOFS stands for Degree Of Freedom For Signal.

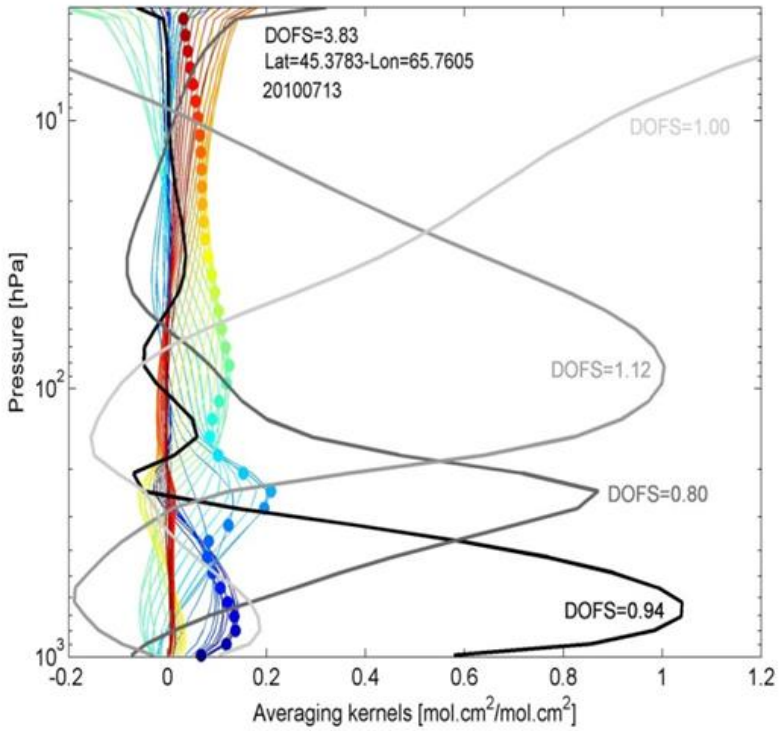

Output product description

Level-2 total ozone data sets derived from the sensors IASI/Metop-A and IASI/Metop-B have been processed with the FORLI v20151001 retrieval algorithm. The data sets are provided for the complete instrumental time series, under the condition of availability of the input parameters, and are based on the Level 1C radiances disseminated by EumetCast.

The format of the Level 2 ozone profile product file from the FORLI algorithm is NetCDF. The FORLI algorithm for IASI operates with multiplication factors, with the a priori as reference, and the profile is adjusted in layer partial columns. The original output profile is in partial columns but is provided here in the units needed to follow the general convention. The values in all groups are taken from the level 1 or other input data files or calculated by the program. Further details on ancillary data, can be found in Section 2.4.6.

There is one ozone profile measurement per ground pixel observed by the sensor and the level-2 data sets are distributed via NetCDF files (one file per day). For each measurement, geolocation information, auxiliary and additional fitted parameters, quality indicators (to be defined yet), a-priori O_3 profile shape and averaging kernels are also provided in the output files. Table 37 describes the main output variables generated by the level-2 processor.

Table 37. Dimension and description of all variables contained in the IASI L2 ozone NetCDF files. N_{obs} represents the total number of IASI measurements. N_{layers} is the number of retrieval vertical layers and $N_{pressures}$ is the number of retrieval pressure levels.

Variable Name	Dimension	Unit	Description
latitude	N_{obs}	degree	latitude of the ground pixel center
longitude	N_{obs}	degree	longitude of the ground pixel center
time	N_{obs}	NA	hour in the day as hhmmss
sun_zen_angle	N_{obs}	degrees	solar zenith angle at the Earth's surface for the pixel center
satellite_zen_angle	N_{obs}	degrees	MetOp zenith angle at the Earth's surface for the pixel center
orbit_number	N_{obs}	NA	MetOp orbit number
scanline_number	N_{obs}	NA	scanline number in the MetOp orbit
pixel_number	N_{obs}	NA	pixel number in the current scanline
cloud_cover	N_{obs}	percent	Eumetsat total cloud coverage in the IASI pixel
dofs	N_{obs}	NA	degrees of freedom of the signal in the retrieved ozone partial column profile
retrieval_quality_flag	N_{obs}		retrieval quality flag summarizing processing flags (to be defined and for the moment, 0 for all observations)
surface_altitude	N_{obs}	m	altitude of the surface
tropopause_altitude	N_{obs}	m	altitude of the tropopause
thermal_contrast	N_{obs}	K	thermal contrast
ozone_total_column	N_{obs}	mol m^{-2}	retrieved ozone total column in mole/m2
ozone_partial_column_profile	N_{obs} x N_{layers}	mol m^{-2}	retrieved ozone partial column vertical profile in mole/m2 in the layers defined by the levels given in the variable atmosphere_pressure_grid

Variable Name	Dimension	Unit	Description
ozone_partial_column_error	N_{obs} x N_{layers}	mol m^{-2}	vertical profile of total retrieval error associated to ozone partial column vertical profile in the layers defined by the levels given in the variable atmosphere_pressure_grid
ozone_apriori_partial_column_profile	N_{obs} x N_{layers}	mol m^{-2}	ozone a priori partial column vertical profile in mole/m2 and in the layers defined by the levels given in the variable atmosphere_pressure_grid
air_partial_column_profile	N_{obs} x N_{layers}	mol m^{-2}	air partial column vertical profile in mole/m2 in the layers defined by the levels given in the variable atmosphere_pressure_grid
atmosphere_pressure_grid	N_{obs} x $N_{pressures}$	hPa	pressures in hPa corresponding to levels used to define inversion layers: 40 layers of about 1 km height between Earth's surface and 40 km with an additional layer from 40 km to the top of the atmosphere
averaging_kernels_matrix	N_{obs} x N_{layers} x N_{layers}	DU/DU	ozone partial column averaging kernels matrix (DU/DU) in the layers defined by the levels given in the variable atmosphere_pressure_grid

Retrieval and quality flags

The IASI L2 data were filtered out in order to keep only O_3 measurements characterized by a good spectral fit based on quality descriptive and fit flags implemented in FORLI. All data meeting the following quality flags were rejected:

Descriptive flags:

- if there is an error related to the L1C data
- if T, H_2O, cloud L2 data associated to L1C data are missing
- if H_2O L2 profile is incomplete or if the skin pressure is missing
- if a partial O_3 column is negative
- if skin temperature is unrealistic

Fit flags:

- if the spectral fit residual root mean square (RMS) is higher than 3.5×10^{-8} W/(cm^2 sr cm^{-1})
- if the spectral fit residual bias is lower than -0.75×10^{-9} W/(cm^2 sr cm^{-1}) or higher than 1.25×10^{-9} W/(cm^2 sr cm^{-1})
- if there were abnormal averaging kernel values
- if the spectral fit diverged
- if the total error covariance matrix is ill conditioned;

It is also recommended to filter IASI L2 data characterized by:

- DOFS <2
- a ratio of the surface-6km column to the total column higher or equal to 0.085

Those last 2 filters have been applied to the IASI L2 data before generating the L3 datasets

3.2.3 Level 2 to Level 3

This section gives a short description of the methodology used to calculate averaged ozone fields on a regular 1°x1° latitude-longitude grid and gives a description of its output files. Input that are provided are IASI/Metop-A and IASI/Metop-B and IASI/Metop-C L2 satellite measurements retrieved from FORLI-O3 v20151001, output is in netcdf format. For each month, all IASI pixels falling into a grid cell are added to the corresponding grid cell. Then the average and standard deviation are calculated. The pixel values are weighted by $1/\sigma^2$ (σ being the total error associated) before adding, so the weighted mean grid cell value and the corresponding standard deviation are given by

$$mean = \frac{\sum_i \frac{x_i}{\sigma_i^2}}{\sum_i \frac{1}{\sigma_i^2}} \qquad \text{Eq. (25)}$$

$$stddev = \sqrt{\frac{1}{\sum_i \frac{1}{\sigma_i^2}}} \qquad \text{Eq. (26)}$$

These values are provided for total ozone column and tropospheric ozone column, for day and night time and for IASI/Metop-A, IASI/Metop-B and IASI/Metop-C separately in the L3 files. Day and night time data are determined with solar zenith angle to the sun <=90° and >90°, respectively. An example is illustrated in Figure 12 for January 2008, based on the L2 dataset. The current parameters included in NetCDF files are presented in Table 38 and the NetCDF files are currently available from 2008 till present.

Figure 12 - L3 mean total ozone column (top) and its uncertainty (bottom) for January 2008, based on IASI/Metop-A L2 data.

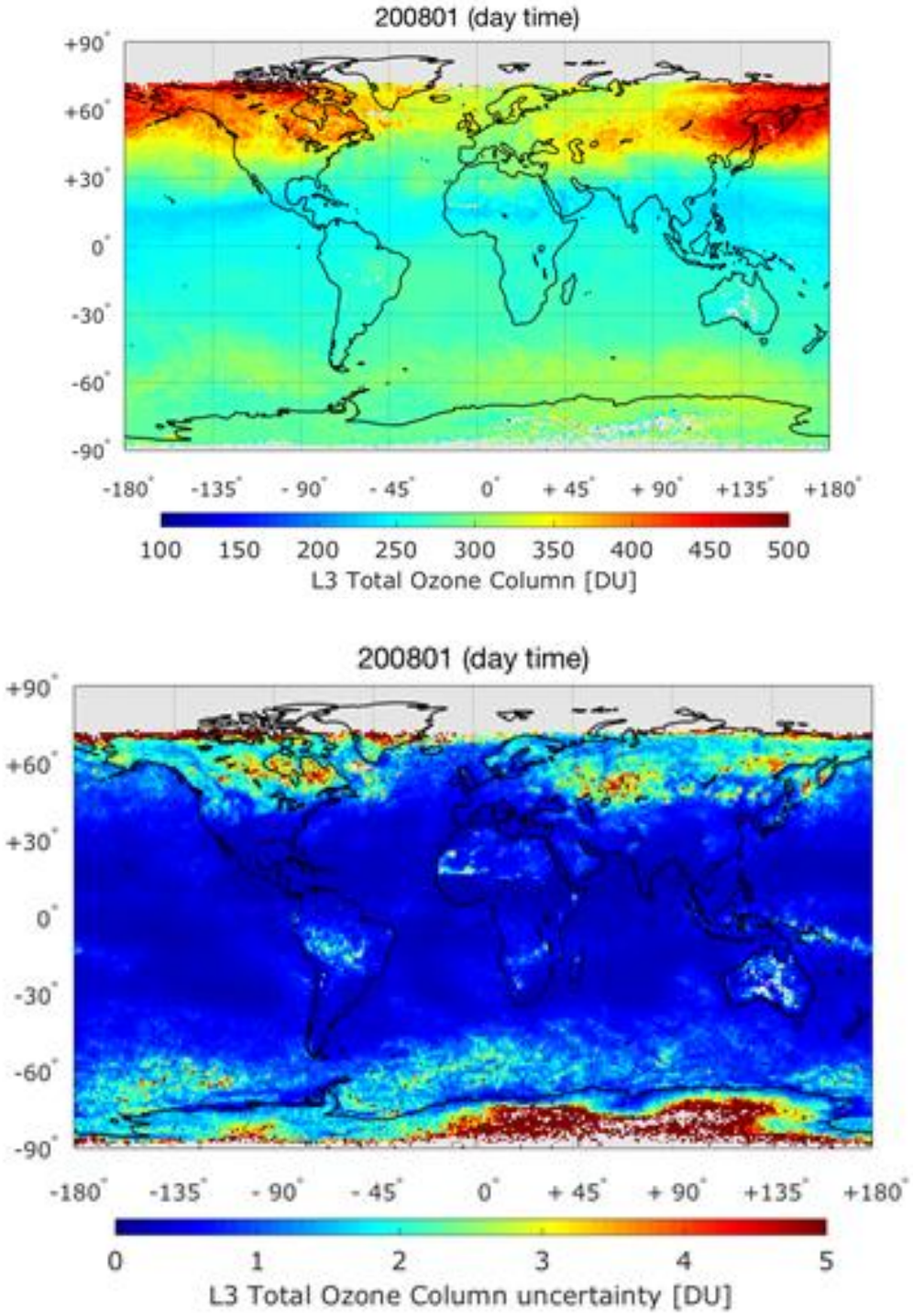

Table 38. Dimension and description of the variables contained in the current IASI-A, IASI-B and IASI-C L3 ozone NetCDF files. N_{lat} and N_{lon} represents the number of latitude and longitude, respectively.

Variable Name	Dimension	Unit	Description
latitude	N_{lat}	degree	latitude, from -90 (south) to +90 (north) given at gridcell centers
longitude	N_{lon}	degree	longitude, from -180 (west) to +180 (east) given at gridcell centers
total_ozone_column	N_{lat} x N_{lon}	mol m^{-2}	weighted average of the total ozone columns
total_ozone_column_error	N_{lat} x N_{lon}	mol m^{-2}	uncertainty in the weighted average of the total ozone columns
tropospheric_ozone_column	N_{lat} x N_{lon}	mol m^{-2}	weighted average of the tropospheric ozone columns
tropospheric_ozone_column_error	N_{lat} x N_{lon}	mol m^{-2}	uncertainty in the weighted average of the tropospheric ozone columns
number_of_measurements	N_{lat} x N_{lon}	-	Number of measurements used to derive the monthly mean total ozone column

3.3 Ozone profile retrieval from UV-nadir sensors

3.3.1 Level 1 to Level 2

3.3.1.1 Overview

The RAL nadir profile ozone scheme for the GOME-class UV sensors uses optimal estimation to directly retrieve the full vertically resolved ozone profile to ground level. Due to its sensitivity to near surface ozone, it was selected as the ESA-CCI nadir profile scheme. The RAL retrieval scheme derives profiles of number density on a set of pressure levels, spaced approximately every 4-6 km in altitude, taken from the SPARC-DI grid (Hegglin et al., 2013). The optimal estimation method is used. Averaging kernels are provided on this basis. It is noted that the vertical resolution of the retrieval is relatively coarse compared to the vertical grid and that tropospheric levels in particular have significant bias towards the assumed *a priori* state. It is therefore important to take account of the characterization of the retrieval provided by the averaging kernels when comparing these results to other data-sets, particularly where those are more highly vertically resolved.

Figure 13 - Retrieved ozone number density on an orbit cross section on 25th August 2008 (nadir pixel). The red line in the right panel denotes the position of the orbit on the globe.

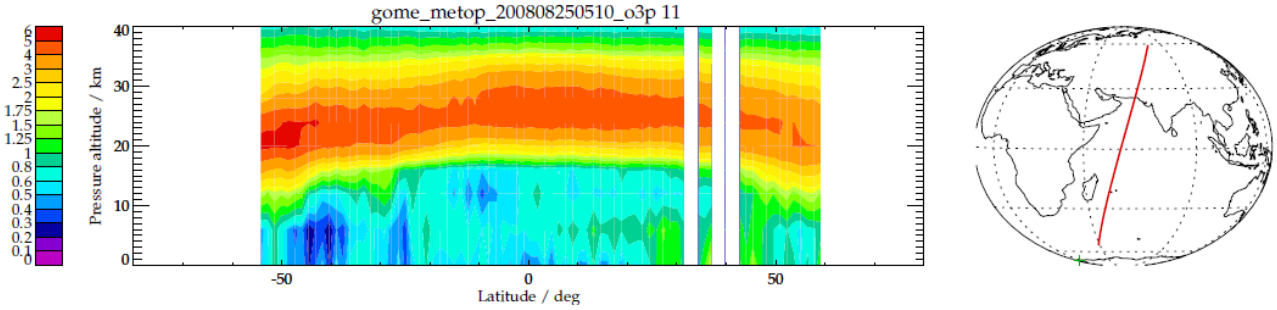

Figure 13 shows an example of retrieved number density profiles over 1 orbit. Retrieved ozone and ozone error are also provided on levels in volume mixing ratio, in addition to sub-column and sub-column error estimates. Figure 14 shows examples of the lowest retrieved sub-column and total column ozone for 1 day in August 2008. For convenience vertically integrated sub-column amounts between the retrieval levels are also reported.

Figure 14 - Lowest layer retrieved sub-column ozone on 25th August 2008 (top), and retrieved total column ozone (bottom) on the same day.

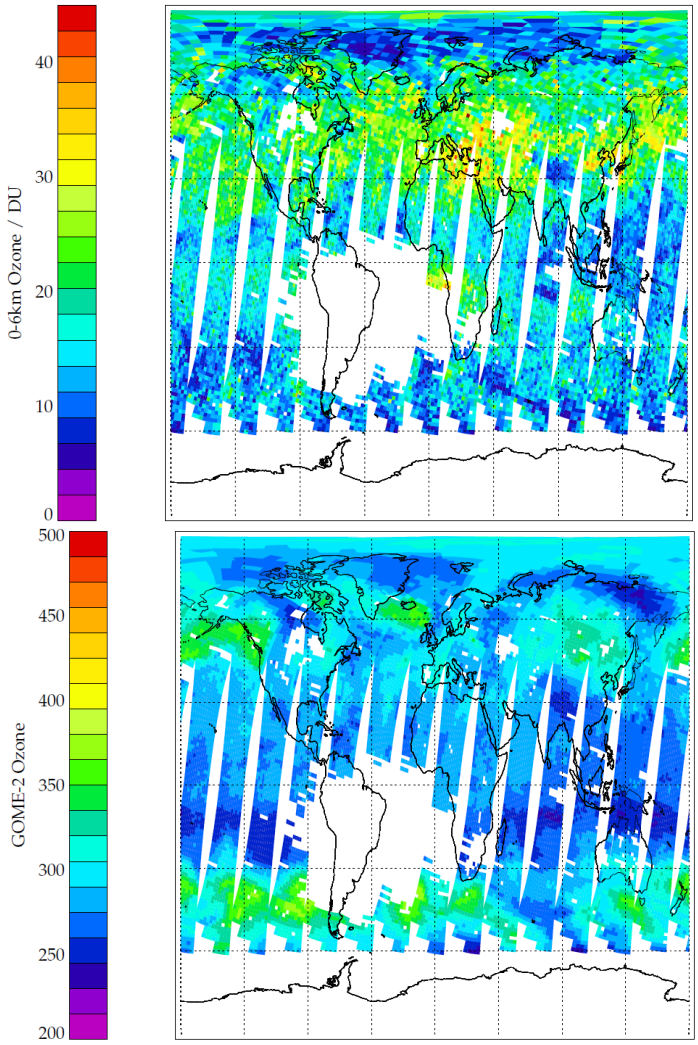

The algorithm is sequential retrieval. It uses information from GOME-2 Band 1 initially before performing surface albedo retrieval in Band 2 and finally ozone profile retrieval in Band 2 incorporating the information derived from Band 1 as input. The output from both retrievals is included in the product with that from Band 1 indicated in the variable name, however it should be highlighted that the output from the Band 1 retrieval is not the algorithm final solution. Other trace gas spectra are fitted as part of the ozone retrieval in order to accurately fit the ozone profile (such as CH_2O and BrO) and their column values are included in the output file, but it should be noted that the chosen fitting window is optimized for ozone rather than these trace gases.

It is recommended that some quality control criteria be applied to the ozone profile data, using parameters also supplied within the NetCDF file:

- 'ncost' (the normalised total fit cost) is less than 2
- 'aconv' (the convergence flag) is equal to 1

- ‘sza’ (solar zenith angle) is less than 80°
- 1/cos (‘lza’)*’o3_b1_tc’ (the line-of-sight zenith component of the Band 1 retrieved total column amount) is less than 500 during the months of January to May. This is due to very high stratospheric ozone at high Northern latitudes which limits the ability to discern tropospheric ozone beneath.

Tropospheric ozone can have a low bias in the presence of thick cloud (as indicated by ‘cloudf’ (cloud fraction) and/or high cloud ‘cloudp’ (effective cloud top pressure).

3.3.1.2 RAL Ozone Profile Algorithm Description

The RAL profile scheme (Munro et al., 1998: Siddans et al., 2003; Miles et al., 2015) scheme differs from the GOME-2 Operational Algorithm (www.temis.nl) in a number of important respects. The most significant difference is the treatment of the Huggins bands which are fitted to a precision of better than 0.1% (close to the noise level) to allow the ozone absorption cross-section temperature dependence to be exploited for tropospheric information. This is achieved by fitting the differential absorption spectrum (log of sun-normalised radiance with polynomial subtracted) in the Huggins range rather than the absolute sun-normalised radiance, which it is necessary to fit in the Hartley band in order to obtain information at higher altitudes. This distinct treatment of the two spectral ranges leads to the formulation of the retrieval problem in 3 steps:

1. “B1 fit”: Fit ozone profile to the sun-normalised radiance in the Harley band (in GOME Band 1) from 265-307nm.
2. “Albedo fit”: Fit effective surface albedo for the Huggins bands GOME from a narrow region (where ozone absorption is low) around 334nm (assuming the B1 ozone to be correct).
3. “B2 fit”: Add information on ozone from the differential absorption spectrum in the Huggins bands. I.e. retrieve the ozone taking the B1 result to define the prior state and errors.

Methods to improve the characterisation of sub-pixel cloud in the GOME field-of-view using Vis-near-IR imagery (ATSR and AVHRR) have been implemented in the RAL GOME scheme and can be used optionally. The potential benefit of using co-located imagery in this way to improve the O_3 ECV has been tested, providing a significant link to the cloud / aerosol ECV projects, which are planned to involve the application of the Oxford-RAL aerosol and cloud scheme to ATSR-2 and AATSR.

3.3.1.3 Basic retrieval equations

Each step of the RAL retrieval is performed using optimal estimation (Rodgers, 2000). The standard equations apply.

However the linear error analysis is somewhat complicated by the 3-step retrieval approach. Particularly as the ozone prior covariance used in step 3 is not identical to the solution covariance output from step 1. This is handled by linearizing each step and propagating the impact of perturbations in parameters affecting the measurements through to the final solution.

The following equations defined the averaging kernel. For the 3-step process, the averaging kernel is:

$$A = D_{y3}K_3 + D_{a3}(M_1^3 A_1 M_1^{3T} + M_2^3 A_2 M_2^{3T}) \qquad \text{Eq. (27)}$$

Where the sub-scripts denote the matrices for each retrieval step and M is the matrix (consisting entirely of 0s and 1s) which maps the elements of the state vector at one step into the corresponding element of the state vector for a later step. Similarly the impact of perturbations in a forward model parameter are propagated via:

$$\Delta X_b = D_{y3}\Delta b_3 + D_{a3}\left[M_1^3\left(D_{y1}\Delta b_3\right)M_1^{3T} + M_2^3\left(D_{y2}\Delta b_2\right)M_2^{3T}\right] \quad \text{Eq. (28)}$$

The estimated standard deviation of the final retrieval (ESD) is taken to be the square-root of the step-3 solution covariance (which includes the contribution from the other steps, in the step-3 a priori covariance).

3.3.1.4 Assumptions, grid and sequence of operations

Spectral ranges

In the region between 240 and 315nm there is a relatively large spectral variation in optical depth and consequent uncertainty in the fractional polarisation, which can lead to errors of the order of a few percent in sun-normalised radiance. There is a trade-off between the improvement in ESD from including as much of this range as possible and the mapping of polarisation errors (also quasi-random due to the variability of the polarisation state introduced by cloud). These errors might be mitigated by including additional retrieval parameters, but the polarisation signature is likely to correlate to the broad absorption in this range. Similarly the benefit of including channels towards the short wave end of the range is offset by increasing measurement errors, including noise and those due to imperfect modelling of dark-current and stray light. The range 265-307nm is selected as the best compromise.

From this range the following sections are ignored to avoid strong Fraunhofer lines (particularly sensitive to errors in modelled leakage current, wavelength calibration and Ring effect) and the NO gamma-bands: 265-269, 278.2-280, 284-286.4, and 287.2-288.8nm.

In order to fit the Huggins bands to the required accuracy it is necessary to model the Ring effect and under-sampling. A pre-requisite of such a model is an accurate knowledge of the slit-function and the wavelength registration relative to the solar reference spectrum used in the model. For GOME-1 Pre-flight spectral calibration of the instrument was insufficient for this purpose and the scheme developed here attempts to derive the required parameters, together with a better estimate of the wavelength calibration in the region by fitting the GOME measured solar spectrum to a high-resolution solar reference spectrum.

The fitting region is restricted to 322.5 to 334nm: Below this range the fit to the solar reference spectrum shows gross changes in spectral resolution and wavelength calibration. Fit residuals are also larger.

Since B2 is primarily of interest for the relatively fine-scale temperature dependent structure, the measurements in B2 are treated in a manner analogous to DOAS. The logarithm of the sun-normalised radiance is taken and a polynomial subtracted. This removes, to a large degree, independent information on the surface reflectance which modulates the mean layer photon-path profile. It is therefore important to specify (not retrieve) an accurate surface albedo as a forward model parameter in this retrieval step. This is obtained from a separate retrieval from measurements in the Huggins absorption minima between 335-340nm. It is assumed that this range is close enough in wavelength to the B2 range used for the retrieval and that the albedo is appropriate, while being

sufficiently insensitive to absorption, so that the B1 fitted profile can be assumed for the Huggins band albedo fit.

After restricting the spectral range and adopting the quasi-DOAS approach above, systematic residuals remained at the 0.2% level (in sun-normalised radiance). For GOME-1 and SCIAMACHY, the mean residual over a single orbit was determined. The retrieval and FM were then modified to allow this pattern to be added to simulated measurements, scaled by a retrieved parameter. For GOME-2 a similar approach is applied, but this is currently being refined to further improve the fit.

The B1 and B2 retrievals both make use of the estimated random error on measurements provided by appropriate photon noise model. In both cases, the matrix is assumed diagonal. However, in both steps noise-floors (upper limits on the fitting precision) are imposed. The noise-floor values are arrived at empirically by inspection of fitting residuals and comparison of retrievals with climatology and validation data. In B1 the noise floor is set to 1% in sun-normalised radiance unit. In B2 the value varies with solar zenith angle, but is typically 0.05% (0.0005 in units of the natural log of the sun-normalised radiance).

Since the absolute sun-normalised radiance is used in the B1 fit, and this is subject to degradation over time (which varies from instrument to instrument), an empirical correction scheme is used to correct the L1 data in the B1 range used. This is based on modelling observed radiances based on climatological ozone distributions and fitting a polynomial in time (sufficient to capture seasonal variations) and wavelength (4th order over the band) which captures the deviations of the observations from the climatological predictions.

Vertical grid

Vertical grids are defined for the retrieval state vector and for the RTM finite-difference computational levels. To minimise changes in the scheme as it is applied globally, the same sets of levels are always used. The levels are defined in terms of pressure, so as to follow the meridional variation in tropopause height more closely than geometric altitude. They are referred to in terms of a scale-height in km, referred to as Z^*:

$$Z^*/\mathrm{km} = 16[3.0 - log_{10}(p/\mathrm{hPa})] \qquad \text{Eq. (29)}$$

Where p is pressure in hPa. This gives a value comparable to geometric height (within about 1km).

Ozone state vector

The state vector elements for ozone are the logarithm of the volume mixing ratio at different altitudes. Retrieval levels are defined to be 0, 6, 12 km, then at 4 km intervals up to 80 km (corresponding always to the same pressure levels of approximately 1000, 422, 177, 100.000, 56, 32, 18, 105.6, 3.2, 1.8, 1.0, 0.56, 0.32, 0.18, 0.10, 0.056, 0.032, 0.018, 0.01 hPa). These over-sample the resolution expected on the basis of averaging kernel analysis. The *a priori* covariance is used to constrain the profile shape.

An *a priori* correlation length of $\Delta z_c = 6\mathrm{km}$ is imposed for the Hartley band fit (Step 1), i.e. the elements of S_a are given by:

$$(S_a)_{ij} = \Delta x_{ai} \Delta x_{aj} e^{-\left(\frac{z_j - z_i}{\Delta z_c}\right)^2} \qquad \text{Eq. (30)}$$

The values of the *a priori* and corresponding errors, Δx_{aj}, at each level i, at altitude z_j, are taken from the *McPeters-Labow* (McPeters et al., 2007) or Fortuin (Fortuin and Langematz, 1994) climatology interpolated in altitude to the retrieval grid.

For the B2 fit, the *a priori* is taken from the B1A retrieval, on the same levels. Instability in the retrieval at UT/LS altitudes was encountered when the full solution covariance, from the B1A retrieval was taken to define for the B2B retrieval. This instability was reduced by using a Gaussian *a priori* covariance with 8km correlation length and *a priori* standard deviation equal to B1A ESD.

The following deviations from the Fortuin climatology are imposed:

- At the surface and 6 km levels, the volume mixing ratio is set to the larger of the climatological value and a value corresponding to a number density of 10^{12} molecules/cm^3. In practice, both levels are always set to this value except at very high latitude where the climatological value is greater on the 6km level. I.e. there is no horizontal structure in the *a priori* at these levels. This approach is intended to minimise the appearance of spurious spatial/temporal patterns in retrievals at tropospheric altitudes due to *a priori* influence.
- To avoid too tight an *a priori* constraint, and to avoid spurious effects in the retrieval due to the imperfect sampling of the tropospheric variance by the climatology, the relative *a priori* errors were set to the larger of the climatological standard deviation and the following:
    - 0-12km: 1 (in logarithmic units corresponding to 100% in fractional terms).
    - 6km: 0.3
    - 20-50km: 0.1
    - 56km: 0.5
    - 60-80km: 1

Other state vector elements: B1 fit

Leakage Current: A leakage current in binary units is fitted in B1, to correct for imperfect prediction of this at L1. A single parameter is fitted for the band, unless the B1A/B1B boundary occurs below 307nm, in which case one parameter is fitted for each sub-band. The leakage current in BU is assumed constant with wavelength.

Lambertian effective surface albedo: A single, wavelength independent albedo is retrieved.

Ring effect: Two parameters are fitted, namely (i): Scaling factor for the single-scattering Ring effect filling-in factor (as modelled via the approach of (Joiner et al., 1995); (ii) Wavelength shift of the pattern relative to the nominal wavelength calibration.

Wavelength shift of the absorption cross-section: A single parameter represents a shift of the GOMETRAN modelled spectrum (before Ring effect or slit-function convolution are simulated), with respect to the measured sun-normalised radiance. The magnitude of the retrieved shift is such that it can be considered to pertain effectively to the trace-gas absorption cross sections, since the scattering coefficient varies relatively weakly with wavelength.

Other state vector elements: B2 fit

Ring effect: A single scaling parameter is fitted (to represent approximately the expected number of scattering events). No wavelength shift is fitted in this case; the mis-registration / under-sampling correction makes the shift of the filling-in spectrum redundant.

Wavelength shift of the absorption cross-section: The parameter has the same meaning as the corresponding B1A state-vector element. In this case a 2nd order polynomial fit to the wavelength shift is fitted across the measurement vector range.

Wavelength mis-registration between solar and back-scattered spectrum: Parameters in 3rd order polynomial expansion (as above) of the wavelength shift between the GOME solar irradiance and back-scattered spectra used to form the sun-normalised radiance.

Column amounts of **NO_2, formaldehyde** and **BrO**.

Residual scaling factor: A single scaling factor for the systematic residual.

Iterations and convergence

The standard Marquardt-Levenberg approach is used. Convergence is judged to occur if (a) the cost function (absolute value, not normalised by the number of elements in the state vector) changes by <1 (b) at this point a Newtonian iteration (i.e. a step without applying the Marquardt-Levenberg damping) also results in a change in cost of <1. This 2nd criterion ensures retrievals do not appear to converge due to a high value of the Marquardt-Levenberg damping parameter.

3.3.1.5 Forward model

Atmospheric state input to the RTM

Temperature and pressure profiles are taken from meteorological analysis. Usually ECMWF profiles are used, though Met Office stratospheric analysis have been used in the past.

A background aerosol profile taken from MODTRAN (Berk et al., 2014) is assumed.

Cloud may be ignored (in which case it is fitted via the retrieved surface albedos) or modelled according to information either from GOME (O_2 A-band retrieval) or co-located imagery (AATSR for GOME-1 and AVHRR for GOME-2).

Radiative Transfer Model (RTM)

The scheme uses a version of the GOMETRAN++ (Rozanov et al., 1997) but with a number of processing speed improvements implemented at RAL.

3.3.1.6 Error description

A quite complete study of the errors pertaining to the profile retrieval is reported in (Siddans, 2003). This was based on performing retrieval simulations for a set of basic geo-physical scenario which had been defined for the GOME-2 Error Study (Kerridge et al., 2002) (which also contains a detailed error budget). For these conditions basic retrieval diagnostics such as averaging kernels and solution covariances were computed.

The following errors are considered:

- Aerosol: Errors in retrieved ozone introduced by deviations in the aerosol profile from the background case assumed in the FM are simulated by mapping measurement perturbations based on the following cases: [HIGH] represents a maximum boundary layer / troposphere optical depth case from the MODTRAN scenarios, with a moderate volcanic stratosphere. [BL10], [SUM] and [MODVOL] are close to the background case except in the boundary layer, troposphere and stratosphere respectively, where they are close to the [HIGH] scenario.
- [PRESSURE]: Effect of a 1% perturbation in surface pressure on scattering profile and hence retrieval (absorber number density not perturbed).
- [TEMP-2KM]: Effect of 1K error in assumed temperature profile on 2km grid. Both temperature errors are propagated through the absorption cross-section only (i.e. not via number density profile).
- [TEMP-10KM]: As above but assuming a Gaussian correlation with 10km half-width.
- [TEMP-FCBKG]: As above, but taking the covariance matrix from a numerical weather prediction background error covariance matrix.
- [TEMP-IASI]: As [TEMP-FCBKG], but using the estimated covariance after assimilation of IASI information.
- [MIRROR]: Errors due to the incidence angle dependence of the scan-mirror degradation.
- [POLERR-G1]: Estimated effect of error in polarisation correction given GOME-1 correction scheme (and PMD data).
- [RADCAL]: 2% Gain error, i.e., mapping of a 2% of the nominal back-scattered radiance is mapped as a systematic error, to represent radiometric calibration errors.

The most important findings of the error assessment described here are summarised as follows:

- The retrieval provides useful information on the ozone profile below 50km.
- Retrieval precision, accounting for measurement noise and other quasi-random errors is expected to be generally in the few-percent range in the stratosphere increasing to a few 10s of percent in the lowest retrieval levels.
- Retrieved quantities should be interpreted as estimates of layer-averaged number density, taking into account the shape of the averaging kernels, and the influence of the a priori.
- The instrumental and RTM errors are generally relatively small, compared to the climatological variance and, in most cases, the ESD. Exceptions are radiometric gain errors including scan-mirror degradation (which has most impact above 40km) and possibly imperfect knowledge of slit-function shape (expected to cause a significant negative bias in the troposphere, though the magnitude is difficult to quantify). These errors are currently addressed in the real scheme by the empirical degradation correction factor, but still represent a significant issue for long-term quality of the retrieved profiles.
- High perturbations in aerosol and errors in the assumed temperature profile give rise to retrieval errors in the troposphere of order 10-20%. (The temperature error is larger at high solar zenith angle.)
- Radiative transfer model approximations in the retrieval scheme are seen to be adequate.
- It was also noted that for GOME-1 a significant error source was lack of pre-flight measurement of the slit-function. Pre-flight characterisation of GOME-2 has much reduced uncertainties for that instrument at the beginning of life but in-orbit changes may mean this source of error is important for GOME-2 as well.

3.3.1.7 Output product description

Retrieval results are output in NetCDF format following CF conventions. See the Product User Guide for details. The product contains the retrieved profile (values on the retrieval levels), partial columns (integrated between retrieval levels), the full error covariance matrix, the retrieval noise covariance matrix, the a-priori profile the averaging kernels and the retrieved auxiliary parameters. Also included are: geolocation, spectral windows used and retrieval diagnostics, like number of iterations, spectral fit indicators. Each file Level 2 to Level 3 - From satellite track to regular longitude-latitude grid

This section gives a short description of the algorithm that calculates averaged ozone fields on a regular latitude-longitude grid and gives a description of its output files. Input that should be provided are L2 satellite measurements, output is in NetCDF format complying with the CF 1.6 metadata conventions.

The pixels in the satellite data (L2) are assumed to be ordered as indicated in Figure 15. If this is not the case, the reading routine should provide the appropriate transformation. A is the first corner in the longitude and latitude arrays, B the second etc. The across track direction is given by the lines A-D and B-C, while the along track direction is given by the lines A-B and D-C. Note that corners C and D are reversed with respect to the GOME/GOME-2 convention.

Figure 15 - Pixel layout assumed in the nadir L3 algorithm.

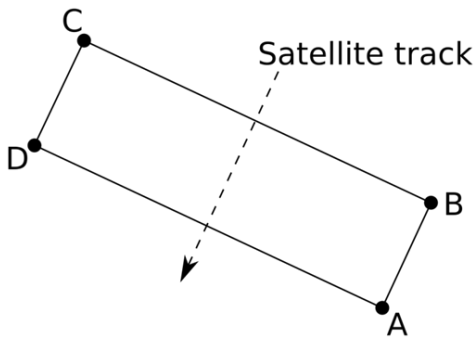

The along track pixel edges AB and DC and cross track pixel edges AD and BC (see Figure 15) are divided into a number of points. The first point on AB and the first on DC form a line which is divided into the same number of points as AD. Each of these points is assigned to a grid cell, see for example Figure 16.

Figure 16 - A L2 pixel is divided into subpixels (diamonds 1-7). Each subpixel is assigned to a TM5 grid cell (dashed) and the average and standard deviation are calculated (see text).

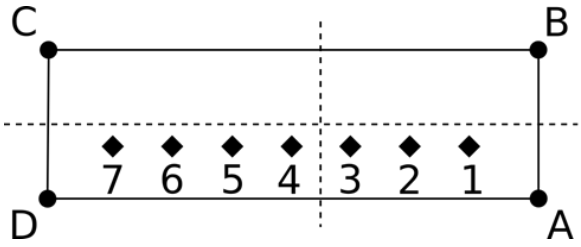

Suppose that ABCD in Figure 16 is the pixel of interest and that the horizontal line marked with the diamonds are the subpixels (numbered 1 to 7). Furthermore, the two dashed lines denote the grid cell boundaries which are numbered the same way as the pixel corners (i.e. grid cell A is the lower right cell). In this case, subpixels $1 \sim 3$ are added to grid cell A, and the counter for grid cell A is increased by 3. Subpixels $4 \sim 7$ are added to grid cell D and the counter for grid cell D is increased by 4. The pixel values are weighted by $1/\sigma^2$ before adding, so the weighted mean grid cell value and the corresponding standard deviation are given by Eq. 25 and 26.

These values are provided for partial columns in the L3 files on a layer-by-layer basis and for the total column. An example is shown in Figure 17 for January 2008, based on the L2 dataset provided in Phase 1 of the ozone CCI project.

Figure 17 - Mean partial ozone column (top) and its uncertainty (bottom) for January 2008, based on L2 data provided in the first phase of the Ozone-CCI project.

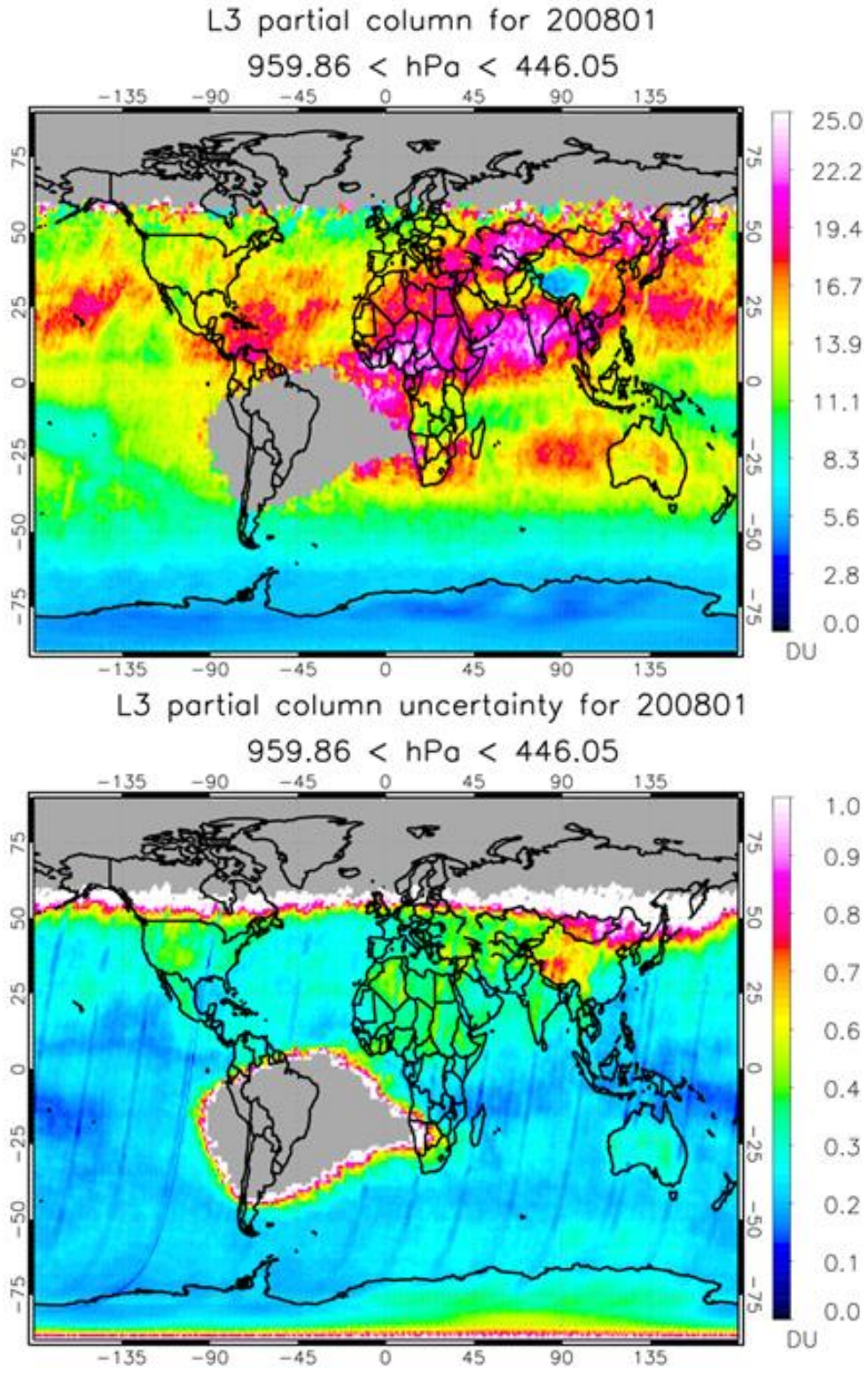

3.3.2 Merged GOME-type Ozone Profile (GOP-ECV)

3.3.2.1 Ozone profile merging algorithm

At first, the individual gridded monthly level-3 ozone profile data are merged into a combined record. The level-3 partial column data are based on the level-2 data retrieved with the RAL nadir profile retrieval scheme as described in the previous section. Data from five sensors are included: GOME (1995-2011), SCIAMACHY (2002-2012), OMI (2004-present), GOME-2A (2007-2021), and GOME-2B (2013-present). The values given in parenthesis denote the complete time periods which are covered by the sensors. These sensors are also used to create the GTO-ECV record. Note that data from TROPOMI and GOME-2C are not yet included in this first version of GOP-ECV. The merging is based on deseasonalized anomalies and similar to the method proposed by Sofieva et al. (2021). Deseasonalized anomalies $\Delta O_{3,i}(\varphi,\lambda,z,t)$ at latitude φ, longitude λ, altitude z, and month t are computed for the time series of all individual instruments *i* following:

$$\Delta O_{3,i}(\varphi,\lambda,z,t) = O_{3,i}(\varphi,\lambda,z,t) - O_{3,i,c}(\varphi,\lambda,z,m), \qquad \text{Eq. (31)}$$

Where $O_{3,i}(\varphi,\lambda,z,t)$ is the monthly mean ozone profile. $O_{3,i,c}(\varphi,\lambda,z,m)$ is the corresponding climatological mean value for the month m with m=January,…, December. Since the individual sensors cover only partially the same periods, the corresponding seasonal cycles have to be computed for different reference periods as follows: GOME (1996-2002), SCIAMACHY (2005-2010), OMI (2005-2020), GOME-2A (2007-2016), GOME-2B (2015-2020). Before merging the anomalies additive offsets w.r.t. OMI anomalies have to be computed and applied in order to account for biases due to different reference periods. These offsets are obtained from the overlap periods and depend on latitude, longitude, and altitude. One exception is the GOME sensor, which lost its global coverage in June 2003. That means for the overlap period with OMI (2004-2011) additive offsets cannot be derived globally, i.e. for each latitude-longitude grid cell. Instead, mean offsets representative for 5 broadband latitude belts (90°N-60°N, 60°N-30°N, 30°N-30°S, 30°S-60°S, and 60°S-90°S) are computed and added to the GOME anomalies. After the application of the offsets, the merged ozone profile for each spatio-temporal bin is obtained from the median of all available instruments as:

$$\Delta O_{3,mer}(\varphi,\lambda,z,t) = \text{median}\left(\Delta O_{3,i}(\varphi,\lambda,z,t)\right) \qquad \text{Eq. (32)}$$

Corresponding uncertainties of the merged data are estimated using the same approach as used for the merged ozone profiles based on limb satellite sensors (MEGRIDOP) as described in Sofieva et al. (2021).

Figure 18 shows the anomalies 1995-2022 for all sensors for the latitude/longitude bin 12.5°N/0.5°E and for altitude 20km. In addition, the adjusted anomalies for GOME, GOME-2A, and GOME-2B are shown. Finally, in order to reconstruct absolute ozone values, the seasonal cycle obtained from OMI measurements is used and added back to the anomalies:

$$O_{3,mer}(\varphi,\lambda,z,t) = \Delta O_{3,mer}(\varphi,\lambda,z,t) + O_{3,\text{omi},c}(\varphi,\lambda,z,m).$$

Figure 18 - Deseasonalized anomalies [DU] 1995-2022 for all satellite sensors for the latitude/longitude bin 12.5°N/0.5°E and for the altitude of 20km. In addition, for GOME, GOME-2A, and GOME-2B the adjusted anomalies w.r.t. OMI anomalies are shown.

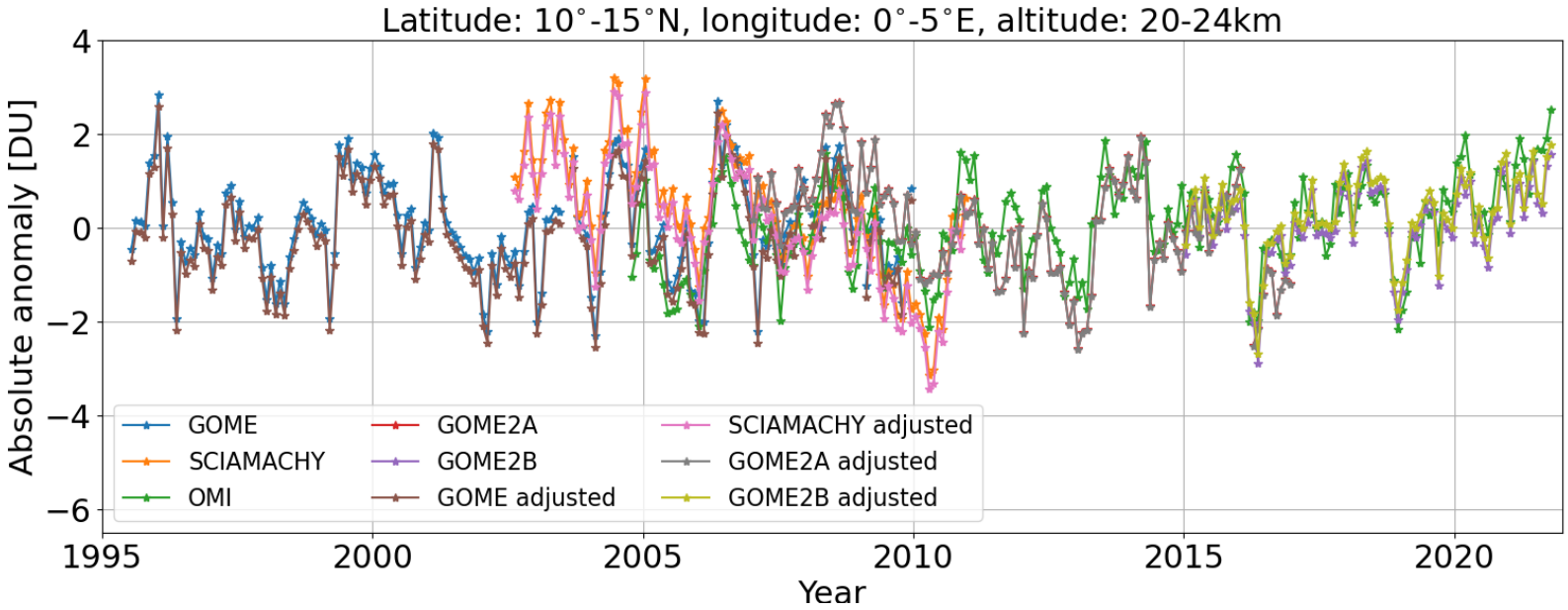

3.3.2.2 Harmonization w.r.t. GTO-ECV total columns

The aim of the harmonization of the merged ozone profiles, generated as described in the previous section, is to achieve consistency between the GTO-ECV total column product and the new GOP-ECV ozone profile record with respect to the total column. The harmonization consists of the following steps:

1. A clustering algorithm is applied to a subset of 80,000 profiles randomly selected from the entire merged data record. We use the same *k*-means clustering procedure as described in Xu et al. (2017) and applied to a set of ozone profiles. From this study we also adopt the optimal number of clusters: K=11. Figure 19 shows the output of the clustering: the ozone profiles in each class. Colors denote the total column of each profile. Profiles of similar shapes are grouped into the same class. Class 03 contains mainly profiles from the Northern Hemisphere middle latitudes in boreal spring (maximum total ozone columns >400DU) and class 05 contains mostly profiles from high latitudes in the Southern Hemisphere from September to November (ozone hole season).
2. For each class of ozone profiles a separate Neural Network is trained using as input the total ozone column and as output the corresponding ozone profile shape. The NNs comprise two hidden layers. From the NN training we extract the derivatives for each class, which provide the information about the altitude-dependent change of the profile, when the total column changes. Figure 20 exemplarily shows the derivatives for class 03. The shape of the derivatives depend on the total column, and derivatives can be negative.
3. In order to assign one of the 11 classes to each of the remaining profiles, which were not used for the clustering procedure (step (1)), a *k*-nearest neighbors classifier method is applied. The training data set for the classifier contains the profiles of the 11 clusters and the class label (1, …, 11). The fitted classifier is then applied to the remaining profiles in order to predict the corresponding class label, which is needed to select the correct set of derivatives for the altitude-dependent scaling.
4. The last step is the application of the scaling procedure to all merged profiles. The difference $\Delta\mathrm{TOZ}$ between the total column from the integrated profile and the corresponding total column from the GTO-ECV data record is computed for each spatiotemporal bin and the adjusted profile is computed as follows:

$$O_{3,new}(\varphi,\lambda,z,t) = O_{3,mer}(\varphi,\lambda,z,t) + \Delta TOZ(\varphi,\lambda,t) * d/dTOZ(z), \qquad \text{Eq. (33)}$$

$O_{3,mer}(\varphi,\lambda,z,t)$ denotes the merged profile from the previous section, $O_{3,new}(\varphi,\lambda,z,t)$ is the adjusted profile which is consistent with GTO-ECV, and d/dTOZ(z) is the derivative derived from the NN in step (2).

Figure 19 - Merged ozone profiles grouped in 11 classes using a *k*-means clustering procedure. The total number of profiles is 80,000 randomly selected from the entire data record. Colours denote the total column of each profile.

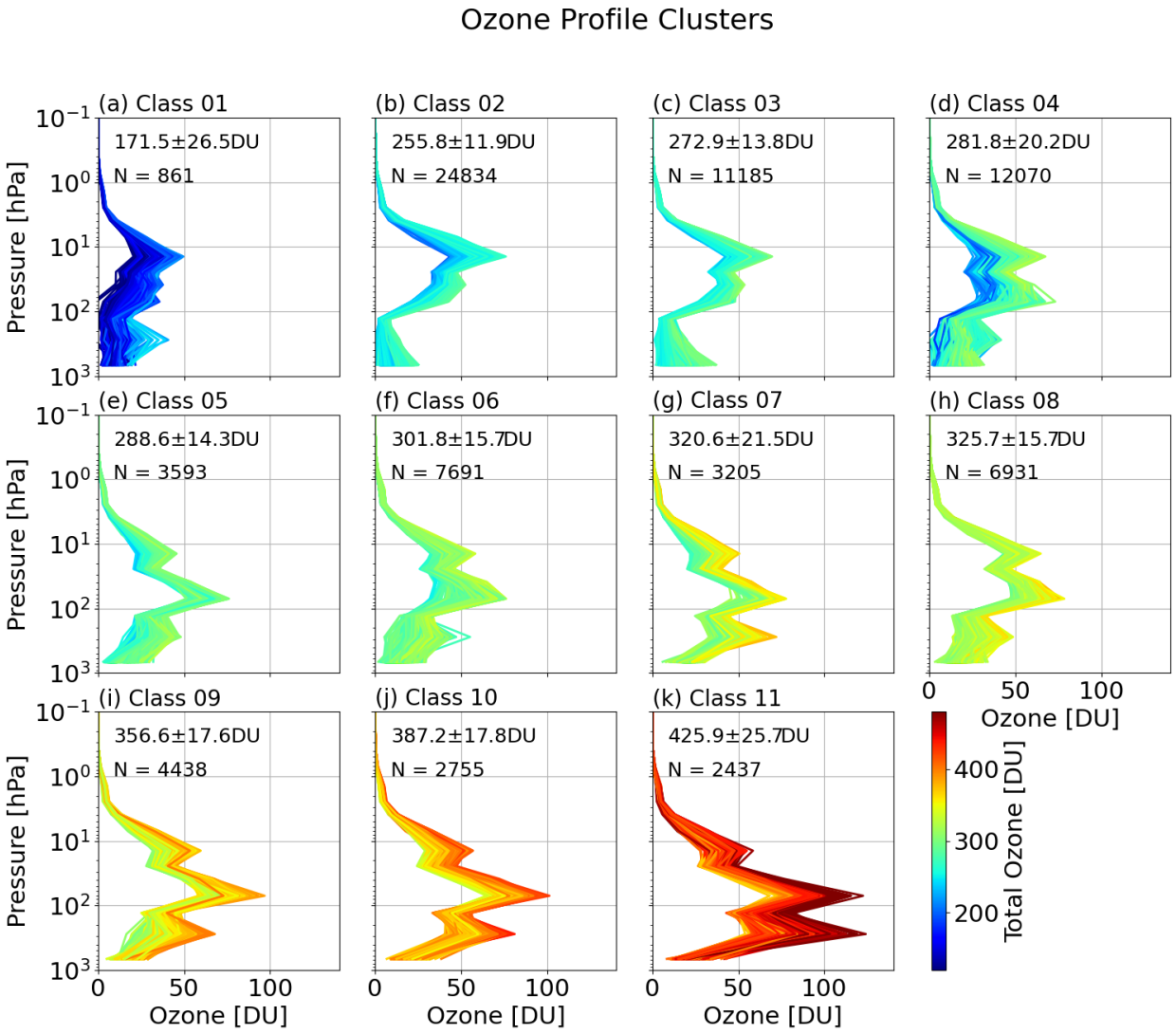

3.3.2.3 Output product description

Results of the merging and harmonization procedure are output in netcdf format following CF conventions. See the Product User Guide and Specification document for details. The product contains the merged profile (partial columns), corresponding error information and the total column.

Figure 20 - Derivatives extracted from the NN training for class 03 (see Figure 19). Colours denote the total column.

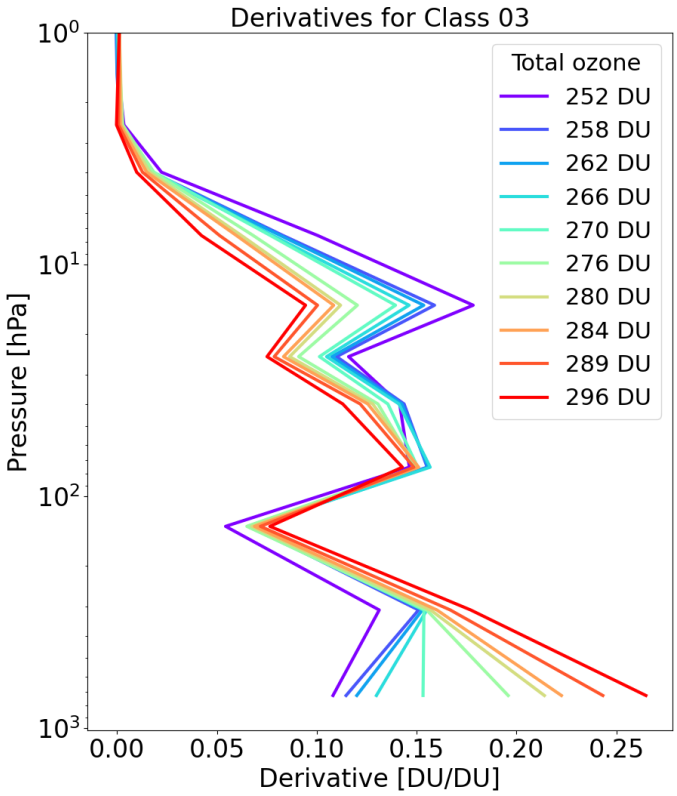

3.4 Ozone profile retrieval from limb and occultation sensors

3.4.1 Heritage

Algorithms applied to the retrieval of Level-2 ozone profiles from Level-1 data collected by limb and occultation sensors are described in the Ozone_CCI ATBD [D22]. In the Ozone_CCI project, the L-2 ozone profiles are harmonized and serve as input to the generation of Level-3 ozone profiles. The same approach is used in the C3S Ozone project.

3.4.2 Harmonisation of Level 2 profiles

The HARMonized dataset of OZone profiles (HARMOZ) is based on limb and occultation measurements from Envisat (GOMOS, MIPAS and SCIAMACHY), Odin (OSIRIS, SMR) and SCISAT (ACE-FTS) satellite instruments (Sofieva et al., 2013). HARMOZ consists of original retrieved ozone profiles from each instrument, which are screened for invalid data by the instrument teams. While the original ozone profiles are presented in different units and on different vertical grids, the harmonized dataset is given on a common pressure grid in NetCDF-4 format. In its original version, HARMOZ used a

pressure grid as a vertical coordinate. The Ozone_cci pressure grid corresponds to a vertical sampling of ~1 km below 20 km and 2-3 km above 20 km. The vertical range of the ozone profiles is specific for each instrument, thus all information contained in the original data is preserved. Based on the altitude and temperature profile information provided in the data product, ozone profiles can be expressed in number density or in mixing ratio on a pressure or altitude vertical grid. Geolocation, uncertainty estimates and vertical resolution are provided for each profile. For each instrument, optional parameters, which are related to the data quality, are also included.

The detailed description of the HARMOZ data can be found in Sofieva et al. (2013). The dataset is available at the ESA Ozone_cci website.

For climate studies, it is preferable to use only the information provided in the dataset (and avoid as much as possible using external data from models and reanalyses). Furthermore, as previously demonstrated by McLinden and Fioletov (2011), ozone trends inferred from measurements expressed in number density on an altitude grid are usually different from those expressed in mixing ratio on a pressure grid. This difference is due to temperature changes in the atmosphere and is more pronounced at upper altitudes.

As a result of these considerations, the HARMOZ dataset is - for C3S - delivered in two different configurations: HARMOZ_PRS and HARMOZ_ALT. The latter is the harmonized dataset of altitude-gridded number density ozone profile. In HARMOZ_ALT, the vertical grid is with 1 km spacing (every integer kilometre). We note that the number density on altitude grid is the "native" representation for the instruments included into the merged ozone dataset (see Section 3.4.3.2 below for more details).

3.4.3 Level 2 to Level 3

For creation of Level 3 data sets, the harmonized Level 2 ozone profiles from the limb/occultation sensors of the Ozone_cci data base are used.

3.4.3.1 Level 3 ozone profiles from individual limb and occultation sensors

The monthly zonal mean data in 10° latitude zones from 90°S to 90°N are created for all Ozone_cci limb and occultation instruments. The most recent versions of HARMOZ data are used as an input.

For all sensors, the monthly zonal average is computed as the mean of ozone profiles. x_k :

$$\rho = \frac{1}{N}\sum x_k \qquad \text{Eq. (34)}$$

Where *N* is the number of measurements, $N > 10$. The mean estimate has been chosen in order to minimize artificial biases, which might appear when using weighted mean or median estimates. The uncertainty of the monthly mean σ_ρ^2 is estimated as the standard error of the mean:

$$\sigma_\rho^2 = \frac{s^2}{N} \qquad \text{Eq. (35)}$$

Where $s^2 = \langle (x_k - \bar{x})^2 \rangle$ is the sample variance. For the sample variance, we used its robust estimate as $s = 0.5\,.\,(P_{84} - P_{16})$, where P_{84} and P_{16} are 84th and 16th percentiles of the distribution, respectively. An example of monthly zonal mean, standard deviation and standard error of the mean at 15-50 km for January 2008, for the Ozone_cci instruments is shown in Figure 21. As observed from Figure 21, the ozone distributions are very similar in the datasets. Due to large number of averaged data, the standard error of the mean is usually less than 1% in the stratosphere.

Both sample standard deviation *s* and the standard error of the mean σ_ρ are stored in the MZM files.

The mean of individual error estimates e_k :

$$\bar{e} = \frac{1}{N}\sum e_k \qquad \text{Eq. (36)}$$

is also provided in the MZM data files.

In order to characterize the non-uniformity of sampling, we provide inhomogeneity measures in latitude,H_{lat}, and in time, H_{time}. The definition of this measures and details of the related analyses can be found in (Sofieva et al., 2014). Each inhomogeneity measure ranges from 0 to 1 (the more homogeneous, the smaller *H*). For dense samplers (MIPAS, SCIAMACHY, OMPS), the inhomogeneity is close to zero nearly for all latitude bins. For other instruments, inhomogeneity measure can be large for some latitude-time bins.

Figure 21 - Left: monthly zonal mean ozone profiles for January 2008 for Ozone_cci instruments, centre: standard deviation of ozone profiles in %, right: standard error of the mean, 0.

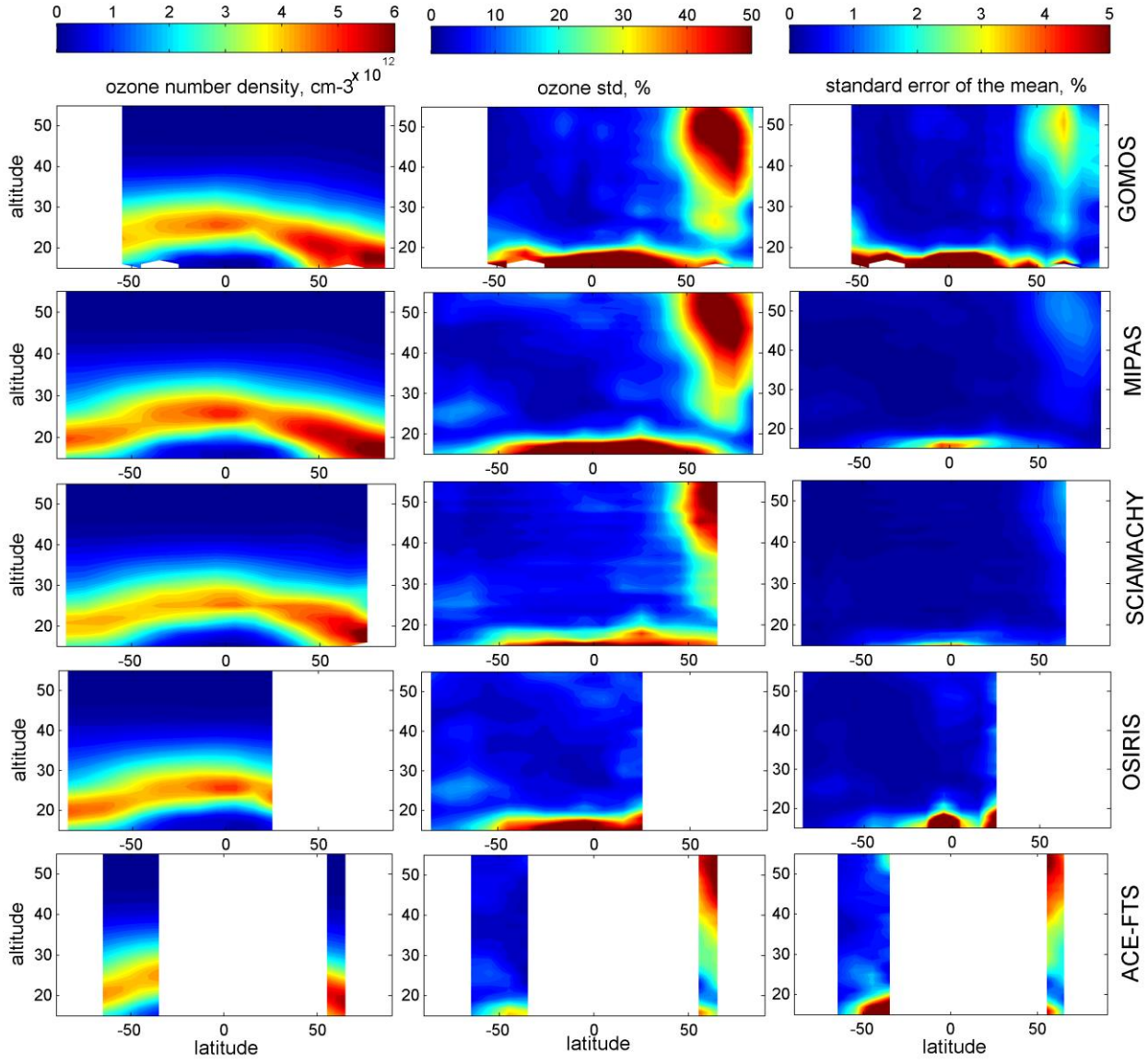

3.4.3.2 Merged monthly zonal mean ozone profiles (SAGE-CCI-OMPS+ dataset)

Overview

For the merged dataset, all reliable satellite data, which provide ozone profiles on altitude grid, are used. The merged dataset is targeted to serve as a climate data record for assessment of ozone trends. This dataset covers the stratosphere and combines measurements by nine limb and occultation satellite instruments – SAGE II, OSIRIS, MIPAS, SCIAMACHY, GOMOS, ACE-FTS, OMPS-LP, POAM III and SAGE III/ISS. The original version of the dataset is referred to as SAGE-CCI-OMPS (Sofieva et al., 2017b), and its updated version as SAGE-CCI-OMPS+ (Sofieva et al., 2023)

The stability of the individual-instrument data records has been extensively studied; only stable data are used for the merged dataset. The merging is performed on the deseasonalized anomalies computed from each individual dataset. This method is often exploited for creating a long-term data record and for trend analysis.

All the data used for creating the merged dataset have a sufficiently good resolution of 2–3 km in the UTLS. For all instruments, ozone profiles are retrieved on the geometric altitude grid. The majority of the datasets - SAGE II, SAGE III, POAM III, GOMOS, OSIRIS, SCIAMACHY and OMPS - provide number density ozone profiles; therefore this representation is used for the merged dataset. For ACE-FTS and MIPAS, the retrievals are in volume mixing ratio on altitude grid. Conversion to number density profiles is performed using temperature profiles retrieved by these instruments, thus providing consistent (i.e., without using external information about temperature and pressure profiles) representation of number density ozone profiles.

The information about individual datasets is collected in Table 39. For some instruments, the selected time period is shorter than the full operation period. The individual datasets have been compared with each other and with ground-based data, and only the time periods when the instruments were operating the best are selected.

Table 39. Information about the datasets used in the merged dataset (ozone profiles from limb and occultation sensors) (Sofieva et al., 2023).

Instrument/ satellite	Processor, data source	Time period	Local time	Vertical resolution	Estimated precision	Profiles per day
SAGE II / ERBS	NASA v7.0, HARMOZ_ALT	Oct 1984 – Aug 2005	sunrise, sunset	~1 km	0.5–5%	14–30
OSIRIS / Odin	USask v7, HARMOZ_ALT	Nov 2011 – present	6 a.m., 6 p.m.	2–3 km	2–10%	~250
GOMOS / Envisat	ALGOM2s v1.0, HARMOZ_ALT	Aug 2002 – Aug 2011	10 p.m.	2–3 km	0.5–5 %	~110
MIPAS / Envisat	KIT/IAA V8, HARMOZ_ALT	Jan 2005 – Apr 2012	10 p.m., 10 a.m.	3–5 km	1–4%	~1000
SCIAMACHY / Envisat	UBr v3.5, HARMOZ_ALT	Aug 2003 – Apr 2012	10 a.m.	3–4 km	1–7%	~1300
ACE-FTS / SCISAT	V4.1/4.2, HARMOZ_ALT	Feb 2004 – present	sunrise, sunset	~3 km	1–3%	14–30
OMPS-LP / Suomi NPP	USask 2D v1.1.0 UBr v3.3 HARMOZ_ALT	Apr 2012 – present	1:30 p.m.	~1 km	2–10%	~1600
SAGE III / ISS	NASA, AO3 v5.2 HARMOZ_ALT	Jun 2017 – present	sunrise, sunset	~1 km	2–4%	14–30
POAM III / SPOT	NASA v.4 HARMOZ_ALT	1998 – 2005	sunrise, sunset	~1 km stratosph., 2–3 km upper troposphere	3–5 %	14–30

The merged dataset is created in 10° latitude zones from 90°S to 90°N, in the altitude range 10 – 50 km.

Merged deseasonalized anomalies

The merging is performed through computation of normalized deseasonalized anomalies from individual instruments and merging them. For each instrument, latitude zone and altitude level, the deseasonalized anomalies are computed as:

$$\Delta(t_i) = \frac{\rho(t_i) - \rho(m)}{\rho(m)} \qquad \text{Eq. (37)}$$

Where $\rho(t_i)$ is monthly zonal mean value at certain altitude and latitude zone corresponding to time t_i and $\rho(m)$ is the mean value for the corresponding month, i.e. $\rho(m) = \frac{1}{N_m}\sum_{j=1}^{N_m}\rho_j$, where N_m is number of monthly mean values ρ_j for month m.

For the Ozone_cci instruments, the seasonal cycle is evaluated using the overlapping period, years 2005-2011. The seasonal cycle for SAGE II is computed using years 1985-2004, for POAM III using its full period 1998-2005, for OMPS using the years 2012-2021, and for SAGE III/ISS using years 2017-2021. In computation of deseasonalized anomalies, we ignore those latitude-time bins with either inhomogeneity measure in latitude H_{lat} or in time H_{time} exceeding 0.9.

Before merging, the deseasonalized anomalies of the individual instruments have been extensively inter-compared with each other by computing and visualizing the time series of difference of individual anomalies from the median anomaly. This method turns out to be a sensitive method for detecting a temporal exceptional behavior of the individual data records. Only reliable datasets, which agree with each other and have no evident drifts or exceptional features with respect to the median anomaly, are selected for the merged dataset.

We perform first pre-merging via computation of the median GOMOS, MIPAS, SCIAMACHY, ACE-FTS and OSIRIS deseasonalized anomalies. Then SAGE II, OMPS, POAM III and SAGE III/ISS deseasonalized anomalies are offset to the pre-merged anomalies using the corresponding overlapping periods. After that, the outlier detection and the final merging (computing the median of all aligned deseasonalized anomalies) is performed.

We computed the merged anomaly as the median anomaly of the anomalies from individual instruments, for each altitude level and for each latitude zone.

Figure 22 illustrates the data merging: the upper panel shows the monthly zonal mean data, while the bottom panel shows individual anomalies and the merged (median) anomaly.

As observed in

Figure 22 the biases between the individual data records are removed by computing the deseasonalized anomalies. In the merging, we filtered individual anomaly values (locally for each latitude zone and altitude level), which differ from the median anomaly more than 10% at latitudes 40S-40N, and more than 20% in other latitude zones. This filtering is ineffective in absolute majority of cases; it removes only a few exceptional anomalies from GOMOS and ACE-FTS data due to their insufficient sampling.

More examples of merged deseasonalized anomalies are shown in *(Sofieva et al., 2017b) and (Sofieva et al., 2023)*. Since absolute values are not important for trend analyses, the merged deseasonalized anomalies can be directly used in time series analyses. The evaluation of ozone trends using the merged SAGE II-CCI-OMPS has been performed in (Sofieva et al., 2017b), (Steinbrecht et al., 2017), (WMO-2018, 2022*).*

Figure 22 - Top: monthly zonal mean ozone at 35 km in the latitude zone 40-50N. Bottom: individual deseasonalized anomalies and the merged anomaly (grey). In both plots, different colours denote data from different sensors as described in the bottom plot.

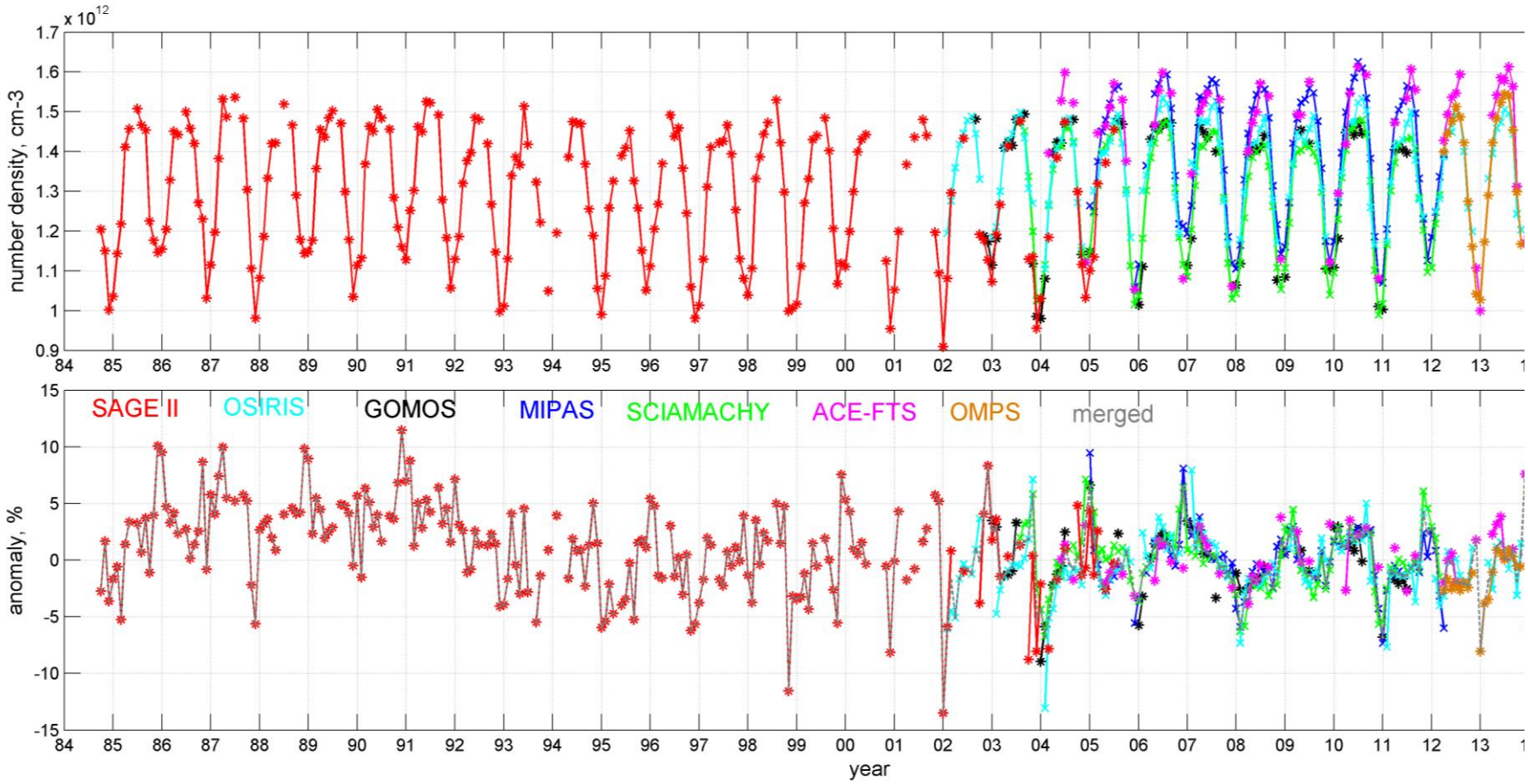

Merged ozone profiles.

The main dataset consists of the merged deseasonalized anomalies and their uncertainties described above. For the purpose of other applications (e.g., comparisons with models etc.), we presented the ozone profile also in number density. The computing of merged number density profiles from the merged deseasonalized anomalies is performed according to Eq. (34): the seasonal cycle is restored in the data. The best estimate of the amplitude of seasonal cycle is given by MIPAS measurements, because they provide all season pole-to-pole measurements with dense sampling. We take the absolute values of the seasonal cycle from SAGE II and OSIRIS in the overlapping period (which are very close to each other and also with GOMOS measurements), thus preserving the consistency in the dataset through the whole observation period.

For trend analyses, it is recommended using the deseasonalized anomalies directly. According to the merging principle, the best quality of the merged dataset is in the stratosphere in the latitude zone from 60°S to 60°N. The data in Polar Regions are affected by large variability and non-uniform data coverage. The quality of the data in Polar Regions is under investigation.

The satellite data quality also degrades in the UTLS. The merging principle seems to be optimal also for the UTLS, as it removed automatically biases, which can be significant in the UTLS. The trends in the UTLS estimated using the merged SAGE II – CCI- OMPS data follow the expectations (declining ozone trends in the tropics just above the tropopause due to intensification of the Brewer-Dobson circulation).

3.4.3.3 Merged monthly mean gridded ozone profiles

Overview

The monthly zonal mean gridded ozone profile dataset (MEGRIDOP, Sofieva et al., 2021) is a merged and gridded dataset generated using the ozone profiles retrieved from several limb and occultation instruments, viz. MIPAS (Michelson Interferometer for Passive Atmospheric Sounding), SCIAMACHY (SCanning Imaging Spectrometer for Atmospheric CHartographY) and GOMOS (Global Ozone Monitoring by occultation of Stars), all on Envisat, OSIRIS (Optical Spectrograph and InfraRed Imaging System) on Odin, OMPS-LP (Ozone Mapping and Profiles Suite - Limb Profiler) on Suomi-NPP, and MLS (Microwave Limb Sounder) on Aura.

These instruments provide high-quality ozone profiles with a good vertical resolution of 2-4 km and a relatively dense spatio-temporal coverage (100-3000 ozone profiles per day with a uniform sampling in longitude). The important information about the datasets is collected in Table 40. More information about the datasets from the individual satellite instruments is found in Petropavlovskikh et al., 2019, Sofieva et al., 2017b and references therein.

Table 40. General information about the datasets ingested in the merged monthly mean gridded ozone profiles product.

Instrument/ satellite	Level 2 processor, references	Years	Vertical range/retrieval coordinate	Local time of Level 2 data	Number of profiles per day
MIPAS/Envisat	KIT/IAA V8	2005-2012	6-70 km, Altitude	10 a.m. and p.m.	~1000
SCIAMACHY/Envisat	UBr v3.5	2002-2012	8-65 km, Altitude	10 a.m.	~1300
GOMOS/Envisat	ALGOM2s v1	2002-2011	10-105 km, altitude	10 p.m.	~110
OSIRIS/Odin	USask v7.2	2001-present	10-59 km, altitude	6 a.m. and p.m	~250
OMLS-LP /SUOMI-NPP	USask 2D v 1.1.0 / UBr V3.3	2012-present	6- 59 km, altitude	1:30 p.m	~1600
MLS/Aura	NASA v5 (Livesey et al., 2013)	2004 - present	261-0.02 hPa (~8-75 km), pressure	1:30 a.m. and p.m.	~3000

For all instruments except MLS, the original retrievals of ozone profiles are performed on an altitude grid. GOMOS, OSIRIS, SCIAMACHY and OMPS provide number density ozone profiles; therefore this representation (number density on an altitude grid) is used for the merged dataset. For MIPAS, the retrievals are performed in volume mixing ratio vs. altitude grid. The conversion to number density profiles is performed using temperature profiles retrieved by MIPAS and the pressure profiles provided with the MIPAS ozone data; the latter are constructed from altitude and temperature using one (z,p,T) data point from the ERA-Interim reanalysis (Dee et al., 2011).

For MLS, retrievals are performed in mixing ratio on a pressure grid. Similarly to the conversion procedure of MIPAS data, we performed the conversion to number density using the retrieved MLS temperatures, but for altitude-pressure conversion, we used the ERA-Interim reanalysis data. Such conversion might introduce some uncertainty in the MLS data. For studies of long-term changes, this uncertainty is associated with a potentially imperfect representation of temperature trends in ERA-Interim, which might influence ozone trends. However, since current stratospheric temperature trends (after 2000) are small (Maycock et al., 2018; Steiner et al., 2020), this uncertainty is expected to be small.

For all the instruments, we use the ozone profiles from the updated HARMonized dataset of Ozone profiles (HARMOZ_ALT) developed in the ESA Ozone_cci project (Sofieva et al., 2013). HARMOZ consists of the original retrieved ozone profiles from each instrument, which are screened for invalid data by the instrument experts and are presented on a vertical grid (altitude-gridded profiles are used here) and in a common netCDF4 format.

Merging method

The merging method used for creating MEGRIDOP is similar to that used in creating the merged monthly zonal mean (MMZM) ozone profiles. The deseasonalized anomalies of all instruments except

OMPS are aligned, as the seasonal cycle was estimated using the same period. First, we offset the OMPS deseasonalized anomalies to the median of the deseasonalized anomalies from all other instruments. These additive offsets are computed using the data from years 2012-2018, and the offsetting procedure is illustrated in Figure 23. In this figure, we selected a spatial bin where the effect of the offsetting is clearly visible. In many other bins, the offsets are small or negligible. As observed, the deseasonalized anomalies from individual datasets are in good agreement.

Figure 23. Illustration of offsetting the OMPS deseasonalized anomalies. The data are shown for altitude 35 km and the latitude/longitude bin 0-10° N/ 0-20° E. The OMPS data are shown in blue, and data from the five other sensor systems are shown in the other colours.

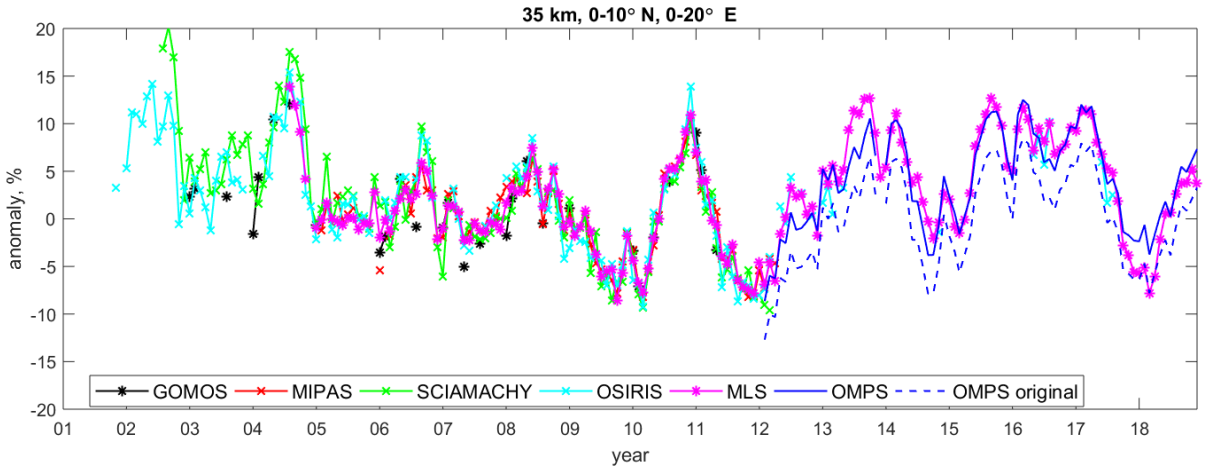

After offsetting OMPS, the merged ozone profiles in each spatiotemporal bin and at each altitude level is obtained from the median of the deseasonalized anomalies corresponding to individual instruments:

$$\Delta_{merged}(z,b,t) = median(\Delta_i(z,b,t)) \qquad \text{Eq. (38)}$$

The advantage of using the median estimate is that the merged anomaly follows the majority of the data, and it is not very sensitive to exclusion/addition of each individual data record, if there are several (and consistent) anomalies. The sensitivity of the dataset and the evaluated trends to the number of instruments is studied in detail for SAGE-CCI-OMPS dataset, which is created with the same merging algorithm (see Sofieva et al., 2017 and its Supplements), and this is valid also for MEGRIDOP.

The uncertainties of the merged deseasonalized anomalies are computed similarly to those used for the merged SAGE-CCI-OMPS dataset (Sofieva et al., 2017). For each instrument, the uncertainty of the deseasonalized anomalies is given by:

$$\sigma_{\Delta i} = \Delta_i \sqrt{\frac{\sigma_i^2}{\rho_i^2} + \frac{\sigma_{m,i}^2}{\rho_{m,i}^2}} \qquad \text{Eq. (39)}$$

Where σ_i is the uncertainty of the gridded ozone profiles (see Sect. 3.1.) and $\sigma_{m,i}$ is the uncertainty of the seasonal cycle $\rho_{m,i}$, which can be estimated via propagation of random uncertainties to the mean value:

$$\sigma_{m,i}^2 = \frac{1}{N_m^2} \sum_{j=1}^{N_m} \sigma_i^2(z,b,t_j) \qquad \text{Eq. (40)}$$

Analogously to (Sofieva et al., 2017b), the uncertainties of the merged deseasonalized anomalies are estimated as:

$$\sigma_{\Delta,merged} = \min\left(\sigma_{\Delta,i_{med}}, \sqrt{\frac{1}{N}\sum_{i=1}^{N}\sigma_{\Delta,i}^2 + \frac{1}{N^2}\sum_{i=1}^{N}\left(\Delta_i - \Delta_{merged}\right)^2} \right) \qquad \text{Eq. (41)}$$

Where $\sigma_{\Delta,i_{med}}$ is the anomaly uncertainty of the instrument corresponding to the median value. In case of even number of measurements, the mean of two neighbors to the median is used. Analogously to uncertainty estimates in the zonal mean merged dataset (Sofieva et al., 2017b), the uncertainties given by Eq. (38) can be interpreted as follows. If individual anomalies are significantly different, the uncertainty of the merged anomaly is the uncertainty corresponding to the median value. In cases where several instruments report a similar anomaly (intersecting error bars), this provides more confidence in this anomaly value, and the resulting uncertainty of the merged anomaly is approximated by the second term in Eq. (38).

4 Output data

A basic description of the C3S ozone output fields is provided in this Section. For further details, please see the C3S Ozone Product User Guide and Specification [D24].

4.1 Overview

All C3S ozone data sets are

- Level-3 or Level 4 data, i.e. are provided on a regular longitude-latitude grid (or latitude bands for zonal averages);
- global coverage;
- Monthly averages;
- Provided in CF-compliant NetCDF format.

The list of all C3S2_312a_Lot2 data products is provided in Table 41.

Table 41. List of the C3S ozone data products available from the C3S CDS (Feb 2024). All products cover the globe and have a monthly temporal resolution. Data are provided in the NetCDF format. The column "Overal temporal coverage" contains the time coverage of the dataset. Note that a fixed end date is not provided in the case there is a corresponding "Update frequency", since these datasets are extended on a regular basis.

Product name	Product definition	Sensor(s)	Processing level	Product type	Overall temporal coverage	Update frequency	Spatial resolution	Uncertainty information	Provision & provenance
TC_GOME	Total ozone column	GOME	3	CDR	06.1995 - 07.2011	N/A	1°x1°	Random and smoothing error	BIRA/DLR
TC_SCIA		SCIAMACHY	3	CDR	08.2002 - 04.2012	N/A	1°x1°		BIRA/DLR
TC_GOME 2A		GOME-2A	3	CDR	01.2007 - 10.2021	N/A	1°x1°		BIRA/DLR
TC_GOME 2B		GOME-2B	3	ICDR	01.2013 -	Quarterly with 4 months delay	1°x1°		BIRA/DLR
TC_GOME 2C		GOME-2C	3	ICDR	07.2019 -		1°x1°		BIRA/DLR
TC_OMI		OMI	3	ICDR	10.2004 -		1°x1°		BIRA/DLR
TC_OMPS		OMPS-NM	3	ICDR	01.2012 -		1°x1°		BIRA/DLR
TC_S5P		S5P-TROPOMI	3	ICDR	05.2018 -		1°x1°		DLR
TC_GTO-ECV		(4)	3	ICDR	07.1995 -	Semi-annually with 4 months delay	1°x1°	Random and sampling error	BIRA/DLR
TC_MSR		(1)	4	ICDR	04.1970 -	Annually with 3 months delay	1°x1°	Random error	KNMI
TC_IASI-A	Total and tropospheric ozone	IASI-A	3	CDR	10.2007 - 08.2021	N/A	1°x1°	Random error	LATMOS
06TC_IASI-A		IASI-A	3	CDR	10.2007 - 08.2021	N/A	1°x1°	Random error	LATMOS
TC_IASI-B		IASI-B	3	ICDR	05.2013 -	Quarterly with 1 month delay	1°x1°	Random error	LATMOS
TC_IASI-C		IASI-C	3	ICDR	10.2019 -		1°x1°	Random error	LATMOS
06TC_IASI-B		IASI-B	3	ICDR	05.2013 -		1°x1°	Random error	LATMOS
06TC_IASI-C		IASI-C	3	ICDR	10.2019 -		1°x1°	Random error	LATMOS
NP_GOME	Ozone profile (nadir)	GOME	3	CDR	06.1995 - 06.2011	N/A	1°x1°	Random and smoothing error	RAL/KNMI
NP_SCIA		SCIAMACHY	3	CDR	08.2002 - 04.2012	N/A	1°x1°		RAL/KNMI
NP_GOME 2A		GOME-2A	3	CDR	01.2007 - 10.2021	N/A	1°x1°		RAL/KNMI
NP_GOME 2B		GOME-2B	3	ICDR	04.2013 –	Annually with 4 months delay	1°x1°		RAL/KNMI
NP_OMI		OMI	3	ICDR	10.2004 -		1°x1°		RAL/KNMI
NP_GOP-ECV		(5)	3	ICDR	07.1995 – 10.2021	N/A	5°x5°		RAL/KNMI /DLR
LMZ_MIPAS	Ozone profile (limb)	MIPAS	3	CDR	07.2002 - 04.2012	N/A	10° lat zones	Random and sampling error	UNI-HB/FMI
LMZ_GOMOS		GOMOS	3	CDR	08.2002 - 12.2011	N/A	10° lat zones		UNI-HB/FMI
LMZ_SCIA		SCIAMACHY	3	CDR	08.2002 - 03.2012	N/A	10° lat zones		UNI-HB/FMI
LMZ_SAGE 2		SAGE-2	3	CDR	10.1984 - 08.2005	N/A	10° lat zones		UNI-HB/FMI
LMZ_HALOE		HALOE	3	CDR	10.1991 - 09.2005	N/A	10° lat zones		UNI-HB/FMI
LMZ_SMR (*)		SMR (*)	3	CDR (*)	07.2001 - 08.2014 (*)	N/A (*)	10° lat zones		UNI-HB/FMI
LMZ_OSIRIS		OSIRIS	3	ICDR	11.2001 -	Annually with 3 months delay	10° lat zones		UNI-HB/FMI

LMZ_ACE		ACE	3	ICDR	02.2004 -		10° lat zones		UNI-HB/FMI
LMZ_SABER		SABER	3	ICDR	01.2002 -		10° lat zones		UNI-HB/FMI
LMZ_MLS		MLS	3	ICDR	08.2004 -		10° lat zones		UNI-HB/FMI
LMZ_OMPS-SASK		OMPS-LP	3	ICDR	02.2012 -		10° lat zones		UNI-HB/FMI
LMZ_OMPS-UB		OMPS-LP	3	ICDR	02.2012 -		10° lat zones		UNI-HB/FMI
LMZ_SAGE-III		SAGE-III	3	ICDR	06.2017 -		10° lat zones		UNI-HB/FMI
LMZ_MERGED		(2)	3	ICDR	10.1984 -		10° lat zones		FMI
LP_MERGED		(3)	3	ICDR	11.2001 -		10°x20°		FMI

TC Total column monthly gridded average product
NP Nadir profile monthly gridded average product
LP Limb profile monthly gridded average product
LMZ Limb monthly zonal profile average product
(*) SMR is still in operation but the L1 data processing has been interrupted in 2014. It may resume later with the reprocessing of the Odin entire data record.
(1) Merged/assimilated product based on GOME, SCIAMACHY, OMI, GOME-2A/B/C, BUV-Nimbus4, TOMS-Nimbus7, TOMS-EP, SBUV-7, -9, -11, -14, -16, -17, -18, -19, OMPS and TROPOMI
(2) Monthly zonal mean merged product (concentration and concentration anomaly) based on MIPAS, GOMOS, SCIAMACHY, SAGE-2, OSIRIS, ACE, POAM-III and OMPS-LP
(3) Latitude-longitude gridded merged product (concentration and concentration anomaly) based on MIPAS, SCIAMACHY, GOMOS, OSIRIS, OMPS-LP and MLS.
(4) Merged product based on GOME, SCIAMACHY, GOME-2A/B/C, OMI and TROPOMI/S5P
(5) Merged product based on GOME, SCIAMACHY, GOME-2A/B, and OMI

4.2 L-3 and L-4 ozone total column derived from UV-nadir sensors

This family of C3S ozone products includes Level-3 and Level-4 monthly mean total columns retrieved from nadir satellite observations. Data are from individual sensors (Table 42), merged (Table 43) or the outcome of multi-sensor reanalysis (Table 44).

Table 42. Level 3 ozone total column monthly mean from individual UV-nadir sensors.

Originating satellite instruments	Nadir-viewing sensors GOME, SCIAMACHY, GOME-2, OMPS, OMI and TROPOMI/S5P (cf. Sections 1.1.1 to 1.1.4)
Data class	Earth Observation Data
Data product names	• TC_GOME • TC_SCIA • TC_GOME2A • TC_GOME2B • TC_GOME2C • TC_OMPS • TC_OMI • TC_S5P
Data specification document	C3S Ozone Product User Guide and Specification [D24]
Geographic coverage	The globe
Horizontal grid	1° longitude x 1° latitude
Temporal coverage	From 1995, 2002, 2004, 2007, 2012, 2013 (depending on satellite) to 2011, 2012 - today (depending on satellite)
Temporal resolution	Monthly
Main variable physical nature and unit	Monthly mean ozone total column (mol.m-2)
Data format	CF-compliant NetCDF

Table 43. Level 3 ozone total column monthly mean from UV-nadir sensors (merged)

Originating satellite instruments	Nadir-viewing sensors GOME, SCIAMACHY, GOME-2, OMI, TROPOMI/S5P (cf. Sections 1.1.1 to 1.1.4)
Data class	Earth Observation Data
Data product name	TC_GTO-ECV
Data specification document	C3S Ozone Product User Guide and Specification [D24]
Geographic coverage	The globe
Horizontal grid	1° longitude x 1° latitude
Temporal coverage	1995 – today
Temporal resolution	Monthly
Main variable physical nature and unit	Monthly mean ozone total column (mol.m-2)
Data format	CF-compliant NetCDF

Table 44. Level 4 ozone total column monthly mean from multi-sensor reanalysis (MSR).

Originating satellite instruments	BUV-Nimbus4, TOMS-Nimbus7, TOMS-EP, SBUV-7, -9, -11, -14, -16, -17, -18, -19, GOME, SCIAMACHY, OMI, GOME-2, TROPOMI, FY-3A and OMPS

Data class	Earth Observation Data
Data product name	TC_MSR
Data specification document	C3S Ozone Product User Guide and Specification [D24]
Geographic coverage	The globe
Horizontal grid	1° longitude x 1° latitude
Temporal coverage	1970 – today
Temporal resolution	Monthly
Main variable physical nature and unit	Monthly mean ozone total column (DU)
Data format	CF-compliant NetCDF

4.3 L-3 ozone total and tropospheric column derived from IASI

The C3S ozone columns retrieved from observations by IASI include Level-3 monthly mean total and tropospheric columns (Table 45).

Table 45. Level 3 ozone total and tropospheric column monthly mean from IASI.

Originating satellite instrument	Nadir-viewing sensor IASI on board the Metop satellites (cf. Section 1.1.6)
Data class	Earth Observation Data
Data product name	• TC_IASI-A • TC_IASI-B • TC_IASI-C • 06TC_IASI-A • 06TC_IASI-B • 06TC_IASI-C
Data specification document	C3S Ozone Product User Guide and Specification [D24]
Geographic coverage	The globe
Horizontal grid	1° longitude x 1° latitude
Temporal coverage	TC_IASI-A & 06TC_IASI-A 2008-2021 TC_IASI-B & 06TC_IASI-B 2013-today TC_IASI-C & 06TC_IASI-C 2019-today
Temporal resolution	Monthly
Main variable physical nature and unit	• Monthly mean ozone total column (DU) • Monthly mean ozone tropospheric column (DU)
Data format	CF-compliant NetCDF

4.4 L-3 ozone profile derived from UV-nadir sensors

The C3S ozone vertical profiles derived from nadir-viewing satellites include Level-3 monthly mean data (Table 46).

Table 46. Level 3 ozone profile monthly mean from UV-nadir sensors.

Originating satellite instruments	Nadir-viewing sensors GOME, SCIAMACHY, GOME-2 and OMI (cf. Sections 1.1.1 to 1.1.4)
Data class	Earth Observation Data

Data product names	• NP_GOME • NP_SCIA • NP_GOME2A • NP_GOME2B • NP_OMI • NP_GOP-ECV
Data specification document	C3S Ozone Product User Guide and Specification [D24]
Geographic coverage	The globe
Horizontal grid	1° longitude x 1° latitude (5° longitude x 5° latitude for GOP-ECV)
Vertical coverage	From surface to top of atmosphere
Vertical scale / levels	20 levels (i.e. 19 layers) in hPa, ranging from 1000 to 0.01 (adjustable)
Temporal coverage	From 1995-today (depending on satellite)
Temporal resolution	Monthly
Main variable physical nature and unit	• Monthly mean vertical profile of the ozone molecular number density (cm^{-3}) • Monthly mean vertical profile of the ozone volume mixing ratio (ppmv) • Monthly mean ozone partial column (mol m^{-2})
Data format	CF-compliant NetCDF

4.5 L-3 ozone profile derived from limb and occultation sensors

The C3S ozone vertical profiles derived from limb and occultation sensors are Level-3 monthly mean data. They include zonal averages retrieved from individual sensors (Table 47) as well as merged zonally averaged (Table 48) and gridded (Table 49) monthly mean profiles.

Table 47. Level 3 ozone profile monthly zonal mean (MZM) from limb and occultation sensors.

Originating satellite instruments	Limb and occultation sensors MIPAS, GOMOS, SCIAMACHY, SAGE-2, HALOE, OSIRIS, SMR, ACE-FTS, MLS, SABER (cf. Section 1.2)
Data class	Earth Observation Data
Data product names	• LMZ_MIPAS • LMZ_GOMOS • LMZ_SCIA • LMZ_SAGE2 • LMZ_HALOE • LMZ_OSIRIS • LMZ_SMR • LMZ_ACE • LMZ_MLS • LMZ_SABER • LMZ_OMPS-SASK • LMZ_OMPS-UB • LMZ_SAGE-III
Data specification document	C3S Ozone Product User Guide and Specification [D24]
Geographic coverage	The globe
Horizontal grid	10°-width latitude zones

Vertical coverage	Instrument-specific
Vertical scale / levels	Altitude grid /pressure grid
Temporal coverage	From 1984, 1991, 2001, 2002, 2004 (depending on satellite) to 2005, 2012-today (depending on satellite)
Temporal resolution	Monthly
Main variable physical nature and unit	Monthly zonal mean (MZM) vertical profile of the ozone molar concentration ($mol.m^{-3}$)
Data format	CF-compliant NetCDF

Table 48. Level 3 ozone profile merged monthly zonal mean (MMZM) from limb and occultation sensors.

Originating satellite instruments	Limb and occultation sensors MIPAS, GOMOS, SCIAMACHY, SAGE-2, OSIRIS, ACE-FTS, POAM-III and OMPS-LP (cf. Section 1.2)
Data class	Earth Observation Data
Data product name	LMZ_MERGED
Data specification document	C3S Ozone Product User Guide and Specification [D24]
Geographic coverage	The globe
Horizontal grid	10°-width latitude zones
Vertical coverage	10 - 50 km
Vertical scale / levels	Altitude grid with 1 km resolution
Temporal coverage	1984 – today
Temporal resolution	Monthly
Main variable physical nature and unit	Monthly zonal mean (MZM) vertical profile of the ozone molar concentration ($mol.m^{-3}$)
Data format	CF-compliant NetCDF

Table 49. Level 3 ozone profile merged horizontally-resolved monthly mean from limb and occultation sensors.

Originating satellite instruments	Limb and occultation sensors MIPAS, SCIAMACHY, GOMOS, OSIRIS, OMPS-LP and MLS (cf. Section 1.2)
Data class	Earth Observation Data
Data product name	LP_MERGED
Data specification document	C3S Ozone Product User Guide and Specification. [D24]
Geographic coverage	The globe
Horizontal grid	10° latitude x 20° longitude
Vertical coverage	10-50 km
Vertical scale / levels	Altitude grid with 1 km resolution
Temporal coverage	2002 – today
Temporal resolution	Monthly
Main variable physical nature and unit	Monthly mean vertical profile of the ozone molar concentration ($mol.m^{-3}$)
Data format	CF-compliant NetCDF

5 References

van der A, R.J., M.A.F. Allaart and H.J. Eskes, Extended and refined multi sensor reanalysis of total ozone for the period 1970-2012, Atmospheric Measurement Techniques, 2015, 8, 3021-3035, doi:10.5194/amt-8-3021-2015.

A. Berk, P. Conforti, R. Kennett, T. Perkins, F. Hawes, and J. van den Bosch, "MODTRAN6: a major upgrade of the MODTRAN radiative transfer code," Proc. SPIE 9088, Algorithms and Technologies for Multispectral, Hyperspectral, and Ultraspectral Imagery XX, 90880H (June 13, 2014); doi:10.1117/12.2050433.

Acarreta, J.R., J.F. de Haan and P. Stammes, Cloud pressure retrieval using the O2-O2 absorption band at 477 nm, J. Geophys. Res., 2004, 109, D05204, doi:10.1029/2003JD003915.

Adams, C., A. E. Bourassa, V. Sofieva, L. Froidevaux, C. A. McLinden, D. Hubert, J.-C. Lambert, C. E. Sioris and D. A. Degenstein, Assessment of Odin-OSIRIS ozone measurements from 2001 to the present using MLS, GOMOS, and ozonesondes, Atmos. Meas. Tech., 7, 49–64, https://doi.org/10.5194/amt-7-49-2014, 2014.

Arosio, C., Rozanov, A., Malinina, E., Eichmann, K.-U., von Clarmann, T. and Burrows, J. P.: Retrieval of ozone profiles from OMPS limb scattering observations, Atmos. Meas. Tech., 11(4), 2135–2149, doi:10.5194/amt-11-2135-2018, 2018.

Arosio, C., Rozanov, A., Gorshelev, V., Laeng, A. and Burrows, J. P.: Assessment of the error budget for stratospheric ozone profiles retrieved from OMPS limb-scatter measurements, Atmos. Meas. Tech. Discuss., 2022, 1–27, doi:10.5194/amt-2022-116, 2022.

August, T., Klaes, D., Schlüssel, P., Hultberg, T., Crapeau, M., Arriaga, A., O'Carroll, A., Coppens, D., Munro, R., and Calbet, X.: IASI on Metop-A: Operational Level 2 retrievals after five years in orbit, J. Quant. Spectrosc. Ra., 113, 1340–1371, doi:10.1016/j.jqsrt.2012.02.028, 2012.

Bass, A. M., and R. J. Paur, The ultraviolet cross-sections of ozone, I, The measurements, in Atmospheric Ozone, edited by C. S. Zerefos and A. Ghazi, pp. 606-610, D. Reidel, Norwell, Mass., 1985.

Bhartia, P. Algorithm Theoretical Baseline Document, TOMS v8 Total ozone algorithm. http://toms.gsfc.nasa.gov/version8/version8_update.html, 2003.

Birch, K. P. and M. J. Downs, Correction to the Updated Edlén Equation for the Refractive Index of Air, Metrologia, 31, 4, 315, doi:10.1088/0026-1394/31/4/006, 1994.

Bovensmann, H., Burrows, J. P., Buchwitz, M., Frerick, J., Noël, S., Rozanov, V. V., Chance, K. V., Goede, A. P. H., Bovensmann, H., Burrows, J. P., Buchwitz, M., Frerick, J., Noël, S., Rozanov, V. V., Chance, K. V. and Goede, A. P. H.: SCIAMACHY: Mission Objectives and Measurement Modes, J. Atmos. Sci., 56(2), 127–150, https://doi.org/10.1175/1520-0469(1999)056<0127:SMOAMM>2.0.CO;2, 1999.

Boynard, A., Hurtmans, D., Koukouli, M. E., Goutail, F., Bureau, J., Safieddine, S., Lerot, C., Hadji-Lazaro, J., Wespes, C., Pommereau, J.-P., Pazmino, A., Zyrichidou, I., Balis, D., Barbe, A., Mikhailenko, S. N., Loyola, D., Valks, P., Van Roozendael, M., Coheur, P.-F., and Clerbaux, C.: Seven years of IASI ozone retrievals from FORLI: validation with independent total column and vertical profile measurements, Atmos. Meas. Tech., 9, 4327–4353, https://doi.org/10.5194/amt-9-4327-2016, 2016.

Boynard, A., Hurtmans, D., Garane, K., Goutail, F., Hadji-Lazaro, J., Koukouli, M. E., Wespes, C., Vigouroux, C., Keppens, A., Pommereau, J.-P., Pazmino, A., Balis, D., Loyola, D., Valks, P., Sussmann, R., Smale, D., Coheur, P.-F., and Clerbaux, C.: Validation of the IASI FORLI/EUMETSAT ozone products using satellite (GOME-2), ground-based (Brewer–Dobson, SAOZ, FTIR) and ozonesonde measurements, Atmos. Meas. Tech., 11, 5125-5152, https://doi.org/10.5194/amt-11-5125-2018, 2018.

Brion, J., A. Chakir, J. Charbonnier, D. Daumont, C. Parisse and J. Malicet, Absorption Spectra Measurements for the Ozone Molecule in the 350–830 nm Region, Journal of Atmospheric Chemistry 30: 291–299, 1998.

Burrows, J.P., M. Weber, and M. Buchwitz, The Global Ozone monitoring experiment (GOME): mission concept and first scientific results, J. Atmospheric Sci., 56, 151-175, 1999.

Chance, K. and Kurucz, R. L.: An improved high-resolution solar reference spectrum for earth's atmosphere measurements in the ultraviolet, visible, and near infrared, J. Quant. Spectrosc. Radiat. Transf., 111(9), 1289–1295, doi:10.1016/j.jqsrt.2010.01.036, 2010.

Chiou, E. W., Bhartia, P. K., McPeters, R. D., Loyola, D. G., Coldewey-Egbers, M., Fioletov, V. E., Van Roozendael, M., Spurr, R., Lerot, C. and Frith, S. M.: Comparison of profile total ozone from SBUV (v8.6) with GOME-type and ground-based total ozone for a 16-year period (1996 to 2011), Atmos. Meas. Tech., 7(6), 1681–1692, doi:10.5194/amt-7-1681-2014, 2014.

Chu, W.P., M.P. McCormick, J. Lenoble, C. Brogniez, and P. Pruvost, SAGE II Inversion Algorithm, J. Geophys. Res., 94, D6, 8339-8352, https://doi.org/10.1029/JD094iD06p08339, 1989.

Clough, S, Shephard, M, Mlawer, E, Delamere, J, Iacono, M, Cady-Pereira K, Boukabara, S., Brown, P.D., Atmospheric Radiative Transfer Modeling: a Summary of the AER Codes, J. Quant. Spectrosc. Radiat. Transfer, 91, 233-244, https://doi.org/10.1016/j.jqsrt.2004.05.058, 2005.

Coldewey-Egbers, M., M. Weber, L. N. Lamsal, R. de Beek, M. Buchwitz, J. P. Burrows, Total ozone retrieval from GOME UV spectral data using the weighting function DOAS approach, Atmos. Chem. Phys. 5, 5015-5025, 2005.

Coldewey-Egbers, M., D.G. Loyola, M. Koukouli, D. Balis, J.-C. Lambert, T. Verhoelst, J. Granville, M. van Roozendael, C. Lerot, R. Spurr, S.M. Frith, and C. Zehner, The GOME-type Total Ozone Essential Climate Variable (GTO-ECV) data record from the ESA Climate Change Initiative, *Atmos. Meas. Tech.*, *8*(9), 3923–3940, doi:10.5194/amt-8-3923-2015, 2015.

Damadeo, R. P., J. M. Zawodny, L. W. Thomason and N. Iyer, SAGE version 7.0 algorithm: application to SAGE II, Atmos. Meas. Tech., 6, 3539–3561, https://doi.org/10.5194/amt-6-3539-2013, 2013.

Daumont, D., Brion, J., Charbonnier, J., and Malicet, J., Ozone UV spectroscopy, I. Absorption cross-sections at room temperature, J. Atmos. Chem. 15, 145-155, 1992.

Dee, D. P., Uppala, S. M., Simmons, A. J., Berrisford, P., Poli, P., Kobayashi, S., Andrae, U., Balmaseda, M. A., Balsamo, G., Bauer, P., Bechtold, P., Beljaars, A. C. M., van de Berg, L., Bidlot, J., Bormann, N., Delsol, C., Dragani, R., Fuentes, M., Geer, A. J., Haimberger, L., Healy, S. B., Hersbach, H., Hólm, E. V, Isaksen, L., Kållberg, P., Köhler, M., Matricardi, M., McNally, A. P., Monge-Sanz, B. M., Morcrette, J.-J., Park, B.-K., Peubey, C., de Rosnay, P., Tavolato, C., Thépaut, J.-N. and Vitart, F.: The ERA-Interim reanalysis: configuration and performance of the data assimilation system, Q. J.

R. Meteorol. Soc., 137(656), 553–597, doi:10.1002/qj.828, 2011.

Degenstein, D. A., Bourassa, A. E., Roth, C. Z. and Llewellyn, E. J.(2009): Limb scatter ozone retrieval from 10 to 60 km using a multiplicative algebraic reconstruction technique, Atmos. Chem. Phys., 9(17), 6521–6529, doi:10.5194/acp-9-6521-2009.

Elsasser, W. M., Heat Transfer by Infrared Radiation in the Atmosphere, Harvard Meteorological Studies N° 6, Harvard University Printing Office, Cambridge, 1942.

Eskes, H. J., van der A, R. J., Brinksma, E. J., Veefkind, J. P., de Haan, J. F., and Valks, P. J. M.: Retrieval and validation of ozone columns derived from measurements of SCIAMACHY on Envisat, Atmos. Chem. Phys. Discuss., 5, 4429-4475, doi:10.5194/acpd-5-4429-2005.

Flynn, L. E., Seftor, C. J., Larsen, J. C. and Xu, P.: The Ozone Mapping and Profiler Suite, in Earth Science Satellite Remote Sensing: Vol. 1: Science and Instruments, edited by J. J. Qu, W. Gao, M. Kafatos, R. E. Murphy, and V. V Salomonson, pp. 279–296, Springer Berlin Heidelberg, Berlin, Heidelberg., 2006.

Fortuin, J. P. F. and U. Langematz, Update on the global ozone climatology and on concurrent ozone and temperature trends, Atmospheric Sensing and Modelling, Satellite Remote Sensing Proceedings, Volume 2311, Rome, Italy, https://doi.org/10.1117/12.198578, 1994.

Froidevaux, L. *et al.*, Validation of Aura Microwave Limb Sounder stratospheric ozone measurements, J. Geophys. Res., 113, D15, https://doi.org/10.1029/2007JD008771, August 2008.

Fussen, D., and C. Bingen. "A volcanism dependent model for the extinction profile of stratospheric aerosols in the UV-visible range." *Geophys. Res. Lett.* 22 (1999): 703-706.

Garane, K., Lerot, C., Coldewey-Egbers, M., Verhoelst, T., Koukouli, M.E., Zyrichidou, I., Balis, D.S., Danckaert, T., Goutail, F., Granville, J., Hubert, D., Keppens, A., Lambert, J.-C., Loyola, D., Pommereau, J.-P., Van Roozendael, M., and Zehner, C.: Quality assessment of the Ozone_cci Climate Research Data Package (release 2017) – Part 1: Ground-based validation of total ozone column data products, Atmos. Meas. Tech., 11, 1385-1402, doi:10.5194/amt-11-1385-2018, 2018.

Gorshelev, V., A. Serdyuchenko, M. Weber, W. Chehade, and J. P. Burrows (2014), High spectral resolution ozone absorption cross-sections – Part 1: Measurements, data analysis and comparison with previous measurements around 293 K, Atmos. Meas. Tech., 7(2), 609–624, doi:10.5194/amt-7-609-2014.

Grainger, J., and J. Ring, Anomalous Fraunhofer line profiles, Nature, 193, 762-762, 1962.

Hao, N., Koukouli, M. E., Inness, A., Valks, P., Loyola, D. G., Zimmer, W., Balis, D. S., Zyrichidou, I., Van Roozendael, M., Lerot, C. and Spurr, R. J. D.: GOME-2 total ozone columns from Metop-A/Metop-B and assimilation in the MACC system, Atmos. Meas. Tech., 7(9), 2937–2951, doi:10.5194/amt-7-2937-2014, 2014.

Hegglin, M. I., *et al.*, SPARC Data Initiative: Comparison of water vapor climatologies from international satellite limb sounders, J. Geophys. Res., 118, 20, 11,824-11,846, https://doi.org/10.1002/jgrd.50752, 2013.

Herman, J.R. and E. A. Celarier, Earth surface reflectivity climatology at 340-380 nm from TOMS data, J. Geophys. Res., 102, 28003-28011, https://doi.org/10.1029/97JD02074, 1997.

Hubert, D., et al. (2016): Ground-based assessment of the bias and long-term stability of 14 limb and occultation ozone profile data records, Atmos. Meas. Tech., 9(6), 2497–2534, doi:10.5194/amt-9-2497-2016, 2016.

Huijnen, V., J. Williams, M. van Weele, T. van Noije, M. Krol, F. Dentener, A. Segers, S. Houweling, W. Peters, J. de Laat, F. Boersma, P. Bergamaschi, P. van Velthoven, P. Le Sager, H. Eskes, F. Alkemade, R. Scheele, P. Nédélec and H.-W. Pätz, The global chemistry transport model TM5: description and evaluation of the tropospheric chemistry version 3.0, Geosci. Model Dev., 3, 445–473, https://doi.org/10.5194/gmd-3-445-2010, 2010.

Hurtmans, D., Coheur, P.-F., Wespes, C., Clarisse, L., Scharf, O., Clerbaux, C., Hadji-Lazaro, J., George, M., and Turquety, S.: FORLI radiative transfer and retrieval code for IASI, J. Quant. Spectrosc. Ra., 113, 1391–1408, doi:10.1016/j.jqsrt.2012.02.036, 2012.

Jia, J., A. Rozanov, A. Ladstätter-Weißenmayer and J. P. Burrows, Global validation of SCIAMACHY limb ozone data (versions 2.9 and 3.0, IUP Bremen) using ozonesonde measurements, Atmos. Meas. Tech., 8, 3369–3383, doi:10.5194/amt-8-3369-2015, 2015.

Joiner, J., P.K. Barthia, R.P. Cebula, E. Hilsenrath, R.D. Mcpeters, and H. Park, Rotational Raman scattering (Ring effect) in satellite backscatter ultraviolet measurements, Applied Optics, 34(21), 4513-4525, https://doi.org/10.1364/AO.34.004513, 1995.

Joiner, J., and P. Bhartia, Accurate determination of total ozone using SBUV continuous spectral scan measurements, J. Geophys. Res., 102, 12957-12969, https://doi.org/10.1029/97JD00902, 1997.

Kerridge, B. J. K.., R. Siddans, B.L. Latter, J.P. Burrows, M. Weber, R. De Beek, I. Aben, and W. Hartman. GOME-2 Error Assessment Study, Final Report EUMETSAT Contract No EUM/CO/01/901/DK, 2002.

Kleipool, Q.L., M.R. Dobber, J.F. De Haan and P.F. Levelt, Earth Surface Reflectance Climatology from Three Years of OMI Data, J. Geophys. Res, 113, D18308, doi:10.1029/2008JD010290, 2008.

Koelemeijer, R. B. A., J. F. de Haan and P. Stammes, A database of spectral surface reflectivity in the range 335–772 nm derived from 5.5 years of GOME observations, J. Geophys. Res., 108, NO. D2, 4070, doi:10.1029/2002JD002429, 2003.

Koukouli, M. E., Lerot, C., Granville, J., Goutail, F., Lambert, J.-C., Pommereau, J.-P., Balis, D., Zyrichidou, I., Van Roozendael, M., Coldewey-Egbers, M., Loyola, D., Labow, G., Frith, S., Spurr, R. and Zehner, C.: Evaluating a new homogeneous total ozone climate data record from GOME/ERS-2, SCIAMACHY/Envisat, and GOME-2/Metop-A, J. Geophys. Res. Atmos., 120(23), 12,296-12,312, doi:10.1002/2015JD023699, 2015.

Krol, M., S. Houweling, B. Bregman, M. van den Broek, A. Segers, P. van Velthoven, W. Peters, F. Dentener and P. Bergamaschi, The two-way nested global chemistry-transport zoom model TM5: algorithm and applications, Atmos. Chem. Phys., 5, 417–432, https://doi.org/10.5194/acp-5-417-2005, 2005.

Kyrölä, E., M. Laine, V. Sofieva, J. Tamminen, S.-M. Päivärinta, S. Tukiainen, J. Zawodny and L. Thomason, Combined SAGE II–GOMOS ozone profile data set for 1984–2011 and trend analysis of

the vertical distribution of ozone, Atmos. Chem. Phys., 13, 10645–10658, https://doi.org/10.5194/acp-13-10645-2013, 2013.

Labow, G. J., Ziemke, J. R., McPeters, R. D., Haffner, D. P. and Bhartia, P. K.: A Total Ozone Dependent Ozone Profile Climatology based on Ozone-Sondes and Aura MLS Data, J. Geophys. Res. Atmos., n/a-n/a, doi:10.1002/2014JD022634, 2015.

Lerot, C., Van Roozendael, M., van Geffen, J., van Gent, J., Fayt, C., Spurr, R., Lichtenberg, G., and von Bargen, A.: Six years of total ozone column measurements from SCIAMACHY nadir observations, Atmos. Meas. Tech., 2, 87–98, https://doi.org/10.5194/amt-2-87-2009, 2009.

Lerot, C., Van Roozendael, M., Spurr, R., Loyola, D., Coldewey-Egbers, M., Kochenova, S., van Gent, J., Koukouli, M., Balis, D., Lambert, J.-C., Granville, J., and Zehner, C., Homogenized total ozone data records from the European sensors GOME/ERS-2, SCIAMACHY/Envisat, and GOME-2/MetOp-A. Journal of Geophysical Research: Atmospheres, 119(Cci), n/a-n/a. https://doi.org/10.1002/2013JD020831, 2014.

Levenberg, A., A method for the solution of certain non-linear problems in least squares, Q. Appl. Math. 2, 164-168, 1944.

Livesey, N. J., W. V. Snyder, and P. A. Wagner, Retrieval algorithms for the EOS Microwave Limb Sounder (MLS) instrument, IEEE Trans. Geosci. Remote Sens., 44 (5), 1144–1155, doi:10.1109/TGRS.2006.872327, 2006.

Lumpe, J. D., Bevilacqua, R. M., Hoppel, K. W. and Randall, C. E., POAM III retrieval algorithm and error analysis, J. Geophys. Res. Atmos., 107(D21), ACH 5-1--ACH 5-32, doi:10.1029/2002JD002137, 2002.

McLinden, C. A. and V. Fioletov, Quantifying stratospheric ozone trends: Complications due to stratospheric cooling, Geophys. Res. Lett., 38, 3, https://doi.org/10.1029/2010GL046012, February 2011.

McPeters, R. D., G. J. Labow, and J. A. Logan, Ozone climatological profiles for satellite retrieval algorithms, J. Geophys. Res., 112, D05308, doi:10.1029/2005JD006823, 2007.

McPeters, R., Frith, S., Kramarova, N., Ziemke, J., and Labow, G.: Trend quality ozone from NPP OMPS: the version 2 processing, Atmos. Meas. Tech., 12, 977-985, https://doi.org/10.5194/amt-12-977-2019, 2019.

Malicet, J., Brion, J., and Daumont, D., Temperature dependence of the absorption cross-section of ozone at 254 nm, Chem. Phys. Lett. 158, 293, https://doi.org/10.1016/0009-2614(89)87338-5, 1989.

Malicet, C., Daumont, D., Charbonnier, J., Parisse, C., Chakir, A. and Brion, J., Ozone UV spectroscopy, II. Absorption cross-sections and temperature dependence, J. Atmos. Chem., 21, 263-273, 1995.

Marquardt, D. W., An algorithm for least-squares estimation of nonlinear parameters, J. Soc. Ind. Appl. Math., 11 (2), 431-441, 1963.

Matthews, E., Global vegetation and land use: new high resolution data bases for climate studies, J. Clim. Appl. Meteo., 22, 474-487, https://doi.org/10.1175/1520-0450(1983)022%3C0474:GVALUN%3E2.0.CO;2, 1983.

Maycock, A. C., Randel, W. J., Steiner, A. K., Karpechko, A. Y., Christy, J., Saunders, R., Thompson, D. W. J., Zou, C.-Z., Chrysanthou, A., Luke Abraham, N., Akiyoshi, H., Archibald, A. T., Butchart, N., Chipperfield, M., Dameris, M., Deushi, M., Dhomse, S., Di Genova, G., Jöckel, P., Kinnison, D. E., Kirner, O., Ladstädter, F., Michou, M., Morgenstern, O., O'Connor, F., Oman, L., Pitari, G., Plummer, D. A., Revell, L. E., Rozanov, E., Stenke, A., Visioni, D., Yamashita, Y. and Zeng, G.: Revisiting the Mystery of Recent Stratospheric Temperature Trends, Geophys. Res. Lett., 45(18), 9919–9933, doi:10.1029/2018GL078035, 2018.

Miles, G. M., R. Siddans, B. J. Kerridge, B. G. Latter, and N. A. D. Richards, Tropospheric ozone and ozone profiles retrieved from GOME-2 and their validation, Atmos. Meas. Tech., 8, 385–398, 2015. www.atmos-meas-tech.net/8/385/2015/, doi:10.5194/amt-8-385-2015.

Miller, A. J., Nagatani, R. M., Flynn, L. E., Kondragunta, S., Beach, E., Stolarski, R., McPeters, R. D., Bhartia, P. K., De-Land, M. T., Jackman, C. H., Wuebbles, D. J., Patten, K. O., and Cebula, R. P.: A cohesive total ozone data set from the SBUV(/2) satellite system, J. Geophys. Res., 107(D23), 4701, doi:10.1029/2001JD000853, 2002.

Munro, R., R. Siddans, W.J. Reburn, and B.J.K. Kerridge, Direct measurement of tropospheric ozone distributions from space, Nature 392 (6672), 168-171, doi:10.1038/32392, 1998.

Munro, R., R. Lang, D. Klaes, G. Poli, C. Retscher, R. Lindstrot, R. Huckle, A. Lacan, M. Grzegorski, A. Holdak, A. Kokhanovsky, J. Livschitz and M. Eisinger, The GOME-2 instrument on the Metop series of satellites: instrument design, calibration, and level 1 data processing – an overview, Atmos. Meas. Tech., 9, 1279–1301, doi:10.5194/amt-9-1279-2016, 2016.

Orphal, J., A critical review of the absorption cross-sections of O3 and NO2 in the ultraviolet and visible, J. Photochem. Photobiology A: Chem. 157, 185–209, https://doi.org/10.1016/S1010-6030(03)00061-3, 2003.

Petropavlovskikh, I., Godin-Beekmann, S., Hubert, D., Damadeo, R., Hassler, B. and Sofieva, V.: SPARC/IO3C/GAW Report on Long-term Ozone Trends and Uncertainties in the Stratosphere, edited by M. Kenntner and B. Ziegele, 2019.

Rahpoe, N., von Savigny, C., Weber, M., Rozanov, A. V., Bovensmann, H., and Burrows, J. P.: Error budget analysis of SCIAMACHY limb ozone profile retrievals using the SCIATRAN model, Atmos. Meas. Tech., 6, 2825–2837, https://doi.org/10.5194/amt-6-2825-2013, 2013.

Rahpoe, N., Weber, M., Rozanov, A. V., Weigel, K., Bovensmann, H., Burrows, J. P., Laeng, A., Stiller, G., von Clarmann, T., Kyrölä, E., Sofieva, V. F., Tamminen, J., Walker, K., Degenstein, D., Bourassa, A. E., Hargreaves, R., Bernath, P., Urban, J., and Murtagh, D. P.: Relative drifts and biases between six ozone limb satellite measurements from the last decade, Atmos. Meas. Tech., 8, 4369–4381, https://doi.org/10.5194/amt-8-4369-2015, 2015.

Randall, C. E., Rusch, D. W., Bevilacqua, R. M., Hoppel, K. W., Lumpe, J. D., Shettle, E., Thompson, E., Deaver, L., Zawodny, J., Kyrö, E., Johnson, B., Kelder, H., Dorokhov, V. M., König-Langlo, G. and Gil, M.: Validation of POAM III ozone: Comparisons with ozonesonde and satellite data, J. Geophys. Res. Atmos., 108(D12), doi:https://doi.org/10.1029/2002JD002944, 2003.

Rodgers, C. D., Inverse Methods for Atmospheric Sounding: Theory and Practice, World Scientific, https://doi.org/10.1142/3171, 2000.

Rothman, L., Gordon, I., Babikov, Y., Barbe, A., Benner, D. C., Bernath, P., Birk, M., Bizzocchi, L., Boudon, V., Brown, L., Campargue, A., Chance, K., Cohen, E., Coudert, L., Devi, V., Drouin, B., Fayt, A., Flaud, J.-M., Gamache, R., Harrison, J., Hartmann, J.-M., Hill, C., Hodges, J., Jacquemart, D., Jolly, A., Lamouroux, J., Roy, R. L., Li, G., Long, D., Lyulin, O., Mackie, C., Massie, S., Mikhailenko, S., Müller, H., Naumenko, O., Nikitin, A., Orphal, J., Perevalov, V., Perrin, A., Polovtseva, E., Richard, C., Smith, M., Starikova, E., Sung, K., Tashkun, S., Tennyson, J., Toon, G., Tyuterev, V., and Wagner, G.: The HITRAN2012 molecular spectroscopic database, J. Quant. Spectrosc. Ra., 130, 4–50, doi:10.1016/j.jqsrt.2013.07.002, 2013.

Rozanov, V. V., D. Diebel, R.J.D. Spurr, and J.P. Burrows. GOMETRAN: A radiative transfer model for the satellite project GOME - the plane-parallel version, J. Geophys. Res., 102 (d14) , 16683-16695, https://doi.org/10.1029/96JD01535, 1997.

Seftor, C. J., Jaross, G., Kowitt, M., Haken, M., Li, J., and Flynn, L., Postlaunch performance of the Suomi National Polar orbiting Partnership Ozone Mapping and Profiler Suite (OMPS) nadir sensors, J. Geophys. Res.-Atmos., 119, 4413–4428, https://doi.org/10.1002/2013JD020472, 2014.

Serdyuchenko, A., Gorshelev, V., Weber, M., Chehade, W., and Burrows, J. P.: High spectral resolution ozone absorption cross-sections – Part 2: Temperature dependence, Atmos. Meas. Tech., 7, 625–636, https://doi.org/10.5194/amt-7-625-2014, 2014.

Siddans, R., Height Resolved Ozone Retrievals from Global Ozone Monitoring Experiment, PhD Thesis, University of Reading, 2003.

Sofieva, V. F., Rahpoe, N., Tamminen, J., Kyrölä, E., Kalakoski, N., Weber, M., Rozanov, A., von Savigny, C., Laeng, A., von Clarmann, T., Stiller, G., Lossow, S., Degenstein, D., Bourassa, A., Adams, C., Roth, C., Lloyd, N., Bernath, P., Hargreaves, R. J., Urban, J., Murtagh, D., Hauchecorne, A., Dalaudier, F., van Roozendael, M., Kalb, N., and Zehner, C.: Harmonized dataset of ozone profiles from satellite limb and occultation measurements, Earth Syst. Sci. Data, 5, 349–363, https://doi.org/10.5194/essd-5-349-2013, 2013.

Sofieva, V. F., Kalakoski, N., Päivärinta, S.-M., Tamminen, J., Laine, M., and Froidevaux, L.: On sampling uncertainty of satellite ozone profile measurements, Atmos. Meas. Tech., 7, 1891–1900, https://doi.org/10.5194/amt-7-1891-2014, 2014.

Sofieva, V. F., Ialongo, I., Hakkarainen, J., Kyrölä, E., Tamminen, J., Laine, M., Hubert, D., Hauchecorne, A., Dalaudier, F., Bertaux, J.-L., Fussen, D., Blanot, L., Barrot, G., and Dehn, A.: Improved GOMOS/Envisat ozone retrievals in the upper troposphere and the lower stratosphere, Atmos. Meas. Tech., 10, 231–246, https://doi.org/10.5194/amt-10-231-2017, 2017a.

Sofieva, V. F., Kyrölä, E., Laine, M., Tamminen, J., Degenstein, D., Bourassa, A., Roth, C., Zawada, D., Weber, M., Rozanov, A., Rahpoe, N., Stiller, G., Laeng, A., von Clarmann, T., Walker, K. A., Sheese, P., Hubert, D., van Roozendael, M., Zehner, C., Damadeo, R., Zawodny, J., Kramarova, N., and Bhartia, P. K.: Merged SAGE II, Ozone_cci and OMPS ozone profile dataset and evaluation of ozone trends in the stratosphere, Atmos. Chem. Phys., 17, 12533–12552, https://doi.org/10.5194/acp-17-12533-2017, 2017b.

Sofieva, V. F., Szeląg, M., Tamminen, J., Kyrölä, E., Degenstein, D., Roth, C., Zawada, D., Rozanov, A., Arosio, C., Burrows, J. P., Weber, M., Laeng, A., Stiller, G. P., von Clarmann, T., Froidevaux, L., Livesey, N., van Roozendael, M., and Retscher, C.: Measurement report: regional trends of

stratospheric ozone evaluated using the MErged GRIdded Dataset of Ozone Profiles (MEGRIDOP), Atmos. Chem. Phys., 21, 6707–6720, https://doi.org/10.5194/acp-21-6707-2021, 2021.

Sofieva, V. F., Szelag, M., Tamminen, J., Arosio, C., Rozanov, A., Weber, M., Degenstein, D., Bourassa, A., Zawada, D., Kiefer, M., Laeng, A., Walker, K. A., Sheese, P., Hubert, D., van Roozendael, M., Retscher, C., Damadeo, R., and Lumpe, J. D.: Updated merged SAGE-CCI-OMPS+ dataset for the evaluation of ozone trends in the stratosphere, Atmos. Meas. Tech., 16, 1881–1899, https://doi.org/10.5194/amt-16-1881-2023, 2023.

Spurr, R., Simultaneous derivation of intensities and weighting functions in a general pseudo-spherical discrete ordinate radiative transfer treatment, J. Quant. Spectrosc. Radiat. Transfer, 75, 129-175, https://doi.org/10.1016/S0022-4073(01)00245-X, 2002.

Spurr, R., LIDORT and VLIDORT: Linearized pseudo-spherical scalar and vector discrete ordinate radiative transfer models for use in remote sensing retrieval problems, in Light Scattering Reviews, Volume 3, by A. A. Kokhanovsky (ed.). Springer, 2008.

Spurr, R., and V. Natraj, A linearized two-stream radiative transfer code for fast approximation of multiple-scatter fields, J. Quant. Spectrosc. Radiat. Transfer, 112, 2630-2637, https://doi.org/10.1016/j.jqsrt.2011.06.014, 2011.

Spurr, R., et al., GOME/ERS-2 – GDP5.0 Upgrade of the GOME Data Processor for Improved Total Ozone Columns, Algorithm Theoretical Basis Document, 2011.

Spurr, R., V. Natraj, C. Lerot, M. Van Roozendael, and D. Loyola, Linearization of the Principal Component Analysis method for radiative transfer acceleration: Application to retrieval algorithms and sensitivity studies, J. Quant. Spectrosc. Radiat. Transfer, 125, 1-17, https://doi.org/10.1016/j.jqsrt.2013.04.002, 2013.

Stamnes, K., S.-C.Tsay, W. Wiscombe, and K. Jayaweera, Numerically stable algorithm for discrete ordinate method radiative transfer in multiple scattering and emitting layered media, App. Opt., 27 (12), 2502-2509, https://doi.org/10.1364/AO.27.002502, 1988.

Steinbrecht, W., Froidevaux, L., Fuller, R., Wang, R., Anderson, J., Roth, C., Bourassa, A., Degenstein, D., Damadeo, R., Zawodny, J., Frith, S., McPeters, R., Bhartia, P., Wild, J., Long, C., Davis, S., Rosenlof, K., Sofieva, V., Walker, K., Rahpoe, N., Rozanov, A., Weber, M., Laeng, A., von Clarmann, T., Stiller, G., Kramarova, N., Godin-Beekmann, S., Leblanc, T., Querel, R., Swart, D., Boyd, I., Hocke, K., Kämpfer, N., Maillard Barras, E., Moreira, L., Nedoluha, G., Vigouroux, C., Blumenstock, T., Schneider, M., García, O., Jones, N., Mahieu, E., Smale, D., Kotkamp, M., Robinson, J., Petropavlovskikh, I., Harris, N., Hassler, B., Hubert, D., and Tummon, F.: An update on ozone profile trends for the period 2000 to 2016, Atmos. Chem. Phys., 17, 10675–10690, https://doi.org/10.5194/acp-17-10675-2017, 2017.

Steiner, A. K., Ladstädter, F., Randel, W. J., Maycock, A. C., Fu, Q., Claud, C., Gleisner, H., Haimberger, L., Ho, S.-P., Keckhut, P., Leblanc, T., Mears, C., Polvani, L. M., Santer, B. D., Schmidt, T., Sofieva, V., Wing, R. and Zou, C.-Z.: Observed temperature changes in the troposphere and stratosphere from 1979 to 2018, J. Clim., 1–72, doi:10.1175/JCLI-D-19-0998.1, 2020.

Stolarski, R. S. and Frith, S. M.: Search for evidence of trend slow-down in the long-term TOMS/SBUV total ozone data record: the importance of instrument drift uncertainty, Atmos. Chem. Phys., 6, 4057–4065, https://doi.org/10.5194/acp-6-4057-2006, 2006.

Turner, D. D., Tobin, D. C., Clough, S. A., Brown, P. D., Ellingson, R. G., Mlawer, E. J., Knuteson, R. O., Revercomb, H. E., Shippert, T. R., Smith, W. L., & Shephard, M. W., The QME AERI LBLRTM: A Closure Experiment for Downwelling High Spectral Resolution Infrared Radiance. Journal of the Atmospheric Sciences, 61(22), 2657-2675, https://doi.org/10.1175/JAS3300.1, 2004.

Van Roozendael, M., D. Loyola, R. Spurr, D. Balis, J.-C. Lambert, Y. Livschitz, P. Valks, T. Ruppert, P. Kenter, C. Fayt, C. Zehner Ten years of GOME/ERS-2 total ozone data—The new GOME data processor (GDP) version 4: 1. Algorithm description, J. Geophys. Res., 111, D14311, doi:10.1029/2005JD006375, 2006.

Van Roozendael, M., R. Spurr, D. Loyola, C. Lerot, D. Balis, J.-C. Lambert, W. Zimmer, J. van Gent, J. van Geffen, M. Koukouli, J. Granville, A. Doicu, C. Fayt, C. Zehner, Sixteen years of GOME/ERS-2 total ozone data: The new direct-fitting GOME Data Processor (GDP) version 5—Algorithm description, J. Geophys. Res., 117, D03305, doi:10.1029/2011JD016471, 2012.

Wang, P., Stammes, P., van der A, R., Pinardi, G., and van Roozendael, M.: FRESCO+: an improved O2 A-band cloud retrieval algorithm for tropospheric trace gas retrievals, Atmos. Chem. Phys., 8, 6565-6576, doi:10.5194/acp-8-6565-2008, 2008.

Waters, J. W. et al., The Earth observing system microwave limb sounder (EOS MLS) on the aura Satellite, *in* IEEE Transactions on Geoscience and Remote Sensing, 44, 5, 1075-1092, doi: 10.1109/TGRS.2006.873771, 2006.

Wellemeyer, C. G., Taylor, S. L., Seftor, C. J., McPeters, R. D., and Bhartia, P. K., A correction for total ozone mapping spectrometer profile shape errors at high latitude, J. Geophys. Res., 102(D7), 9029–9038, doi:10.1029/96JD03965, 1997.

WMO: Scientific assessment of ozone depletion, Global Ozone Research and Monitoring Project-Report No. 52, Geneva, Switzerland, https://www.esrl.noaa.gov/csd/assessments/ozone/, 2014.

Zawada, D. J., Dueck, S. R., Rieger, L. A., Bourassa, A. E., Lloyd, N. D. and Degenstein, D. A.: High-resolution and Monte Carlo additions to the SASKTRAN radiative transfer model, Atmos. Meas. Tech., 8(6), 2609–2623, doi:10.5194/amt-8-2609-2015, 2015.

Zawada, D. J., Rieger, L. A., Bourassa, A. E. and Degenstein, D. A.: Tomographic retrievals of ozone with the OMPS Limb Profiler: algorithm description and preliminary results, Atmos. Meas. Tech. Discuss., 2017, 1–26, doi:10.5194/amt-2017-236, 2017.

Zhou, D. K., A. M. Larar, X. Liu, W. L. Smith Sr., L. Strow, P. Schluessel and X. Calbet, Global Land Surface Emissivity Retrieved From Satellite Ultraspectral IR Measurements, IEEE Transactions on Geoscience and Remote Sensing, 49, 4, 1277-1290, doi:10.1109/TGRS.2010.2051036, 2011.

Ziemke, J. R., Chandra, S., Labow, G. J., Bhartia, P. K., Froidevaux, L., and Witte, J. C.: A global climatology of tropospheric and stratospheric ozone derived from Aura OMI and MLS measurements, Atmos. Chem. Phys., 11, 9237-9251, doi:10.5194/acp-11-9237-2011, 2011.

Copernicus Climate Change Service

ECMWF - Robert-Schumann-Platz 3, D-53175 Bonn, Germany

Contact: https://support.ecmwf.int/